Doctoral Dissertation of 2018

Observation of Two-Photon Interference with Continuous Variables

Daohua Wu

Department of Engineering Science
The University of Electro-Communications
January 2018

概　要

量子光学および量子情報の実験研究については大きくわけて (1) 離散変数と (2) 連続変数の二つである。前者には光の粒子性を注目し、識別できない光子間の量子干渉を根幹として行う。また、後者は光 (電磁場) の波動性を注目し、電場の二つ直交位相振幅を観測量として扱う。二つ分野分けますが、いずれもいろいろな量子もつれの生成するのは、量子光学と量子情報においてとても重要で、量子情報提案を実現することのキーとなる。その中で我々は光の粒子性に注目し, その特徴の一つである二光子干渉を観測することを目指している. 従来, 二光子干渉はアバランシェフォトダイオード (APD) による光子数を直接的に評価する離散的な測定が良く報告されてきた. 一方, ホモダイン検出器を用いて連続変数である直交位相振幅のデータから光子数の情報を評価する方法は, 新たな手法として期待される. 本研究は、連続変数を用いて位相空間における奇妙な二光子干渉現象を実験的に検証することを目的としている。

光源として波長 1064 nm で連続波 (CW) の Nd:YAG レーザーを使用した. 光源からの光は第二高調波発生 (SHG) と雑音低減のためのモードクリーナー共振器 (MCC) に入射するため, 2 つに分割した. SHG からの 532 nm の光はポンプ光として用い, 光パラメトリック増幅器 (OPA) に入射し, 真空スクイーズド状態を生成した. MCC からの光は seed 光, コヒーレント光, ローカルオシレーター (LO) 光として用いるため 3 つに分割した. コヒーレント光は電気光学変調器 (EOM) による振幅変調 (AM) もしくは位相変調 (PM) によって生成した. 真空スクイーズド状態とコヒーレント光を 95%反射ミラーで干渉させることでディスプレイススクイーズド状態の生成を実現した. ディスプレイススクイーズド状態は EOM による AM 方式, PM 方式によってそれぞれ振幅スクイーズド状態, 位相スクイーズド状態となる. それぞれのディスプレイススクイーズド状態が正しく生成されているかはホモダイントモグラフィを用いて Wigner 関数を構築することによって確認した.

二光子干渉の観測では, 位相スクイーズド状態, 振幅スクイーズド状態について二次強度相関 $g^{(2)}(0)$ を測定した. 位相クイーズド状態では常に $g^{(2)}(0) > 1$ となるバンチング状態となり, 二光子確率が増大していることが観測された, 一方, 振幅スクイーズド状態の測定では最小値が $g^{(2)}(0) = 0.81 \pm 0.03$ と 1 を下回るアンチバンチング状態となり二光子確率の低減を観測した. この結果から, 直交位相振幅を測定対象としてホモダイン検出器を使用し, 二光子干渉が観測出来ていることが示された.

更に今後の光子数確率の測定に向け, 実際に二光子確率がどのように変化していると考えられるのか, 測定のためにはどのような光源が必要となるかを考察した.

Abstract

Two-photon interference is highly important, fundamental, and indefeasible features of quantum mechanics. It has numerous applications in production of quantum state, which is useful in quantum communications, quantum information processing, and quantum metrology. In this thesis, we experimentally observed a two-photon interference between a squeezed vacuum state and a coherent state with continuous variables by homodyne detection for the first time. The photon anti-bunching effect and bunching effect of the measured field were investigated by calculating the second-order correlation function from the measured quadrature amplitudes, which were obtained by two homodyne detection systems. This provides another method to observe two-photon interference, and the method has the following merits:

First, we gave a new method to calculate the second-order correlation function. It provides a link to close the gap between discrete variables and continuous variables in the field of quantum optics.

Then, we experimentally observed two-photon interference (particle property) by measuring amplitude quadratures (wave property) of the light field. In other words, we used a wave method to investigate the particle property of light. It may give another evidence to show the wave-particle duality of light.

At last, we experimentally observed the two-photon interference at two sideband frequencies of laser light. As applications, it opens a new method to generate a single-photon frequency comb and leads to potential applications in multi-channel quantum communications technology.

The detail of this thesis is included as follows:

1. We experimentally generated a squeezed vacuum state from a below threshold optical parametric amplifier (OPA) with periodically poled KTiOPO4 (PPKTP) crystal. The OPA could be controlled so as to de-amplify or amplify the injection beam by choosing the relative phase between pump and injection beams. This ensures to produce the amplitude quadrature or phase quadrature squeezed state with the squeezing level of -1 dB and anti-squeezing of 1.7 dB in the range of 5 MHz to the cavity linewidth of 35 MHz.

2. We reconstructed the Winger function of generated states by homodyne tomography. Using homodyne detection, we measured a set of probability densities for the quadrature amplitudes of the generated states. These histograms were inverted using inverse Radon transform to reconstruct the Winger distribution which showed the fluctuation of the light fields in phase space. It intuitively characterizes the generated vacuum states, coherent states, squeezed vacuum states and displaced squeezed states in our experiment.

3. We experimentally observed a continuous-wave two-photon interference between a squeezed vacuum state from an OPA and a weak coherent state on a beam splitter by measuring the second-order correlation function with the homodyne detection system. A second-order correlation function of $g^{(2)}(0) = 0.81 < 1$, indicating the two-photon destructive interference, was observed when an amplitude squeezed vacuum state acts as one of interference sources. On the other hand, the two-photon constructive interference of $g^{(2)}(0) = 1.37 > 1$ was also obtained when the phase squeezed vacuum state is employed.

CONTENTS

Chapter1 Introduction

Two-photon interference has played an important role in fundamental investigations of quantum mechanics and has widely used in quantum communications, quantum information processing, and quantum metrology [1–7]. Since 1980s, both two-photon interference and its applications have been extensively studied in theoretically and experimentally [8–14].

This chapter presents the the background and the motivations of our research. Firstly, we will briefly introduce the background of this thesis. then, the originality and motivation of our research will be introduced. At last, we will give the structure of this thesis.

1.1 Introduction

Quantum optics is a relatively young branch of physics. One of its goals is to interpret the nonclassical phenomena from semi-classical and quantum-mechanical physics point of view. This may lead to a deeper understanding of nature of light. Up to now, lots of physical systems, such as photons, atoms, ions and superconducting devices, have been employed in quantum optics and quantum information processing. Quantum optics and quantum information processing divide into two different regimes which depend on the degree of freedom of the observable. If the observable is discrete in nature (e.g. the polarization and the orbital angular momentum degree of freedom for a single photon), we refer to discrete variable regime. One the other hand, if the observable has continuous values (e.g. the amplitude quadratures of a light field), we refer to continuous variable regime. In other words, the discrete variables and continuous variables pictures can be alternated depending on whether one is interested in probing the particle-like or wave-like property of light. From the beginning of the last century, lots of great achievements, such as generation of quantum states and quantum teleportations, have been made on quantum optics or quantum information processing in both continuous variables and discrete variables regime [15–20]. In these experiments, the two different observable was recorded either by photon counting or homodyne detection. However, both dealing with quantum information processing with continuous variables and discrete variables have the intrinsic limitations. For example, with discrete variables, the transformation efficiency is low and the projection measurement with the photons combined is random. One the other hand, with continuous variables, there are demerits such as sensitivity to loss and difficult to information transmission. Recently, A hybrid technique which combines continuous and discrete variables techniques attracts more and more attention [21–25]. For example, Schrodinger kitten state [21] has been experimentally produced by subtracting a single photon (discrete variables) from a quadrature squeezed vacuum state

(continuous variables) . In this protocol, the preparation of Schrodinger kitten state was realized by combining a photon counter measurement with a homodyne measurement where the photon counter was used to prepare a single photon state, whereas the homodyne detector employed as a squeezing operation. This technique opens a new research direction, which will bring innovative developments in the research fields of quantum optics and quantum information processing, for linking the continuous variables and discrete variables in the field of quantum optics.

In this thesis, by measuring the the amplitude quadratures of light with homodyne detection, we will observe the two-photon interference, which indicates the particle property of light, between a squeezed vacuum state and a coherent state on a beam splitter. To evaluate the two-photon interference, a well known approach is to reconstruct the photon number probability distributions using homodyne tomography technique. However, in this research, we will provide a novel method to demonstrate the quantum interference of light, in which photon bunching and anti-bunching effects of the mixed field will be investigated by calculating the second-order correlation function from the measured amplitude quadratures which can be obtained by two homodyne detections systems. Since the squeezed vacuum state can be observed over a range of analysis frequencies, the interfered coherent state should be prepared on one of the frequencies which can be realized by performed an amplitude modulation or phase modulation on laser light . In other words, the two-photon interference occurred at the two sidebands frequencies of the laser frequency. Since the two-photon interference has been widely used to generate single-photon states and entangled photon states for quantum information processing. Hence, this makes it possible to produce quantum states at the sidebands frequencies. It is easy to further extend to other sideband components using modern techniques, such as an optical frequency comb generator. It maybe lead to potential applications in multi-channel quantum communications technology in the future.

1.2 Motivation of this thesis

In this thesis, we will experimentally observe two-photon interference with continuous variables by homodyne detection system for the first time. The nonclassical effect of photon anti-bunching occurs when an amplitude squeezed vacuum state acts as one of the interference source, which indicates the two-photon destructive interference. On the other hand, the photon bunching effect appears, indicating the two-photon constructive interference, will be obtained when the phase squeezed vacuum state is employed. The originality and motivation of my thesis are:

1. Different from other experiments, homodyne detection technique is used in our experiment. It gives the quadrature amplitudes of the measured field, which relates to the wave property of the light. On the other hand, the result (photon interference) relates to the particle property of the light. We believe this gives another evidence for the wave-particle duality of light [26–31].

2. Usually, the technique of single photon counting modules (SPCMs) is employed to interrogate the strong correlation photons [32,33]. In general, using the SPCM, experimentalists do quantum optics experiments in the discrete variables regime. In our experiment, we measure the second-order correlation function with homodyne detection which measure the quadrature amplitudes of the measured field, and they are regarded as continuous variables.This provides opportunity to close the gap between discrete variables and continuous variables in quantum optics field [34].

3. The two-photon interference in our experiment was observed at two sideband frequencies of laser frequency. It is easy to further extend sideband components using optical frequency comb technique. Adding the generation of the wideband squeezed state, it gives a new method to produce a single-photon frequency comb. We believe it leads to potential applications for future multi-channel quantum communications technology.

1.3 Structure of the thesis

The structure of this thesis is given as:

In chapter 2, we will introduce the background for quantum optics and the formalism which is required to model the experiments in this thesis.

In chapter 3, we will introduce a scheme to generate an amplitude and phase quadrature squeezed states which will be acted as interference sources in our experiment. We will also introduce a method to reconstruct the Wigner function of quantum states with homodyne tomography.

In chapter 4, we will perform the two-photon interference by producing a displaced squeezed state. By measuring the second-order correlation function with two set of homodyne detections, we observed two different photon statistics of the generated state due to two different results of the two-photon interference.

Finally, I will summarize the most important theoretical and experimental results of the two-photon interference with continuous variables and make suggestions for improvements and further studies that may yield interesting results.

Chapter2 Foundation of Quantum Optics

This chapter presents the basic theory of quantum optics which will be used in this thesis. Firstly, we will briefly introduce the quantization of the electromagnetic field. Secondly, we will introduce some states of light and their properties. Thirdly, balanced homodyne detection and the main method for detecting states of light, will be introduced. Fourthly, We will introduce the second-order correlation function $g^{(2)}(0)$ and $g^{(2)}(0)$ in two-photon interference. At last, we will introduce the two-photon number probabilities of displaced squeezed states.

2.1 The quantized field of light

2.1.1 Quantization of a single-mode field

A quantum mechanical picture of light begins with quantization of the electro-magnetic(EM) field. Here we will briefly introduce this procedure. We start it with a single-mode radiation field which is confined to a one-dimensional cavity along the z-direction with perfectly conducting walls at z=0 and z=L [35–38]. The free electro-magnetic field obeys the Maxwell equations,

$$\nabla \cdot \mathbf{B} = 0, \tag{2.1.1}$$

$$\nabla \cdot \mathbf{E} = 0, \tag{2.1.2}$$

$$\nabla \times \mathbf{E} = \frac{\partial B}{\partial t}, \tag{2.1.3}$$

$$\nabla \times \mathbf{B} = \mu_0 \varepsilon_0 \frac{\partial E}{\partial t}. \tag{2.1.4}$$

Assuming the electro-magnetic field to be polarized along the x-direction, the electric field of a standing wave cavity with perfectly reflecting mirrors(the boundary conditions of the single-mode field) can be written as,

$$E_x(z,t) = (\frac{2\omega^2}{V\varepsilon_0})^{1/2} q(t) \sin(kt), \tag{2.1.5}$$

where ω is the frequency of the mode and k is the wave number related to the frequency according to $k = \omega/c$. The boundary condition at z=L can be $\omega_m = \frac{mc\pi}{L}$, where $m = 1, 2, 3, \cdots$, and ω in Eq.(2.1.5) is one of these frequencies. V in Eq.(2.1.5) is the effective volume of the cavity and a time-dependent factor having the dimension of length is given by q(t). As we shall see, q(t) will act as a canonical position. From Eq(2.1.2) and Eq.(2.1.5),the magnetic field, which is

polarized along y-direction, can be described as,

$$B_y(z,t) = \frac{\mu_0\varepsilon_0}{k}(\frac{2\omega^2}{V\varepsilon_0})^{1/2}\dot{q(t)}\cos(kt), \tag{2.1.6}$$

Here $\dot{q(t)}$ plays the role of a canonical momentum for a harmonic oscillator, i.e. $p(t) = \dot{q(t)}$. From Eq.(2.1.5) and Eq.(2.1.6), we can derive the Hamiltonian $\boldsymbol{H}$

$$\boldsymbol{H} = \frac{1}{2}(p^2 + \omega^2 q^2), \tag{2.1.7}$$

Similarly with the canonical variables p and q for classical system, we use the correspondence rule to replace them by their operator equivalents $p \to \hat{p}$, $q \to \hat{q}$ with $[\hat{q}, \hat{p}] = i\hbar$. Thus the electric field $E_x(z,t)$ and magnetic field become the operators $\hat{E}_x(z,t)$ and $\hat{B}_y(z,t)$, respectively. And the Hamiltonian becomes

$$\hat{H} = \frac{1}{2}(\hat{p}^2 + \omega^2\hat{q}^2), \tag{2.1.8}$$

Where the operators $\hat{p}$ and $\hat{q}$ are Hermitian and correspond to observable quantities. Actually, in quantum optics, we usually use another non-Hermittian creation operator $\hat{a}^\dagger$ and annihilation operators $\hat{a}$ which are described as

$$\hat{a} = (2\hbar\omega)^{-\frac{1}{2}}(\omega\hat{q} + i\hat{p}), \tag{2.1.9}$$

$$\hat{a}^\dagger = (2\hbar\omega)^{-\frac{1}{2}}(\omega\hat{q} - i\hat{p}). \tag{2.1.10}$$

The operators $\hat{a}^\dagger$ and $\hat{a}$ satisfy the commutation relation

$$[\hat{a}, \hat{a}^\dagger] = \hat{a}\hat{a}^\dagger - \hat{a}^\dagger\hat{a} = 1. \tag{2.1.11}$$

and the Hamiltonian operator can be re-expressed as

$$\hat{H} = \hbar\omega(\hat{a}^\dagger\hat{a} + \frac{1}{2}), \tag{2.1.12}$$

To see how the system work, we first propose an energy eigenstate of the system $|n\rangle$, such as

$$\hat{H}|n\rangle = \hbar\omega(\hat{a}^\dagger\hat{a} + \frac{1}{2})|n\rangle = E_n|n\rangle, \tag{2.1.13}$$

where E_n is the energy eigenvalue. We apply the creation operator to both sides of the energy eigenvalue equation

$$\hbar\omega(\hat{a}^\dagger\hat{a}^\dagger\hat{a} + \frac{1}{2}\hat{a}^\dagger)|n\rangle = E_n\hat{a}^\dagger|n\rangle. \tag{2.1.14}$$

Using the commutation relation of Eq.(2.1.11), we get a new energy eigenvalue equation,

$$\hat{H}\hat{a}^\dagger|n\rangle = (E_n + \hbar\omega)\hat{a}^\dagger|n\rangle, \tag{2.1.15}$$

We can interpret it as the eigenvalue problem for a new state $\hat{a}^\dagger|n\rangle$ with a new energy eigenvalue $E_{n+1} = E_n + \hbar\omega$. It is also why the $\hat{a}^\dagger$ is called the creation operator: it creats a quantum of

energy $\hbar\omega$. Similarly, we can apply the annihilation operator to both sides of the Eq.(2.1.13) and use the commutation relation,

$$\hat{H}\hat{a}|n\rangle = (E_n - \hbar\omega)\hat{a}|n\rangle. \tag{2.1.16}$$

Obviously, it shows an opposite produce for the eigenstate $\hat{a}|n\rangle$ with the energy eigenvalue $E_{n-1} = E_n - \hbar\omega$, and clears annihilation operator $\hat{a}$ annihilates one quantum of erergy $\hbar\omega$. For the energy of the harmonic oscillator must always be positive, there must be a lowest energy state $|0\rangle$ which is called vacuum state or ground state. we define

$$\hat{a}|0\rangle = 0. \tag{2.1.17}$$

We act Hamiltonian operator $\hat{H}$ on the state,

$$\hat{H}|0\rangle = \hbar\omega(\hat{a}^\dagger\hat{a} + \frac{1}{2})|0\rangle = \frac{1}{2}\hbar\omega|0\rangle, \tag{2.1.18}$$

so that the lowest energy eigenvalue is not zero, but so-called zero-point energy $E_0 = \frac{1}{2}\hbar\omega$. As mentioned above, the creation operator $\hat{a}^\dagger$ creates each time one quantum of energy $\hbar\omega$, namely, $E_{n+1} = E_n + \hbar\omega$, the energy eigenvalue of eigenstate $|n\rangle$ are

$$E_n = \hbar\omega(n + \frac{1}{2}), n = 0, 1, 2, \cdots \tag{2.1.19}$$

Comparing Eq.(2.1.19) with Eq.(2.1.13), we can difine number operator $\hat{n} = \hat{a}^\dagger\hat{a}$ and

$$\hat{n}|n\rangle = n|n\rangle. \tag{2.1.20}$$

This kind of number states should be normalized according to $\langle n|n\rangle = 1$. For the state $\hat{a}|n\rangle$, we have

$$\hat{a}|n\rangle = c_n|n-1\rangle, \tag{2.1.21}$$

where c_n is a constant to be determined by inner product of $\hat{a}|n\rangle$ with itself, namely,

$$\begin{aligned}(\langle n|\hat{a}^\dagger)(\hat{a}|n\rangle) &= \langle n|\hat{a}^\dagger\hat{a}|n\rangle = n \\ &= \langle n-1|c_n^* c_n|n-1\rangle = |c_n^2|.\end{aligned} \tag{2.1.22}$$

then we can obtain $|c_n^2| = n$ and $c_n = \sqrt{n}$. Thus

$$\hat{a}|n\rangle = \sqrt{n}|n-1\rangle, \tag{2.1.23}$$

$$\hat{a}^\dagger|n\rangle = \sqrt{n+1}|n+1\rangle. \tag{2.1.24}$$

From Eq.(2.1.24), any number state $|n\rangle$ can be generated from the ground state $|0\rangle$ by repeated action of creation operator $\hat{a}^\dagger$,

$$|n\rangle = \frac{(\hat{a}^\dagger)^n}{\sqrt{n}}|0\rangle. \tag{2.1.25}$$

The number state described in Eq.(2.1.25) is also called "Fock state" and is important for single photon experiments. Furthermore, states with different number are orthogonal:

$$\langle n'|n\rangle = \delta_{nn'} = \begin{cases} 1 & n = n' \\ 0 & n \neq n'. \end{cases} \tag{2.1.26}$$

2.1.2 Quadrature Operators for a single-mode field

We can use the annihilation operator $\hat{a}$ and creation operator $\hat{a}^\dagger$ to describe the electric field:

$$\hat{E}_x = \varepsilon_0(\hat{a}e^{-i\omega t} + \hat{a}^\dagger e^{i\omega t})\sin(kz). \tag{2.1.27}$$

But they are not Hermitian, and are therefore not observable. In order to be measured in the lab, let us define the dimensionless pair of conjugate variables which play the role of position q and momentum p. It is so-called quadrature operators,

$$\hat{X}^0 = \frac{\omega}{2\hbar}q = \hat{a}^\dagger + \hat{a}, \tag{2.1.28}$$

$$\hat{X}^{\frac{\pi}{2}} = \frac{1}{2\hbar\omega}q = i(\hat{a}^\dagger - \hat{a}), \tag{2.1.29}$$

in term of quadrature operators, the Eq.(2.1.27) is expressed as

$$\hat{E}_x = \frac{1}{2}\varepsilon_0[\hat{X}^0\cos(\omega t) + \hat{X}^{\frac{\pi}{2}}\sin(\omega t)]\sin(kz). \tag{2.1.30}$$

It is evident that $\hat{X}^0$ and $\hat{X}^{\frac{\pi}{2}}$ are associated with field amplitudes oscillating out of phase with each other by 90^o, and satisfy the commutation relation

$$[\hat{X}^0, \hat{X}^{\frac{\pi}{2}}] = 2i. \tag{2.1.31}$$

Here we set the $\hbar = 2$, and then the Heisenberg Uncertainty relation can be derived as

$$\Delta^2\hat{X}^0\Delta^2\hat{X}^{\frac{\pi}{2}} \geq 1, \tag{2.1.32}$$

in which $\Delta^2\hat{X}^0$ and $\Delta^2\hat{X}^{\frac{\pi}{2}}$ are variances for the two quadrature operators. For a number state $|n\rangle$, we can obtain

$$\langle n|\hat{X}^0|n\rangle = \langle n|\,(\hat{a}^\dagger + \hat{a})\,|n\rangle = \langle n|\hat{a}^\dagger|n\rangle + \langle n|\hat{a}|n\rangle = 0. \tag{2.1.33}$$

Similarly, $\langle n|\hat{X}^{\frac{\pi}{2}}|n\rangle = 0$. On the other hand,

$$\begin{aligned}\langle n|(\hat{X}^0)^2|n\rangle &= \langle n|\,((\hat{a}^\dagger)^2 + (\hat{a})^2 + \hat{a}^\dagger\hat{a} + \hat{a}\hat{a}^\dagger)\,|n\rangle \\ &= \langle n|\,((\hat{a}^\dagger)^2 + (\hat{a})^2 + 2\hat{a}^\dagger\hat{a} + 1)\,|n\rangle \\ &= 2n + 1,\end{aligned} \tag{2.1.34}$$

and

$$\langle n|(\hat{X}^{\frac{\pi}{2}})^2|n\rangle = 2n + 1. \tag{2.1.35}$$

Obviously, the uncertainties in both quadratures are the same, and the variances are calculated as

$$\begin{aligned}\Delta^2\hat{X}^0 &= \langle 0|(\hat{X}^0)^2|0\rangle - \langle 0|\hat{X}^0|0\rangle^2 = 2n + 1 \\ \Delta^2\hat{X}^{\frac{\pi}{2}} &= \langle 0|(\hat{X}^{\frac{\pi}{2}})^2|0\rangle - \langle 0|\hat{X}^{\frac{\pi}{2}}|0\rangle^2 = 2n + 1.\end{aligned} \tag{2.1.36}$$

And

$$\Delta^2\hat{X}^0\Delta^2\hat{X}^{\frac{\pi}{2}} = (2n+1)^2. \tag{2.1.37}$$

Here $n \geq 0$ and we can obtain $\Delta^2\hat{X}^0\Delta^2\hat{X}^{\frac{\pi}{2}} \geq 1$ which accords with the Heisenberg uncertainty relation Eq.(2.1.32). For a special number state $|0\rangle$, we have

$$\Delta^2\hat{X}^0_{vac} = \Delta^2\hat{X}^{\frac{\pi}{2}}_{vac} = 2n+1 = 1(n=0). \tag{2.1.38}$$

and call it the minimum uncertainty state.

2.2 States of light

In this section, I will introduce several states [35] of light which are important in quantum optics and will be used in this thesis. It includes vacuum state, coherent state, squeezed state and displaced squeezed state.

2.2.1 Vacuum state

The vacuum state is a state with the lowest energy. It satisfies

$$\hat{a}|0\rangle = 0. \tag{2.2.1}$$

the vacuum state has no coherent amplitude and contains no physical particles.

$$\langle 0|\hat{X}^0_{vac}|0\rangle = \langle 0|\hat{X}^{\frac{\pi}{2}}_{vac}|0\rangle = 0 \tag{2.2.2}$$

$$\langle 0|\hat{n}|0\rangle = \langle 0|\hat{a}^\dagger\hat{a}|0\rangle = 0 \tag{2.2.3}$$

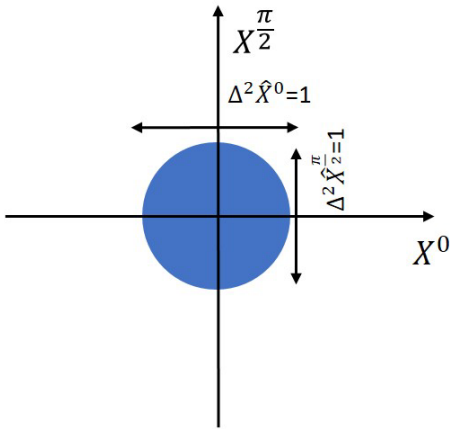

Fig. 2.1. Phase-space representation of a vacuum state.

Although there is no coherent amplitude, the vacuum state has quantum fluctuations. It is a minimum uncertainty state with equal quantum noise in both quadratures. It can be shown in Fig. 2.1.

$$\Delta^2 \hat{X}^0_{vac} = \Delta^2 \hat{X}^{\frac{\pi}{2}}_{vac} = 1. \tag{2.2.4}$$

These fluctuations are produced from the zero-point energy of ground state of the quantum harmonic oscillator. We also called these fluctuations vacuum noise or shot noise or quantum noise limit. These fluctuations occur in every possible optical mode and play important roles in quantum optics. For example, they have important ramifications when considering optical loss.

2.2.2 Coherent state

Coherent state is the closest possible quantum analogy of the corresponding classical state. The coherent state can be produced by applying the unitary displacement operator on a vacuum state:

$$|\alpha\rangle = \hat{D}(\alpha)|0\rangle. \tag{2.2.5}$$

where $\hat{D}(\alpha)$ is defined as

$$\hat{D}(\alpha) = \exp(\alpha\hat{a}^\dagger - \alpha^*\hat{a}). \tag{2.2.6}$$

It has the following properties

$$\hat{D}^\dagger(\alpha) = \hat{D}^{-1}(\alpha) = \hat{D}(\alpha) \tag{2.2.7}$$

$$\hat{D}^\dagger(\alpha)\hat{a}\hat{D}(\alpha) = \hat{a} + \alpha \tag{2.2.8}$$

$$\hat{D}^\dagger(\alpha)a^\dagger\hat{D}(\alpha) = \hat{a}^\dagger + \alpha^* \tag{2.2.9}$$

Coherent state can also be described as the eigenstate of the annihilation operator $\hat{a}$

$$\hat{a}|\alpha\rangle = \alpha|\alpha\rangle. \tag{2.2.10}$$

Since the annihilation operation is not Hermitian, the eigenvalues of $\hat{a}$ are complex values. Hence, the coherent state has a well-defined amplitude and phase. The set of coherent state $|\alpha\rangle$ are parameterised by their complex coherent amplitude $\alpha = |\alpha|e^{i\theta}$ in which the real and imaginary components show up in the amplitude quadrature and phase quadrature, respectively. This effect is shown in Fig. 2.2 using the phase diagram.

We can also expand coherent state $\langle\alpha|$ in terms of the Fock states as form of

$$|\alpha\rangle = \sum_n c_n |n\rangle. \tag{2.2.11}$$

Acting an annihilation operator a on both sides of the equation, using Eq.(2.2.10), we can obtain

$$a|\alpha\rangle = \alpha \sum_n c_n |n\rangle = \sum_n c_n\sqrt{n}\,|n-1\rangle\,. \tag{2.2.12}$$

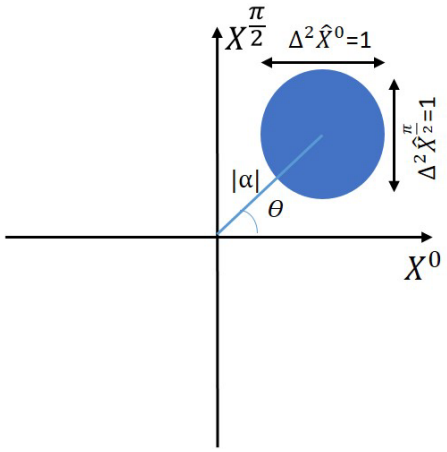

Fig. 2.2. Phase-space representation of a coherent state.
the $|\alpha|$ and θ are the amplitude and phase of the coherent state, respectively.

Equating coefficients of $|n\rangle$ on both sides, we can obtain the recursion relation

$$c_n\sqrt{n} = \alpha c_{n-1}, \tag{2.2.13}$$

whose solution is

$$c_n = \frac{\alpha^n}{\sqrt{n!}}c_0, \tag{2.2.14}$$

and the c_0 can be determined by

$$\begin{aligned}\langle\alpha|\alpha\rangle &= |c_0|^2 \sum_n \sum_{n'} \frac{(\alpha^*)^n \alpha^{n'}}{\sqrt{n!n'!}} \langle n|n'\rangle \\ &= |c_0|^2 \sum_n \frac{|\alpha|^{2n}}{n!} = |c_0|^2 e^{|\alpha|^2} = 1,\end{aligned} \tag{2.2.15}$$

and c_0 can be calculated as

$$c_0 = e^{-\frac{1}{2}|\alpha|^2}. \tag{2.2.16}$$

Thus the coherent state $|\alpha\rangle$ can be expanded as

$$|\alpha\rangle = e^{-|\alpha|^2/2} \sum_n \frac{\alpha^n}{\sqrt{n!}}|n\rangle. \tag{2.2.17}$$

Next we will introduce some properties of coherent state. Firstly, we calculate the mean of photon number operator $\hat{n} = \hat{a}^\dagger\hat{a}$ for a coherent state $|\alpha\rangle$ with $\alpha = |\alpha|e^{i\theta}$,

$$\langle\hat{n}\rangle = \langle\alpha|\hat{n}|\alpha\rangle = \langle\alpha|\hat{a}^\dagger\hat{a}|\alpha\rangle = |\alpha|^2 \tag{2.2.18}$$

To calculate the variance of the photon number operator $\Delta^2\hat{n}$, we also calculate

$$\begin{aligned}\langle\hat{n}^2\rangle &= \langle\alpha|\hat{a}^\dagger\hat{a}\hat{a}^\dagger\hat{a}|\alpha\rangle \\ &= \langle\alpha|(\hat{a}^\dagger\hat{a}^\dagger\hat{a}\hat{a} - \hat{a}^\dagger\hat{a})|\alpha\rangle \\ &= |\alpha|^4 + |\alpha|^2,\end{aligned} \tag{2.2.19}$$

here we used Eq.(2.1.11). Thus we can obtain $\Delta^2\hat{n}$ of a coherent state as

$$\Delta^2\hat{n} = \langle\hat{n}^2\rangle - \langle\hat{n}\rangle^2 = |\alpha|^2. \tag{2.2.20}$$

Then we calculate the mean and variance of quadrature amplitude.

$$\langle\hat{X}^0\rangle = \langle\alpha|\hat{X}^0|\alpha\rangle = \langle\alpha|(\hat{a}^\dagger + \hat{a})|\alpha\rangle = \alpha + \alpha^* \tag{2.2.21}$$

$$\langle\hat{X}^{\frac{\pi}{2}}\rangle = \langle\alpha|\hat{X}^{\frac{\pi}{2}}|\alpha\rangle = \langle\alpha|i(\hat{a}^\dagger + \hat{a})|\alpha\rangle = i(\alpha + \alpha^*) \tag{2.2.22}$$

$$\Delta^2\hat{X}^0 = \langle(\hat{X}^0)^2\rangle - \langle\hat{X}^0\rangle^2 = 1 \tag{2.2.23}$$

$$\Delta^2\hat{X}^{\frac{\pi}{2}} = \langle(\hat{X}^{\frac{\pi}{2}})^2\rangle - \langle\hat{X}^{\frac{\pi}{2}}\rangle^2 = 1. \tag{2.2.24}$$

At last we look at the probability of the detecting n photon. Using the Eq.(2.2.16), we obtain

$$P_n = |\langle n|\alpha\rangle|^2 = e^{-|\alpha|^2}\frac{|\alpha|^{2n}}{n!} \tag{2.2.25}$$

Obviously, the probability of finding n photons for a coherent state is given by the Poisson distribution Eq.(2.2.24). In Fig.2.3 we give some the photon number probability distributions in a coherent state with different amplitudes. From Fig. 2.3, we can see that when the amplitude $|\alpha|$ is large, such as $|\alpha| = 2$, the photons have apparent probability distributions. When $|\alpha|$ decreases, such as $|\alpha| = 0.5$, the probability of $|1\rangle$ and $|2\rangle$ become $P(1) = 0.14$ and $P(2) = 0.011$, respectively. While the probability of $|3\rangle$ becomes $P(3) = 0.0006$ which can be ignored compared to $P(2)$. It can be used as one of interference sources to perform the two-photon interference in this thesis.

2.2.3 Squeezed vacuum state

Different from coherent states, the squeezed vacuum states are another member of the family of the minimum uncertainly states which take on unequal variances for the amplitude and phase quadratures. The variances of one quadrature of squeezed states are squeezed by cost of the increasing of the variances at the other quadrature.

Squeezed vacuum state is generated by applying the unitary squeezing operator on a vacuum state.

$$|\zeta\rangle = \hat{S}(\zeta)|0\rangle. \tag{2.2.26}$$

where $\hat{S}(\zeta)$ is defined as

$$\hat{S}(\zeta) = \exp(\frac{1}{2}\zeta^*\hat{a}^2 - \frac{1}{2}\zeta(\hat{a}^\dagger)^2). \tag{2.2.27}$$

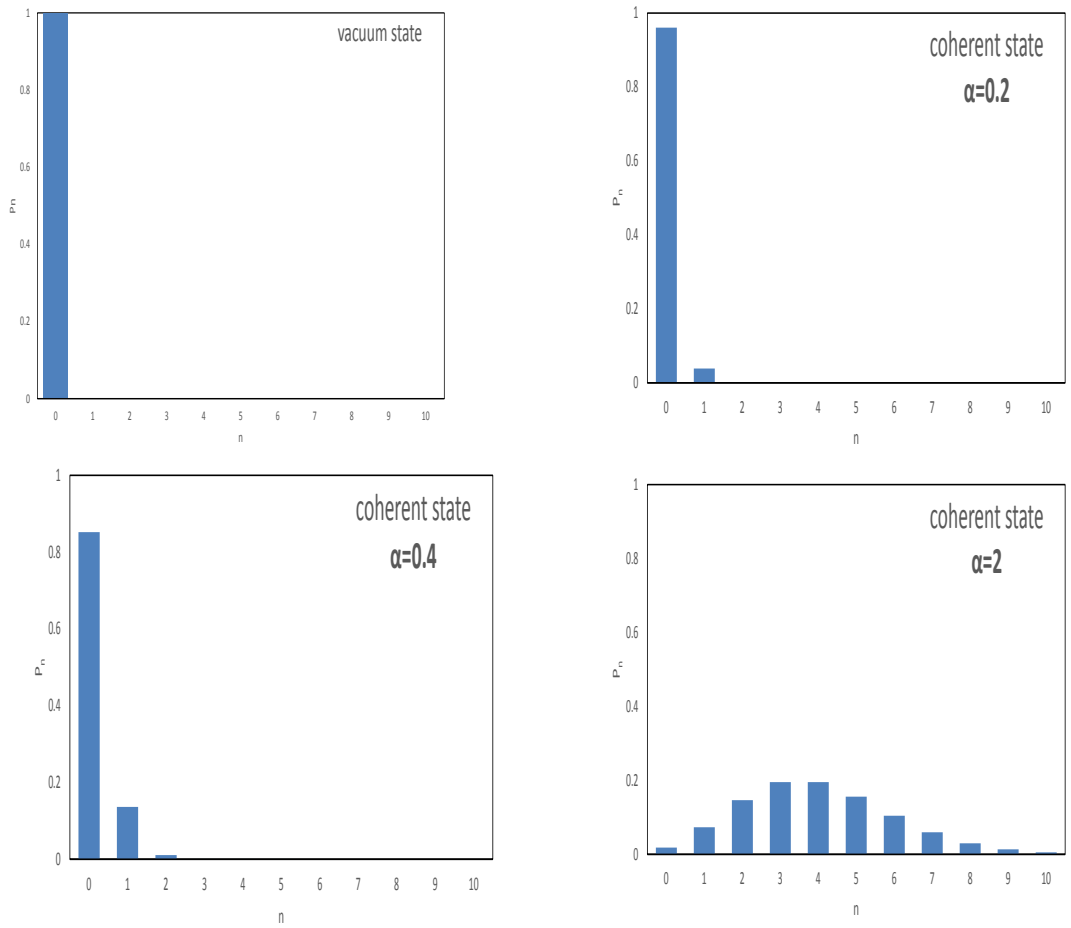

Fig. 2.3. photon number probability distribution of coherent state with different amplitudes.

where $\zeta = r\exp(i\varphi)$ and $r \in R$. The squeezing operator $\hat{S}(\zeta)$ satisfies

$$\hat{S}^{\dagger}(\zeta) = \hat{S}^{-1}(\zeta) = \hat{S}(-\zeta), \tag{2.2.28}$$

$$\hat{S}^{\dagger}(\zeta)\hat{a}\hat{S}(\zeta) = \hat{a}\cosh r - \hat{a}^{\dagger}\exp(i\varphi)\sinh r, \tag{2.2.29}$$

$$\hat{S}^{\dagger}(\zeta)\hat{a}^{\dagger}\hat{S}(\zeta) = \hat{a}^{\dagger}\cosh r - \hat{a}\exp(-i\varphi)\sinh r. \tag{2.2.30}$$

A squeezed vacuum state of light is shown in Fig. 2.4.

For a squeezed vacuum state, the mean of photon number operator is

$$\langle\hat{n}\rangle = \langle\zeta|\hat{n}|\zeta\rangle = \sinh^2 r. \tag{2.2.31}$$

And the variance of the quadrature is found to be

$$\Delta^2\hat{X}^0 = e^{(2r)}\sin^2(\varphi/2) + e^{(-2r)}\cos^2(\varphi/2) \tag{2.2.32}$$

$$\Delta^2\hat{X}^{\frac{\pi}{2}} = e^{(2r)}\cos^2(\varphi/2) + e^{(-2r)}\sin^2(\varphi/2) \tag{2.2.33}$$

For $\varphi = 0$, these reduce to

$$\Delta^2\hat{X}^0 = e^{-2r}, \tag{2.2.34}$$

$$\Delta^2\hat{X}^{\frac{\pi}{2}} = e^{2r}. \tag{2.2.35}$$

The corresponding uncertainty relation is

$$\Delta^2\hat{X}^0\Delta^2\hat{X}^{\frac{\pi}{2}} = 1. \tag{2.2.36}$$

It implies the minimum uncertainty state which may reduce in one quadrature at the expense of increasing quadrature in the other.

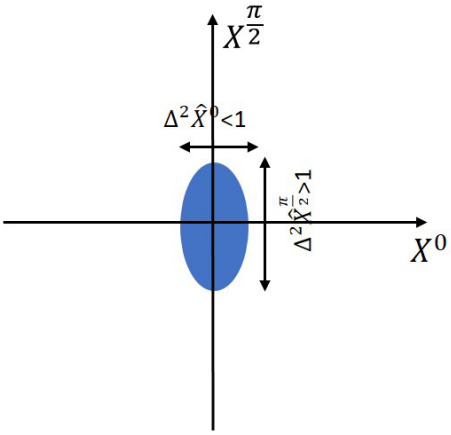

Fig. 2.4. Phase-space representation of a squeezed state.

Next, we will discuss the photon number probability of squeezed vacuum state. We start from the vacuum state.

$$\hat{a}\,|0\rangle = 0. \tag{2.2.37}$$

Since the squeezing operator $\hat{S}(\zeta)$ is unitary, we can re-write Eq.(2.2.25) as

$$\hat{S}(\zeta)\hat{a}\hat{S}^{\dagger}(\zeta)\,|\zeta\rangle = 0. \tag{2.2.38}$$

Using Eq.(2.2.28), the Eq.(2.2.37) can be re-expressed as

$$(\hat{a}\mu + \hat{a}^{\dagger}\nu)\,|\zeta\rangle = 0 \tag{2.2.39}$$

where $\mu = \cosh r$ and $\nu = e^{i\varphi}\sinh r$. We also can expand the squeezed vacuum state as

$$|\zeta\rangle = \sum_{n=0}^{\infty} C_n\,|n\rangle \tag{2.2.40}$$

Insert Eq.(2.2.38) into Eq.(2.2.39), the coefficients of left side of Eq.(2.2.39) satisfy the relation,

$$C_{n+1} = -\frac{\nu}{\mu}\Big(\frac{n}{n+1}\Big)^{\frac{1}{2}} C_{n-1}. \tag{2.2.41}$$

Obviously, the relation connects every even-photon state or every odd-photon state. So there are two solutions to this relation. Since only the even solution contains the vacuum, we only consider the amplitude probability of even-photon state.

$$C_{2m} = (-1)^m(\mathrm{e}^{i\varphi})^m[\frac{(2m-1)!!}{(2m)!!}]^{\frac{1}{2}} C_0, \tag{2.2.42}$$

where the coefficients satisfy

$$\sum_{m=0}^{\infty} |C_{2m}|^2 = \sum_{m=0}^{\infty} C_{2m} C_{2m}^* = 1. \tag{2.2.43}$$

Insert the Eq.(2.2.40) into Eq.(2.2.41), we can obtain

$$|C_0|^2 [1 + \sum_{m=0}^{\infty} \frac{\tanh^2 r m (2m-1)!!}{(2m)!!}] = 1. \tag{2.2.44}$$

Using a mathematical identity

$$1 + \sum_{m=0}^{\infty} x^m [\frac{(2m-1)!!}{(2m)!!}] = (1-x)^{\frac{1}{2}}, \tag{2.2.45}$$

Compare Eq.(2.2.42) and Eq.(2.2.43), we can re-write the Eq.(2.2.43) as

$$|C_0|^2 [1 - \tanh^2 r]^{-\frac{1}{2}} = 1, \tag{2.2.46}$$

we can easily obtain

$$C_0 = \sqrt{\cosh r}, \tag{2.2.47}$$

And then we use the identities

$$(2m)!! = 2^m m!, \tag{2.2.48}$$

$$(2m-1)!! = (2m)!/2^m m!. \tag{2.2.49}$$

Thus we can calculate the coefficients for the even-photon state as

$$C_{2m} = (-1)^m \frac{\sqrt{(2m)!}}{2^m m!} \frac{(\mathrm{e}^{i\varphi} \tanh r)^m}{\sqrt{\cosh r}}, \tag{2.2.50}$$

and the squeezed vacuum state is re-written as

$$|\zeta\rangle = \frac{1}{\sqrt{\cosh r}} \sum_{m=0}^{\infty} \frac{\sqrt{(2m)!}}{m!} (-\frac{\mathrm{e}^{i\varphi} \tanh r}{2})^m |2m\rangle . \tag{2.2.51}$$

The probability of even-photon state is

$$P(2m) = |C_{2m}|^2 = \frac{(2m)!}{(\cosh r)(m!)^2} (\frac{\tanh r}{2})^{2m} \tag{2.2.52}$$

while the probability of odd-photon state is

$$P(2m+1) = 0. \tag{2.2.53}$$

From Eq.(2.2.51) and Eq.(2.2.52), we can find the photon number probability of a squeezed vacuum state is oscillatory. For all odd-photon state, the probability becomes zero. Choosing

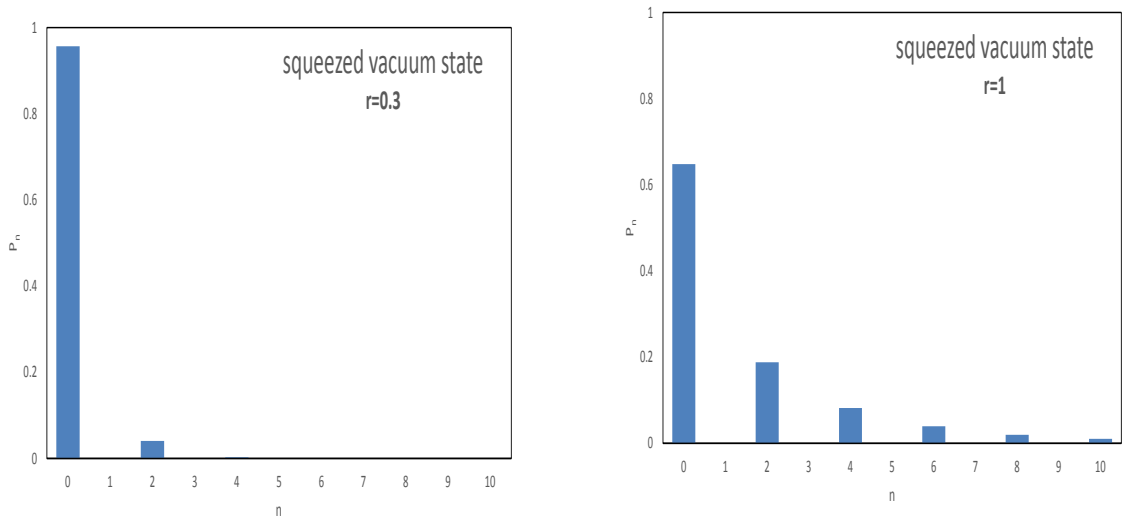

Fig. 2.5. photon number probability distribution of squeezed vacuum state.

different squeezing parameter r, the corresponding photon number probability distribution are shown in Fig.2.5.

From Fig. 2.5, we can also find that when the squeezing parameter is large, such as $r = 1$, the probability of $|2\rangle, |4\rangle, |6\rangle$ and $|8\rangle$ in the the squeezed state all have larger values, while as the squeezing parameter decreases, the probability of the $|4\rangle, |6\rangle$ and $|8\rangle$ decrease. Such as when $r = 0.3$, the probability of the $|2\rangle$ becomes $P(2) = 0.04$, while $P(4) = 0.0025$ and $P(6) = 0.0002$ which can be ignored compared to $P(2)$, and such a squeezed vacuum state can be regarded as a two-photon state.

2.2.4 Displaced squeezed state

The squeezed vacuum state can be displaced in similar to the way that the vacuum state displaced to form the coherent state.The effect is shown in Fig.2.6 using phasor diagram. Acting the displacement operator and squeezing operator on a vacuum state,

$$|\alpha, \zeta\rangle = \hat{D}(\alpha)\hat{S}(\zeta)|0\rangle. \tag{2.2.54}$$

The $\hat{S}(\zeta)$ and $\hat{D}(\alpha)$ satisfy,

$$\hat{D}^\dagger(\alpha)\hat{S}^\dagger(\zeta)\hat{a}\hat{S}(\zeta)\hat{D}(\alpha) = \hat{a}\cosh r - \hat{a}^\dagger \exp(i\varphi)\sinh r + \alpha, \tag{2.2.55}$$

$$\hat{D}^\dagger(\alpha)\hat{S}^\dagger(\zeta)\hat{a}^\dagger\hat{S}(\zeta)\hat{D}(\alpha) = \hat{a}^\dagger \cosh r - \hat{a}\exp(-i\varphi)\sinh r + \alpha^*. \tag{2.2.56}$$

The displaced squeezed states are another member of the family of the minimum uncertainly states which take on unequal variances for the amplitude and phase quadratures. Then we also discuss the photon number probability distribution of displaced squeezed state. Similar to

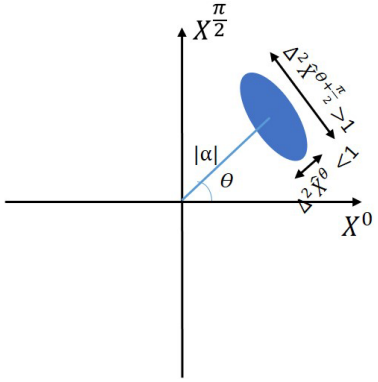

Fig. 2.6. Phase-space representation of a displaced squeezed state.

coherent state and squeezed vacuum state, the displaced squeezed state can also be expanded to

$$\begin{aligned}|\alpha,\zeta\rangle &= \sum_{n=0}^{\infty} C_n\,|n\rangle \\ &= \frac{1}{\sqrt{\cosh r}}\exp\{-\frac{|\alpha|^2}{2}-\frac{1}{4}\tanh r[(\alpha^*)^2\mathrm{e}^{i\varphi}+\alpha^2\mathrm{e}^{-i\varphi}]\}\times\sum_{n=0}^{\infty}\frac{(\frac{1}{2}\tanh r)^{n/2}}{\sqrt{n!}}H_n(z)\,|n\rangle\,,\end{aligned} \tag{2.2.57}$$

where $H_n(z)$ is the Hermite polynomial, and z can be described as

$$z=\frac{\alpha+\alpha^*\mathrm{e}^{i\varphi}\tanh r}{\sqrt{2\mathrm{e}^{i\varphi}\tanh r}}. \tag{2.2.58}$$

The probability of n-photon state is given as

$$P(n)=\frac{1}{2^n n!\cosh r}\Big(\tanh r\Big)^n\exp\{-|\alpha|^2-\frac{1}{2}\tanh r[(\alpha^*)^2\mathrm{e}^{i\varphi}+\alpha^2\mathrm{e}^{-i\varphi}]\}|H_n(z)|^2. \tag{2.2.59}$$

$$=\frac{1}{2^n n!\cosh r}\Big(\tanh r\Big)^n\times\exp\{-|\alpha|^2-\frac{1}{2}\tanh r[(|\alpha|^2\mathrm{e}^{-i(2\theta-\varphi)}+|\alpha|^2\mathrm{e}^{i(2\theta-\varphi)}]\}|H_n(z)|^2, \tag{2.2.60}$$

where $\alpha=|\alpha|e^{i\theta}$, and $2\theta-\varphi=0$ and $2\theta-\varphi=\pi$ correspond to displaced amplitude squeezed state and displaced phase squeezed state, respectively. The Fig.2.6 shows the photon probability distribution of two different displaced squeezed states for squeezing parameter $|r|=0.09$ and displacement $|\alpha|=0.3$ and coherent state with $|\alpha|=0.3$. From Fig.2.6, for the probability of $|1\rangle$ $(P(1))$, we can find that $P_{ASS}(1)$ is lager than that of the coherent state $P_{COH}(1)$, while $P_{PSS}(1)$ is smaller $P_{COH}(1)$. One the other hand, for the probability of $|2\rangle$, we obtain opposite results. Hence, the displaced squeezed states can be regarded as the result states of the two-photon interference between a squeezed vacuum state and a coherent state. The displaced amplitude squeezed state comes from destructive two-photon interference in which the two-photon state $|2\rangle$ are suppressed and the single-photon state $|1\rangle$ are increased. The displaced phase squeezed state comes from constructive two-photon interference in which the two-photon state $|2\rangle$ are increased

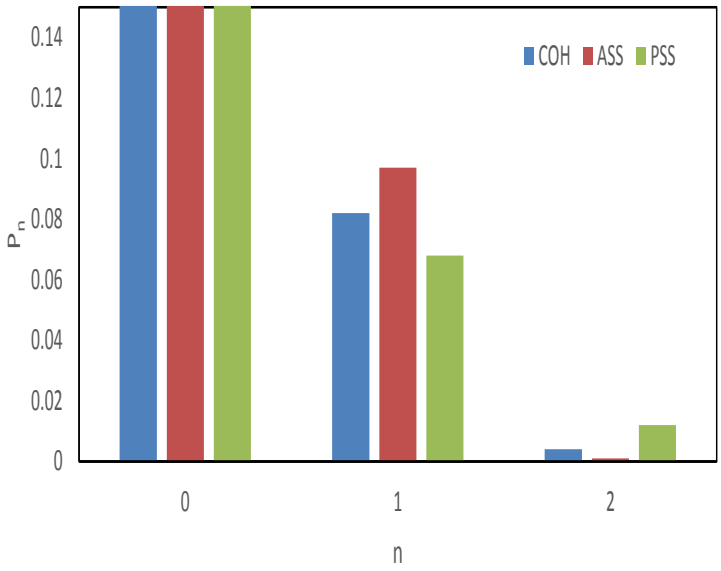

Fig. 2.7. photon number probability of displaced squeezed state and coherent state. COH: coherent state, ASS: displaced amplitude squeezed state, PSS: displaced phase squeezed state.

and the single-photon state $|1\rangle$ are suppressed. The other properties of displaced squeezed state are listed in Table 2.1.

Since the displaced squeezed states can be regarded as the results of the two-photon interference between squeezed vacuum state and coherent state, especially the probability of the two-photon state, we will discuss it in section 2.6 in detail.

Table 2.1. properties of quantum states.

	Number state	Coherent state	Squeezed vacuum state	Displaced squeezed state
State vector	$\|n\rangle = \hat{N}(n)\|0\rangle$ $\hat{N}(n) = \frac{(\hat{a}^\dagger)^n}{\sqrt{n!}}$, where $n = 0, 1, 2, 3....$	$\|\alpha\rangle = \hat{D}(\alpha)\|0\rangle$ $\hat{D}(a) = \exp(\alpha\hat{a}^\dagger - \alpha^*\hat{a})$ where $\alpha = \|\alpha\| \exp i\theta$	$\|\zeta\rangle = \hat{S}(\zeta)\|0\rangle$ $\hat{S}(\zeta) = \exp(\frac{1}{2}\zeta^*\hat{a}^2 - \frac{1}{2}\zeta(\hat{a}^\dagger)^2)$ where $\zeta = r\exp(i\varphi)$	$\|\alpha, \zeta\rangle = \hat{D}(\alpha)\hat{S}(\zeta)\|0\rangle$ $\hat{D}(a) = \exp(\alpha\hat{a}^\dagger - \alpha^*\hat{a})$ $\hat{S}(\zeta) = \exp(\frac{1}{2}\zeta^*\hat{a}^2 - \frac{1}{2}\zeta(\hat{a}^\dagger)^2)$
$\langle\hat{n}\rangle$	n	$\|\alpha\|^2$	$\sinh^2 r$	$\|\alpha\|^2 + \sinh^2 r$
$\Delta^2(\hat{n})$	0	$\|\alpha\|^2$	$2(\sinh^2 r + 1)\sinh^2 r$	$\|\alpha\|^2[e^{2r}\sin^2(\theta - \frac{\varphi}{2}) + e^{-2r}\cos^2(\theta - \frac{\varphi}{2})] + 2(\sinh^2 r + 1)\sinh^2 r$
$\langle\hat{X}^0\rangle$	0	$2\|\alpha\|\cos\theta$	0	$2\|\alpha\|\cos\theta$
$\langle\hat{X}^{\frac{\pi}{2}}\rangle$	0	$2\|\alpha\|\sin\theta$	0	$2\|\alpha\|\sin\theta$
$\Delta^2(\hat{X}^0)$	$2(n + \frac{1}{2})$	1	$e^{(2r)}\sin^2(\varphi/2) + e^{(-2r)}\cos^2(\varphi/2)$	$e^{(2r)}\sin^2(\theta - \varphi/2) + e^{(-2r)}\cos^2(\theta - \varphi/2)$
$\Delta^2(\hat{X}^{\frac{\pi}{2}})$	$2(n + \frac{1}{2})$	1	$e^{(2r)}\cos^2(\varphi/2) + e^{(-2r)}\sin^2(\varphi/2)$	$e^{(2r)}\cos^2(\theta - \varphi/2) + e^{(-2r)}\sin^2(\theta - \varphi/2)$
P_n	1	$\exp(-\\|\alpha\|^2)\\|\alpha\|^{2n}/2$	$P_{2m} = \frac{(\mathrm{sech}\, r)(2m)!}{(m!)^2}(\frac{\tanh r}{2})^{2m}$, $P_{2m+1} = 0$, where $m = 0, 1, 2, 3.....$	$\frac{(\frac{1}{2}\tanh r)^n \exp\{-\\|\alpha\|^2 - \frac{1}{2}\tanh r[(\alpha^*)^2 e^{i\varphi}]\}\\|H_n(z)\|^2}{n!\cosh r}$, where $z = \frac{\alpha + \alpha^* e^{i\varphi}\tanh r}{\sqrt{2e^{i\varphi}\tanh r}}$ and $H_n(z)$ are the Hermite polynomials
$g^{(2)}(0)$	$1 - \frac{1}{n}$, where $n \geq 1$	1	$3 + \frac{1}{\sinh^2 r}$	$1 + [\|\alpha\|^2 + \sinh^2(r)]^{-2}\{\|\alpha\|^2[e^{2r}\sin^2(\theta - \frac{\varphi}{2}) + e^{-2r}\cos^2(\theta - \frac{\varphi}{2}) + \sinh^2 r\cosh 2r - \|\alpha\|^2\}$

$\langle n\rangle$: Mean of photon number, $\Delta^2(\hat{n})$: Variance of photon number, $\langle\hat{X}^0\rangle$:Mean of amplitude quadrature, $\langle\hat{X}^{\frac{\pi}{2}}\rangle$:Mean of phase quadrature, $\Delta^2(\hat{X}^0)$: Variance of amplitude quadrature. $\Delta^2(\hat{X}^{\frac{\pi}{2}})$:Variance of phase quadrature, P_n: Probability of n photons, $g^{(2)}(0)$: second-order correlation function

2.3 Detection of squeezed state of light

Since a single photodetector is only able to measure fluctuations in the intensity or in the number of photons, it is not a suitable detector to characterize a squeezed state. For a more accurate description of a squeezed state, the least the squeezing and anti-squeezing level should be measured to be able to derive the purity of the state, or quantum state tomography can be down, which requires the measurement of a great number of consecutive quadratures. An appropriate measurement technique is homodyne detection.

2.3.1 Balanced homodyne detection

The observation of quantum noise of generated state is performed by a balanced homodyne detector which is the most adequate detection scheme since both the amplitude and phase quadrature of the generated state can be measured [39–42]. The detection principle is shown in Fig. 2.7, a weak signal beam $\hat{a}$ combines with a strong local oscillator (LO) beam $\hat{a}_{LO}$ on a 50:50 beam splitter. The signal and the local oscillator have a relative phase θ which is normally adjusted by controlling the path length of the local oscillator beam. The power of local oscillator is much stronger than the signal power. Each output light $\hat{c}$ and $\hat{d}$ is detected with a photodiode and finally the difference of two photocurrents is taken.

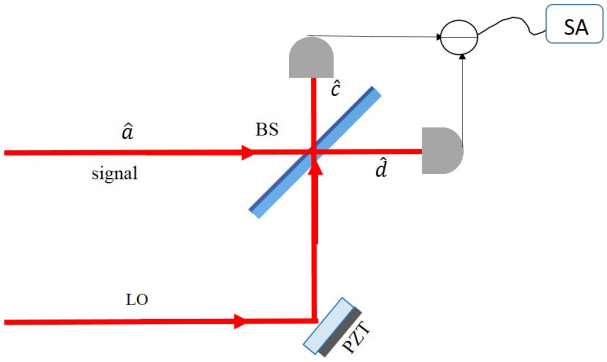

Fig. 2.8. Schematic of a homodyne detection scheme.

The output states of beam splitter can be expressed in terms of their input states via

$$\hat{c}(t) = \frac{\hat{a}(t) + e^{i\theta}\hat{a}_{LO}(t)}{\sqrt{2}}, \tag{2.3.1}$$

$$\hat{d}(t) = \frac{\hat{a}(t) - e^{i\theta}\hat{a}_{LO}(t)}{\sqrt{2}}, \tag{2.3.2}$$

The output beams are detected by two detectors and transformed into photocurrents. The

difference between the output photocurrents from two detectors can be written as

$$\begin{aligned}\hat{i}_-(t) &= \hat{i}_c - \hat{i}_d \\ &= \eta[\hat{c}^\dagger(t)\hat{c}(t) - \hat{d}^\dagger(t)\hat{d}(t)] \\ &= \frac{1}{2}\eta[e^{i\theta}\hat{a}^\dagger(t)\hat{a}_{LO}(t) + e^{-i\theta}\hat{a}^\dagger_{LO}(t)\hat{a}(t)],\end{aligned} \tag{2.3.3}$$

where η is the detection efficiency. Since the LO beam is far stronger than the signal beam, so that we can treat the local oscillator wave classically, the operator $\hat{a}^\dagger_{LO}(t)$ and $\hat{a}_{LO}(t)$ is replaced by $|a_{LO}(t)|$, and the current difference is re-written as we can obtain the noise variance by measuring the photocurrent from the subtractor,

$$\hat{i}_-(t) = \frac{1}{2}\eta|a_{LO}(t)|[e^{i\theta}\hat{a}^\dagger(t) + e^{-i\theta}\hat{a}(t)]. \tag{2.3.4}$$

Inserting $\hat{a} = \frac{\hat{X}^0 + i\hat{X}^{\frac{\pi}{2}}}{2}$ and $\hat{a}^\dagger = \frac{\hat{X}^0 - i\hat{X}^{\frac{\pi}{2}}}{2}$ into Eq. (2.3.4), we obtain

$$\hat{i}_-(t) = \frac{1}{2}\eta|a_{LO}(t)|[\hat{X}^0(t)\cos\theta + \hat{X}^{\frac{\pi}{2}}\sin\theta]. \tag{2.3.5}$$

Equation (2.3.5)simply tells us that the measurement of the difference current $\hat{i}_-(t)$ is equivalent to the measurement of the θ quadrature amplitude. If we change relative phase θ, we can measure any quadrature amplitude.

What a spectrum analyzer can measure is the noise equivalent power of the photocurrent $\hat{i}_-(t)$, such as the variance $\Delta^2\hat{i}_-(\Omega)$.

$$\Delta^2\hat{i}_-(t) = \frac{1}{4}\eta^2|a_{LO}(t)|^2[\Delta^2\hat{X}^0(t)\cos^2\theta + \Delta^2\hat{X}^{\frac{\pi}{2}}\sin^2\theta]. \tag{2.3.6}$$

Obviously, the variances of the amplitude and phase quadratures of the signal beam can be measured. Especially, when $\theta = 0$, the variances of amplitude quadrature of the signal beam is measured, while $\theta = \pi/2$, the variances of phase quadrature is detected.

2.3.2 Sideband modulation field in quantum optics

An amplitude modulation (AM) or phase modulation (PM) signal can be produced on the light beam by applying a coherent excitation to its upper and lower sidebands [43]. In experiments, we can produce the coherent state at the upper and lower sidebands ($\omega_0 \pm \Omega$) of the central frequency ω_0 by modulating the laser light. In this section, we will introduce amplitude modulation and phase modulation at frequency Ω relative to the central frequency ω_0, respectively.

A beam of light is amplitude modulated by a modulation index M at modulation frequency Ω can be written as

$$\begin{aligned}a_{am}(t) &= a_0(1 + M\cos(\Omega t))\exp(i\omega_0 t) \\ &= a_0[1 + \frac{M}{2}(\exp(i\Omega t) + \exp(-i\Omega t)]\exp(i\omega_0 t) \\ &= a_0\{\exp(i\omega_0 t) + \frac{M}{2}\exp[i(\omega_0 + \Omega)t] + \frac{M}{2}\exp[i(\omega_0 - \Omega)t]\}.\end{aligned} \tag{2.3.7}$$

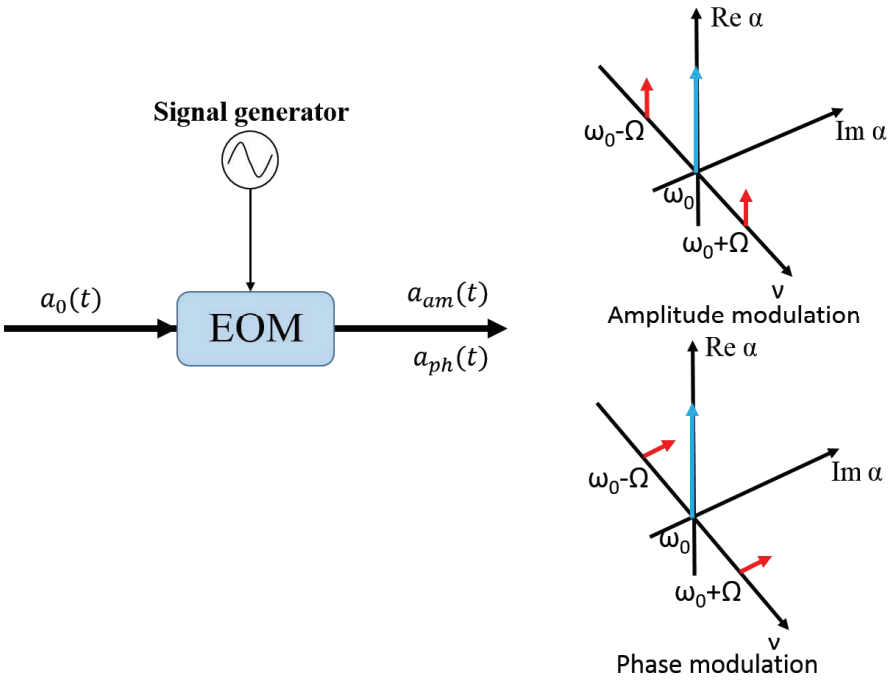

Fig. 2.9. Amplitude and phase modulation with the sideband frequency Ω.

here a_0 is complex. We can see that the effect of the amplitude modulation is to create two modulation sidebands at $\omega_0 - \Omega$ and $\omega_0 + \Omega$.

Similarly, a light beam with phase modulation can be described as

$$\begin{aligned}
a_{pm}(t) &= a_0 \exp\left[iM\cos\left(\Omega t\right)\right]\exp\left(i\omega_0 t\right) \\
&= a_0[1 + iM\cos\left(\Omega t\right) - \frac{M^2}{2}\cos^2\left(\Omega t\right) + \cdots]\exp\left(i\omega_0 t\right) \\
&= a_0\{1 + \frac{iM}{2}[\exp\left(i\Omega t\right) + \exp\left(-i\Omega t\right)] - \frac{M^2}{8}[\exp\left(i2\Omega t\right) + \exp\left(-i2\Omega t\right) + 2] + \cdots\}\exp\left(i\omega_0 t\right) \\
&= a_0[(1 - \frac{M^2}{4} + \cdots)\exp\left(i\omega_0 t\right) + i(\frac{M}{2} + \cdots)(\exp\left[i(\omega_0 + \Omega)t\right] + \exp\left[i(\omega_0 - \Omega)t\right]) \\
&- (\frac{M^2}{8} + \cdots)(\exp\left[i(\omega_0 + 2\Omega)t\right] + \exp\left[i(\omega_0 - 2\Omega)t\right]) + \cdots], \qquad (2.3.8)
\end{aligned}$$

we assume the modulation depth is small with $M \ll 1$, the phase modulated light is approximately

$$a_{pm}(t) \approx a_0 \exp\left(i\omega_0 t\right) + i\frac{M}{2}a_0 \exp\left[i(\omega_0 + \Omega)t\right] + i\frac{M}{2}a_0 \exp\left[i(\omega_0 - \Omega)t\right]. \qquad (2.3.9)$$

The sidebands will only provide on measurements of the phase quadrature. It is the phase of the sidebands with respect to the carrier that distinguishes amplitude modulation from phase modulation. Fig. 2.9 shows the amplitude modulation and phase modulation, respectively.

Quantum noise can be understood as sidebands due to the vacuum fluctuations of signals beating local oscillator with a carrier frequency. Thus the sidebands are a consequence of the zero-point energy of harmonic oscillator, and the quantum noise can be regarded as a continuum of sidebands spanning all frequencies. All sidebands are uncorrelated with each other, and the quantum noise is distributed equally between the amplitude quadrature and phase quadrature.

2.4 Second-order correlation function and two-photon interference

In quantum optics, correlation functions are used to characterize the coherence propertied of a light field [32,33,36]. For example, a first-order correlation function $g^{(1)}(t)$ is used to quantify the coherence of a light field. A second-order correlation function is used to quantify the non-classical nature of a light field. It is also used to distinguish a quantum interference from a classical optical interference.

In this section, we will briefly introduce second-order correlation function and the relationship between it and two-photon interference. We will begin with a review of the notions of classical first-order correlation function and first-order coherence from a simple case, Young's double-slit interference experiment.

2.4.1 First-order correlation function

Classical optical interference experiments correspond to a measurement of the first-order correlation function. In this section, we will introduce the first-order correlation from Young's double-slit interference.

As shown in Fig. 2.10, we use $E(t_1)$ and $E(t_2)$ to describe two electric fields (S_A, S_B) which pass through the two slits, respectively. Thus the electric field at position P can be written as a linear superposition of fields.

$$E(t) = E(r_1, t_1) + E(r_2, t_2), \tag{2.4.1}$$

The intensity of light is given by

$$I(r) = \langle |E(r,t)|^2 \rangle = \langle E^*(r,t)E(r,t) \rangle, \tag{2.4.2}$$

Inserting Eq. (2.4.1) into Eq. (2.4.2) , we can obtain

$$I_P(r_1, r_2) = \langle |E(r_1, t_1)|^2 \rangle + \langle |E(r_2, t_2)|^2 \rangle + 2Re[\langle E^*(r_1, t_1)E(r_2, t_2) \rangle]. \tag{2.4.3}$$

Obviously, we can find the first term and the second term are the intensities related with the field from two slits, while the third term is a cross term which relates to the coherence of the light field.

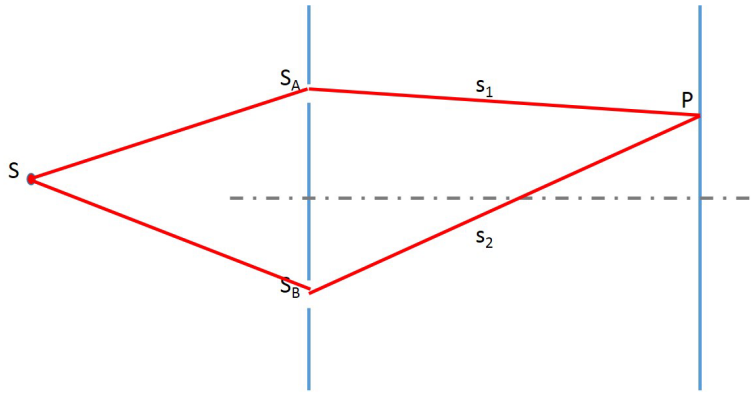

Fig. 2.10. Sketch of the Young's double-slit interference experiment.

We define the first-order correlation function of field from S as

$$g^{(1)}(r_1, r_2) = \frac{\langle E^*(r_1)E(r_2)\rangle}{\sqrt{\langle|E(r_1)|\rangle\langle|E(r_2)|\rangle}}. \tag{2.4.4}$$

Thus we can write the intensity measured at P in terms of component intensities plus a coherence term:

$$I_P(t) = I(r_1) + I(r_2) + 2\sqrt{I(r_1)I(r_2)}Re[g^{(1)}(r_1, r_2)]. \tag{2.4.5}$$

Thus when $|g^{(1)}(r_1, r_2)| = 1$, the two light fields are complete coherence which indicates complete interference occurs. When $0 < |g^{(1)}(r_1, r_2)| < 1$ indicates partial coherence and partial interference. While $|g^{(1)}(r_1, r_2)| = 0$ exhibits complete incoherence and there is no interference occurs.

2.4.2 Second-order correlation function

In 1956, Hanbury-Brown-Twiss (HBT) extended an optical intensity interferometer to second-order coherence of light [32, 36]. Later the coherence was further generalized to nth-order by Glauber in a comprehensive quantum theory of optical coherence [33].The HBT experiment gave a new method on optical interference. In this section, we will introduce the second-order correlation function from the HBT experiment.

The scheme setup of HBT interferometer is shown in Fig. 2.11. A input mode $\hat{a}$ is split by a 50:50 beam splitter, each output is detected by a photo-detector. The setup measures a delayed intensity correlation between the two detectors register intensity at time t_1 and $t_2 = t_1 + \tau$, respectively. The intensity correlation is proportional to the time average, namely,

$$I(t, t+\tau) \propto \langle I(t)I(t+\tau)\rangle, \tag{2.4.6}$$

in which $I(t)$ and $I(t+\tau)$ are the intensities at the two detectors. Consider a stationary wave field, if the average of the intensity at each detector is $I(t)$, the second-order correlation function

with time delay τ is defined as

$$g^{(2)}(\tau) = \frac{\langle I(t)I(t+\tau)\rangle}{\langle I(t)\rangle\langle I(t+\tau)\rangle}. \tag{2.4.7}$$

For a stationary wave, the average of the intensity is independent with time delay τ, namely, $\langle I(t)\rangle = \langle I(t+\tau)\rangle$. Thus, the Eq. (2.4.7) can be re-written as

$$g^{(2)}(\tau) = \frac{\langle I(t)I(t+\tau)\rangle}{\langle I(t)\rangle^2}. \tag{2.4.8}$$

The second-order correlation function is limited by classical bounds $1 \leq g^{(2)}(\tau) \leq \infty$.

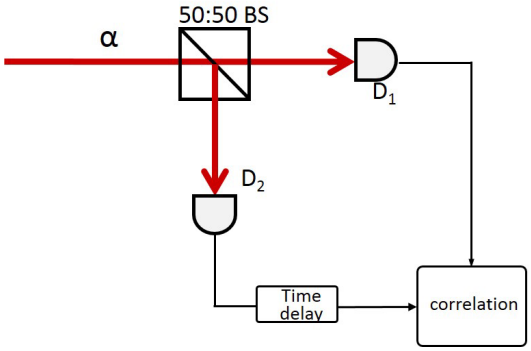

Fig. 2.11. Scheme of setup for Hanbury-Brown-Twiss experiment.

Equation (2.4.8) is a classical second-order correlation function. When the second-order correlation function is expressed in the quantum theory of light, the intensities become normally-ordered products of the creation ($\hat{a}^\dagger(t)$) and annihilation ($\hat{a}(t)$) operators of the input field. Here we consider a single-mode light field, the second-order correlation function can be described as

$$g^{(2)}(\tau) = \frac{\langle \hat{a}^\dagger(t+\tau)\hat{a}^\dagger(t)\hat{a}(t+\tau)\hat{a}(t)\rangle}{\langle \hat{a}^\dagger(t)\hat{a}(t)\rangle^2}. \tag{2.4.9}$$

After applying the Schwarz inequality $|\langle u, v\rangle|^2 \leq \langle u, u\rangle \langle v, v\rangle$, we can find that the second-order correlation function is bounded by one.

$$(1) \quad g^{(2)}(0) > 1, \quad \text{classical field, non-classical field, bunching effect,} \tag{2.4.10}$$

$$(2) \quad g^{(2)}(0) = g^{(2)}(\tau) = 1, \quad \text{coherent state,} \tag{2.4.11}$$

$$(3) \quad g^{(2)}(0) < 1, \quad \text{non-classical field, anti-bunching effect.} \tag{2.4.12}$$

In experiments, we usually measure the $g^{(2)}(\tau)$ with zero-time delay.

$$\begin{aligned} g^{(2)}(0) &= \frac{\langle \hat{a}^\dagger\hat{a}^\dagger\hat{a}\hat{a}\rangle}{\langle \hat{a}^\dagger\hat{a}\rangle^2} \\ &= \frac{\langle \hat{n}(\hat{n}-1)\rangle}{\langle \hat{n}\rangle^2}. \\ &= \frac{\langle (\Delta\hat{n})^2\rangle - \langle \hat{n}\rangle}{\langle \hat{n}\rangle^2} + 1. \end{aligned} \tag{2.4.13}$$

From Eq. (2.4.13), we also can identify the Schwarz inequality by Poissonian statistics (super-Poissonian statistics or sub-Poissonian statistics). Table 2.2 gives the relationship between the $g^{(2)}(0)$ and photon statistics properties of a single-mode light field.

Table 2.2. Relationship between $g^{(2)}(0)$ and statistics properties of light field.

$g^{(2)}(0)$	photon distribution	statistics property	light field
$g^{(2)}(0) = 1$	Poissonian statistics	random	coherent state
$g^{(2)}(0) < 1$	sub-Poissonian statistics	anti-bunching	non-classical field
$g^{(2)}(0) > 1$	super-Poissonian statistics	bunching	classical or non-classical field

2.5 Two-photon interference between squeezed vacuum state and coherent state

2.5.1 Two-photon rate in two-photon interference

In this section, we will consider two-photon interference between an squeezed vacuum state and a weak coherent state on a beam splitter.

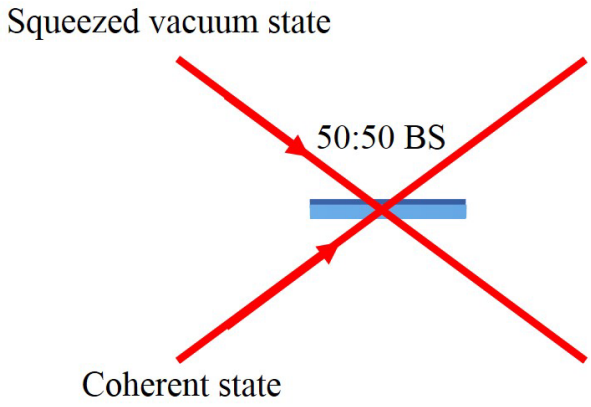

Fig. 2.12. Two-photon interference between a squeezed state and a coherent state

To understand how two-photon interference occurs, let us consider a principle scheme shown in Fig. 2.12. A coherent state and a squeezed state from the OPO are combined on a beam splitter to produce the measured field on one of its outputs. For simplicity, we only treat it with a simple single mode model and both parametric gain of the OPO and the amplitude of coherent state are not significant. It means that the average photon number of both squeezed

state and coherent sate are far less than one. Hence, the input states have the form of [44]

$$\begin{aligned} |\Psi_{in}\rangle &= |\zeta\rangle \otimes |\alpha\rangle \\ &\approx |0,0\rangle + \alpha\,|0,1\rangle + \frac{\alpha^2}{\sqrt{2}}\,|0,2\rangle - \frac{\zeta}{\sqrt{2}}\,|2,0\rangle\,, \end{aligned} \tag{2.5.1}$$

in which $|\zeta\rangle$ is a squeezed state with a complex-valued squeezing parameter ζ,

$$|\zeta\rangle \approx |0\rangle - \frac{\zeta}{\sqrt{2}}\,|2\rangle\,, \tag{2.5.2}$$

and $|\alpha\rangle$ is a coherent state with a complex amplitude α,

$$|\alpha\rangle \approx |0\rangle + \alpha\,|1\rangle + \frac{\alpha^2}{\sqrt{2}}\,|2\rangle\,, \tag{2.5.3}$$

where we neglect the contribution from more than two photons. Since the two-photon interference is independent with reflectivity of beam splitter, to simplify the system, we combine them on a 50:50 beam splitter and obtain the output of the beam splitter,

$$\begin{aligned} |\Psi_{out}\rangle = |0,0\rangle &+ \frac{\alpha}{\sqrt{2}}(|1,0\rangle + |0,1\rangle) + \frac{(\alpha^2+\zeta)}{2}|1,1\rangle \\ &+ \frac{\alpha^2-\zeta}{2\sqrt{2}}(|2,0\rangle + |0,2\rangle). \end{aligned} \tag{2.5.4}$$

We are only interested in the state from one output of the beam splitter, it can be written as

$$\begin{aligned} |\Psi_{out1}\rangle &= |0\rangle + \frac{\sqrt{2}\alpha + \alpha^2 + \zeta}{2}|1\rangle + \frac{\alpha^2-\zeta}{2\sqrt{2}}|2\rangle \\ &\approx |0\rangle + \frac{\alpha}{\sqrt{2}}|1\rangle + \frac{\alpha^2-\zeta}{2\sqrt{2}}|2\rangle. \end{aligned} \tag{2.5.5}$$

In Eq. (2.5.5), $|\alpha^2| \sim |\zeta| << |\alpha|$ is used since $|\alpha| << 1$. And the detectable two-photon rate at one arm is given by

$$\begin{aligned} R_2 &= |\frac{\alpha^2-\zeta}{2\sqrt{2}}|^2 \\ &= \frac{||\alpha|^2 \exp 2i\theta - |r|\exp i\varphi|^2}{8} \\ &= \frac{|\alpha|^4 - 2|\alpha|^2|r|\cos(2\theta-\varphi) - |r|^2}{8}, \end{aligned} \tag{2.5.6}$$

where $\zeta = |r|e^{i\varphi}$ and $\alpha = |\alpha|e^{i\theta}$. With the selection of the relative phase between the squeezed vacuum state and the coherent state, R_2 can be bigger than two-photon rate of the coherent state derived from Eq. (2.5.3) giving rise to photon bunching effect or smaller for the photon anti-bunching effect. Especially when $\alpha^2 = \zeta$, the coefficient of $|2\rangle$ is zero, and there will be no two-photon state in the output, which indicates complete destructive two-photon interference. Fig 2.13 and Fig 2.14 show the two-photon rate with the function of the amplitude of the coherent state and squeezing parameter of the squeezed vacuum state in constructive and destructive interference , respectively.

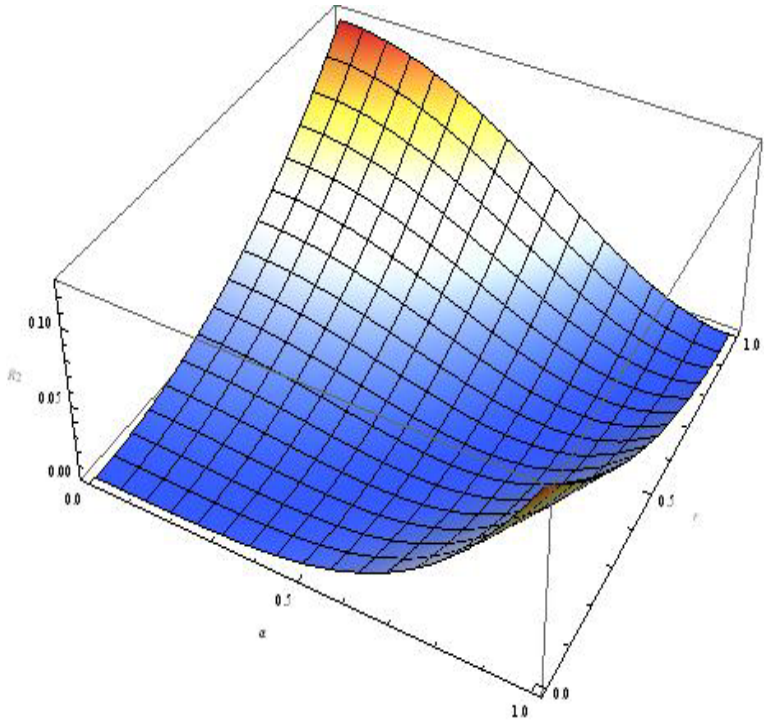

Fig. 2.13. Two-photon rate in destructive interference ($2\theta - \varphi = 0$).

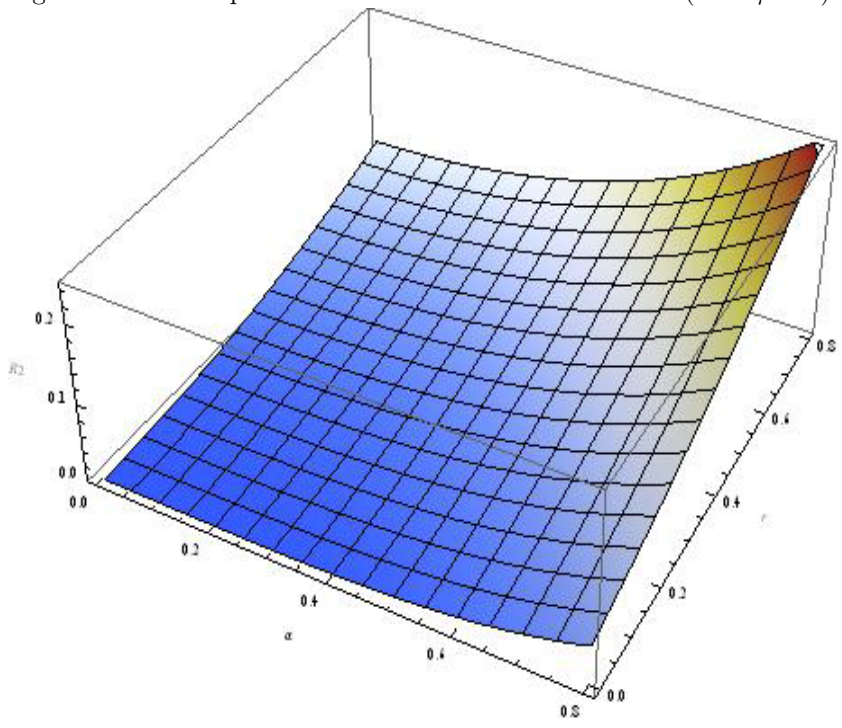

Fig. 2.14. Two-photon rate in constructive interference ($2\theta - \varphi = \pi$).

2.5.2 $g^{(2)}(0)$ in the two-photon interference

Up to now, most of experiments on two-photon interference were extensively demonstrated by directly measuring the two-photon rate with two single photon counting modules (SPCMs). Actually, we also can demonstrate the two-photon interference by calculating the second-order correlation function of the interfered field. We assume that α^2 and ζ are of the same order, the second-order correlation function of the interfered field in Eq. (2.5.5) is given as

$$\begin{aligned} g^{(2)}(0) &= \frac{\langle \Psi_{out1}|\hat{a}^\dagger\hat{a}^\dagger\hat{a}\hat{a}|\Psi_{out1}\rangle}{\langle \Psi_{out1}|\hat{a}^\dagger\hat{a}|\Psi_{out1}\rangle^2} \\ &= \frac{|\alpha^2-\zeta|^2}{|\alpha|^4} \\ &= 1-\frac{2|\alpha|^2|r|\cos(2\theta-\varphi)-|r|^2}{|\alpha|^4}, \end{aligned} \tag{2.5.7}$$

Fig. 2.15 is a plot of $g^{(2)}(0)$ for the two different phase difference ($2\theta-\varphi=0$ and $2\theta-\varphi=\pi$) with various of amplitude of coherent state α. The squeezing parameter is fixed with $|r|=0.09$.

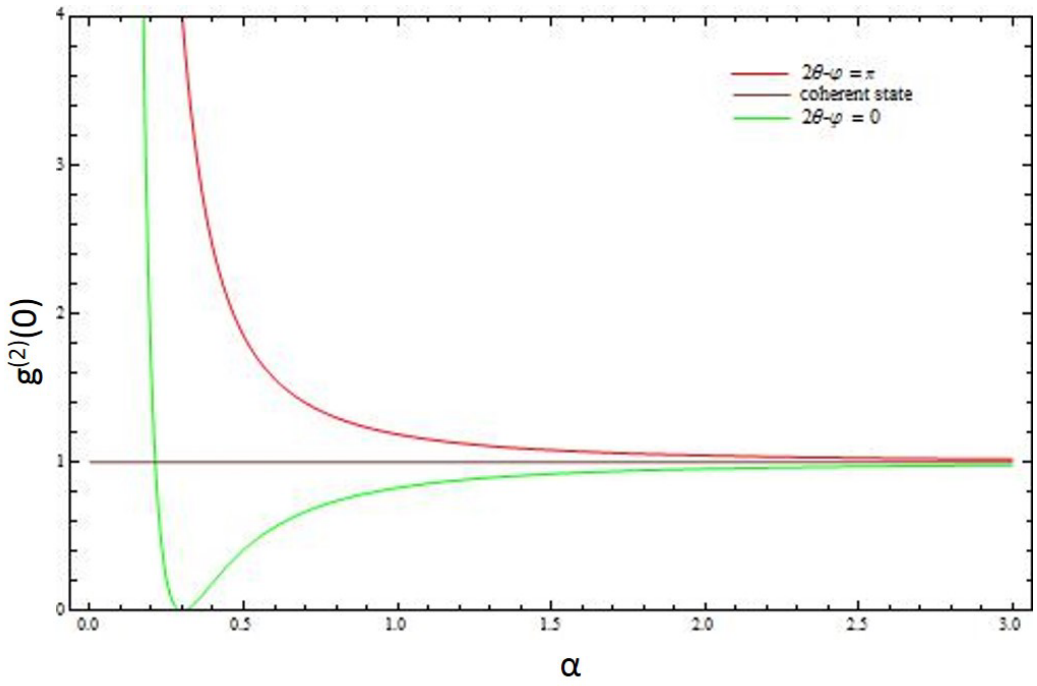

Fig. 2.15. The relationship of $g^{(2)}(0)$ with α for different phase difference.

From Fig. 2.15, we can see that the $g^{(2)}(0)$ shows a appreciable deviation from one, which corresponds to a coherent state, when the amplitude of coherent state α is less than a specific value, while approach one when α is lager than this value. For $2\theta-\varphi=0$, $g^{(2)}(0)$ decreases below one when $|\alpha|^2>|r|/2$ which indicates anti-bunching effect, and find a minimum value $g^{(2)}(0)=0$

at $|\alpha|^2 = |r| = 0.09$ on increasing the α. As the α increases further, $g^{(2)}(0)$ grows larger and approaches one. One the other hand, the $g^{(2)}(0)$ for $2\theta - \varphi = \pi$ decreases monotonously to one as α increases and indicates bunching effect.

2.6 The two-photon probability of displaced squeezed states

Actually, the two-photon interference between a squeezed vacuum state and coherent state can be regarded as generation of displaced squeezed state. In this section, we will discuss the two-photon probability for displaced squeezed states, which will appear in our experiment.

In two-photon interference between squeezed vacuum state and coherent state, we usually compare the two-photon rate of the generated displaced squeezed state $P_{dis}(2)$ with the interference coherent state $P_{coh}(2)$. With the selection of the relative phase between the squeezed vacuum state and the coherent state, the two-photon rate of the displaced squeezed state can be bigger than that of the interfered coherent state $P_{dis}(2) > P_{coh}(2)$. It exhibits photon bunching effect due to constructive two-photon interference. Similarly, with section of another relative phase, we can obtain $P_{dis}(2) < P_{coh}(2)$ which indicates destructive two-photon interference. Especially when $|\alpha|^2 = |r|$, $P_{dis}(2) = 0$, we obtain complete destructive two-photon interference.

We first give the two-photon probability of coherent state and two kind of displaced squeezed states from Eq.(2.2.24) and Eq.(2.2.59).

$$P_{co}(2) = \frac{1}{2}|\alpha|^4 e^{-|\alpha|^2} \tag{2.6.1}$$

$$P_{am}(2) = \frac{1}{2\cosh r}\Big(\frac{1}{2}\tanh r\Big)^2 \exp\big\{-|\alpha|^2(1+\tanh r)\big\}H_2^2(z), \tag{2.6.2}$$

$$P_{ph}(2) = \frac{1}{2!\cosh r}\Big(\frac{1}{2}\tanh r\Big)^2 \exp\big\{-|\alpha|^2(1-\tanh r)\big\}H_2(z)H_2(z^*). \tag{2.6.3}$$

Then, we plot the relationship between the two-photon probability P(2) with $|\alpha|$ for displaced squeezed states with $|r| = 0.09$, as shown in Fig. 2.16.

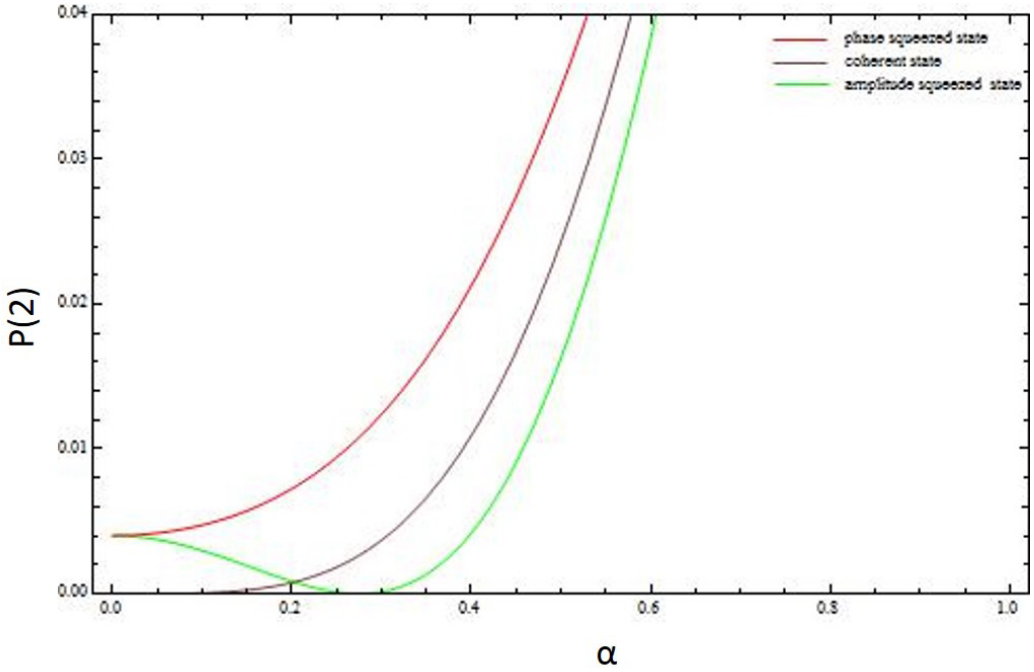

Fig. 2.16. The relationship of P(2) with α for different states.

For the amplitude squeezed state, when α= 0, the statistics properties are decided by the two-photon term in squeezed vacuum state, the $P_{am}(2)$ is bigger than that of the coherent state. With the increasing in α, the $P_{am}(2)$ decreases to smaller than those of the coherent state when $|\alpha|^2 > |r|/2$ and find minimum value 0. as the α increasing further, $P_{am}(2)$ increases and approach to the coherent state. For the phase squeezed state, with the increasing in α, the statistics properties is gradually decided by the coherent state, and the $P_{ph}(2)$ monotonously decreases to value of the coherent state and larger than $P_{co}(2)$ at all the time.

Chapter3 Generation of squeezed vacuum state

Reduction or even completely suppressing the quantum noise of the light field has been a research focus in quantum optics. The squeezed state, which quantum noise in one quadrature is less than the quantum-noise-limit (QNL) in coherent state, has become a key resource in quantum optics [45–47], with applications in quantum communications [48], quantum informations processing [49], ultra high-precision measurement [50] and ultra-weak signal measurement. In this chapter, we will introduce a scheme for generation of squeezed states. In the first section, we will briefly introduce the history of squeezing results from various cavity systems. In the second section, we will introduce optical parametric process which was used in producing squeezed state. In the third section , we will describe a experimental setup to generate the squeezed vacuum state which is used to interfere with a coherent state in the next chapter. In the forth section, we will present the measurement results of various quantum states, including vacuum states, coherent states, squeezed vacuum states and displaced squeezed state. At last, we will introduce the method to reconstruct the Wigner function of generated states.

3.1 Introduction

Theoretical considerations about the possible existence of light with squeezed quantum noise can be traced back to 1920s [51–53]. However, the first experimental generation of squeezing was produced by an American research group led by R. E. Slusher in 1985 [54] . In their experiment, they used a four-wave mixing in a Na atomic beam and observed a squeezed state with 0.7 dB. Another alternative technique for squeezed light generation is the phase-sensitive amplification in an optical-parametric oscillator (OPO). The first experimental realisation of squeezing in an OPO was performed in 1986 [55] resulting in almost 3 dB of noise reduction. In 1987, parametric down conversion was used to generate pulsed squeezed light [56]. It resulted in squeezed pulses of 100 ps length 0.6 dB below shot-noise level. In 1992, the record level of quadrature noise suppression in an OPO was pushed to 6 dB below the standard quantum limit [57]. This result was improved in 1998 to 6.5 dB [58]. In recent years, this technique has benefited from advances in nonlinear materials, low-loss coatings, and low-noise detectors. This resulted in dramatic improvements in degree of squeezing to 10 dB below standard quantum limit [59] in 2008. In subsequent experiments, the observed squeezing levels are further increased. Recently, a 12.3dB at 1550nm and 12.7dB at 1064nm quantum noise squeezing of a laser field was produced by a

German group [60, 61]. In 2016, a very great step forward was achieved by the same group and a squeezed state with 15dB at 1064nm was observed [62].

Table 3.1 shows a short list of relevant squeezing measured results from the first experiment with 0.7dB in 1985 to the lastest experiment with 15dB at a measurement frequency of 3MHz. Most of them are based on optical parametric amplifier process and performed in the continuous-wave regime.

Squeezed light is not only a special quantum mechanical state but has also several applications: Any measurement that uses only one quadrature for detection can be improved to a sensitivity below the standard quantum limit by using squeezed light for the measurement. Following the proposal by Caves [69] squeezed light was used to improve interferometric measurements. To our knowledge, the first experiment which employed squeezed light to improve a measurement sensitivity was made at University of Texas in 1987 [70]. In that experiment the squeezed light was used to improve the detection of phase modulation in an interferometer. The measurement resulted in 3 dB increase in signal to noise ratio. The improvement of the sensitivity of the interferometers can be used in practice for the detection of gravitational waves. At the moment the most sensitive classical gravitational wave detector is Laser Interferometer Gravitational wave Observatory (LIGO) with the interferometer arm length of 2 to 4 km. A strong gravitational wave would change the arm length by at most 10^{-17} m. The high sensitivity necessary for this measurement can currently only be reached at low frequencies (below 1 kHz). At high frequencies the detection is limited by the standard quantum limit. Here the measurements below standard quantum limit could be performed using squeezed light. This application was the motivation to be built a source of squeezed light with very high level of squeezing close to 15 dB below shot-noise level [62].

The applications mentioned above are emphasize on the squeezing level of the squeezed state. However, there are some other applications which are sensitive to the purity of the squeezed state with weak squeezing level. In 2007, N. B. Grosse [71] performed an experiment to demonstrate the non-classical statistics (anti-bunching effect) of light, in which the best result was observed using a squeezed state with squeezing $0.5dB$ and purity $V^0 * V^{\frac{\pi}{2}} = 1.005$. Recently, a complex wave function [72, 73], which provided complete knowledge of a state was been measured by optical interference, in which a weak but purity squeezed state was used as one of the interference source.

In this thesis, we will discuss a two-photon interference between a squeezed state and a coherent state, in which a squeezed vacuum state with weak squeezing level and high purity will be used.To realize the two-photon interference, we will generate two different squeezed states (amplitude squeezed state and phase squeezed state).

3.2 Optical parametric processes

Until last century, the history of optics was assumed that the optical media were linear which has led to some simple rules in optics, such as the frequency of light do not change when it

Table 3.1. A brief list of groups and results in generating squeezed state.

Year	author	wavelength(nm)	non-linear crystal	Frequency	Squeezing
1985	Slusher [54]	589	four-wave mixing	594.6MHz	0.7dB
1986	Wu [55]	532,1064	MgO:LN	1.8MHz	3dB
1992	Ou [45]	540,1080	KTP	1.1MHz	3.6dB
1992	Polzik [57]	856	KNB	1.4MHz	6dB
1998	Schneider [58]	1064	MgO:LN	6.5MHz	6.5dB
1999	Lam [63]	1064	MgO:LN	3MHz	7.1dB
2002	Bowen [64]	1064	MgO:LN	220kHz	2.5dB
2006	Suzuki [65]	860	PPKTP	1MHz	7dB
2007	Takeno [66]	860	PPKTP	1MHz	9dB
2008	Vahlbruch [59]	1064	MgO:LN	5MHz	10dB
2010	Mehmet [67]	1064	MgO:LN	5MHz	11.5dB
2010	Eberle [61]	1064	PPKTP	5MHz	12.7dB
2011	Mehmet [60]	1550	PPKTP	60kHz	12.3dB
2012	Stefskzy [68]	1064	PPKTP	10Hz	10dB
2016	Vahlbruch [62]	1064	PPKTP	3MHz	15dB

propagates through an optical medium, optical properties of a medium are independent with the intensity of the light. But since the laser was invented in 1960's, high optical intensities previously unattainable have revealed observations deviating from all of the simple rules mentioned above. Here we will introduce some optical nonlinear processes involving second-order nonlinearity $\chi^{(2)}$ and how these processes can produce squeezed state. We can write the induced polarisation, $\vec{P}$, in a non-linear dielectric medium due an external electromagnetic, $\vec{E}$, as

$$\vec{P} = \epsilon_0(\chi\vec{E} + \chi^{(2)}\vec{E}^2 + \chi^{(3)}\vec{E}^3 + \cdots), \tag{3.2.1}$$

where the ϵ_0 is the electric permittivity of the free space and the $\chi^{(n)}$ are the nrd-order non-linear susceptibility. $\chi^{(1)}$ is the first-order linear susceptibility which is usually used to described the absorption, refraction of a medium and satisfies $n = \sqrt{1+\chi^{(1)}}$. The third-order nonlinear susceptibility, $\chi^{(3)}$ is responsible for four-wave processes such as the Kerr effect, third harmonic generation and self phase modulation. The second-order nonlinear processes $\chi^{(2)}$ can be used to drive processes such as second harmonic generation (SHG), optical parametric amplification (OPA) and optical parametric oscillation (OPO). It actually involves the interaction of three photons, so it is also called three-wave mixing processes. Two lower frequency photons combining to produce a more higher frequency photon is known as the parametric up-conversions which is called sum frequency processes. The processes of one higher frequency photon being converted into two photons of low frequencies is known as parametric down-conversions which is also called difference frequency processes.

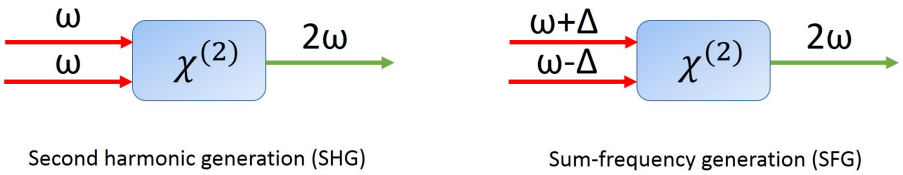

Fig. 3.1. The up-conversion processes of SHG and SFG.

3.2.1 Parametric up conversion process

The optical parametric up conversion processes include sum frequency generation (SFG) where two photons with different frequencies, $\omega + \Delta$ and $\omega - \Delta$, are combined to produce one photon with frequency 2ω, as shown in Fig. 3.1. When the input photons have the same frequency ω, the combined process is called second harmonic generation (SHG). Here, we only discuss the SHG process which was first experimentally achieved by Franken [74] in 1961. Considering two photons at a lower frequency, ω, combining to produce one photon at a higher frequency, in this case at 2ω. Thus we can write

$$\omega_{SHG} = 2\omega = \omega + \omega, \tag{3.2.2}$$

where ω_{SHG} is the frequency of the second harmonic field and the ω is the frequency of the fundamental field. The systems are often placed inside a resonator such that the fundamental field undergoes many passes through the material, substantially improving the efficiency of the conversion.

3.2.2 Parametric down conversion process

Down conversion processes are ones in which higher frequency photons are converted into lower frequency photons. With different conditions, the down conversion processes can be divided into four categories: degenerate optical parametric amplifier (DOPA), non-degenerate optical parametric amplifier (NDOPA), degenerate optical parametric oscillator (DOPO) and non-degenerate optical parametric oscillator (NDOPO). These various processes are integral in squeezed state generation from a second-order nonlinearity $\chi^{(2)}$ system. The down conversion process is shown in Fig. 3.2.

We can different these processes by the features of the sub-harmonic outputs: The degenerate processes where the two output photons are identical and non-degenerate processes where the modes of the two output photons are different. Unlike the up conversion processes, the down conversion processes have associated threshold powers below which the dissociations of higher frequency photons into lower frequency sub-harmonic photons does not happen. The processes only occur when the pump power is above the threshold . We call these processes DOPO and NDOPO. However, even the threshold condition can not be satisfied, we can realize the processes by introducing a seed field into the non-linear medium. These processes are called DOPA and

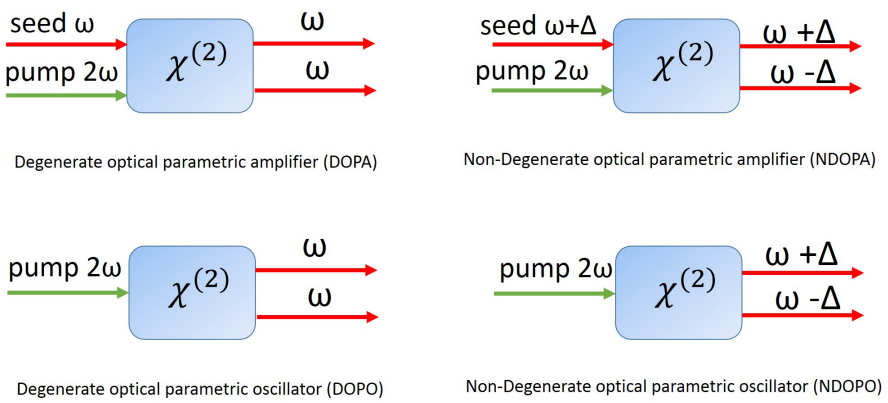

Fig. 3.2. The down-conversion processes of OPA and OPO.

NDOPA. Thus the DOPA and NDOPA needn't satisfy the threshold conditions. Actually, the DOPO and NDOPO can be regarded introducing vacuum fields as seed fields.

The degenerate down conversion processes (DOPO and DOPA) have been proved to be the most efficient source of generating single-mode quadrature squeezed state, such as squeezed vacuum state, amplitude squeezed state and phase squeezed state. For non-degenerate modes, the NDOPA and NDOPO have become key sources to generate two-mode squeezed state and Einstein-Podolsky-Rosen (EPR) entangled state when they are operated below or above the threshold.

3.2.3 Phase matching

In the previous section, we introduced various non-linear optical processes in which energies (frequencies) are converted. Like all physical processes, these conversions must satisfy the energy conservation law. For three photons with $\omega_1, \omega_2, \omega_3$, thus the non-linearity process should satisfy,

$$\omega_1 = \omega_1 + \omega_2. \tag{3.2.3}$$

Actually, in these processes, another law also should be satisfied, momentum conservation law. The conservation of momentum in a nonlinear optical process is often referred as phase matching condition. For the momentum of three photons to be conserved, we require their optical wave vectors to fulfill the following equation,

$$\vec{k}_1 = \vec{k}_2 + \vec{k}_3, \tag{3.2.4}$$

where $|\vec{k}_i| = \frac{n_i \omega_i}{c}$, and n_i is the index of refraction of the nonlinear medium for the ω_i field and the c is the speed of light in a vacuum. When the Eq. (3.2.4) is satisfied, we say the process is phase matched. To understand easily, we can rewrite Eq.(3.2.4) as

$$\frac{n_1}{\lambda_1} = \frac{n_2}{\lambda_2} + \frac{n_3}{\lambda_3}. \tag{3.2.5}$$

It is obviously that in order to phase matching to occur, the refractive indexes must be matched. If the nonlinear processes is done in a birefringent crystal material, we can achieve phase matching with two methods :

1. **Angle matching:** If the nonlinear processes is done in a birefringent crystal material, and the refractive index depends on the polarization and direction of the light that passes through, we can match the refractive indexes by changing the direction of the light. This method is called angle matching.

2. **Temperature matching:** Since the characteristics of the crystals, such as refractive index, can be changed by tuning the temperature of the crystal, we can realize the refractive indexes matching by controlling the temperature of the crystal. This method is called temperature matching.

3.3 Generation of squeezed vacuum state

In this section, we will introduce the generation of squeezed vacuum state using the degenerate optical parametric amplifier (DOPA). The experimental setup is shown in Fig. 3.3. The main laser source is a commercially available continuous wave Nd:YAG laser which emits 2.0 W of coherent light at 1064 nm. A major fraction of this light is frequency-doubled by a SHG and used to pump the an OPA which is composed of a periodically poled $KTiOPO_4$ (PPKTP) crystal. The remaining light from the laser was first transmitted through a high finesse mode clean cavity (MCC) and split into two parts: injection beam for OPA and local oscillator (LO) for homodyne detector. By choosing appreciate relative phase between pump beam and injection beam, we can generate amplitude quadrature and phase quadrature squeezed state with squeezing level of -1dB and anti-squeezing of 1.7dB in the range of 5MHz to 35MHz. All parts of the experiment including second harmonic generation (SHG) cavity, optical parameter amplifier (OPA) cavity, mode clean cavity (MCC) and the homodyne detector, will be introduced in detail in the following section.

3.3.1 Second harmonic generation

The pump beam of the OPA cavity is frequency-doubled by a SHG cavity [75, 76]. The experimental layout is sketched in Fig. 3.4. All the optical parts of the SHG system were arranged in a $9cm \times 36cm$ box. The SHG cavity is made by four mirrors in a bow-tie cavity, using two plane mirrors (M_1, M_2) and two curved mirrors (M_3, M_4) with $r = 50mm$ radius of curvature. The total length of the cavity is about 398 mm, the free spectral range (FSR) and full width half maximum (FWHM) are 753 MHz and 12.7MHz, thus the finesse can be calculated as 59. The mirror M_1 is 90% refectivity mirror at 1064nm light. The output mirror M_4 is coated dichromatically so that it transmits 98% of the power for 532 nm light and reflects more than 99.9% for 1064 nm light. The mirrors M_2 and M_3 are high reflectivity mirrors at 1064nm

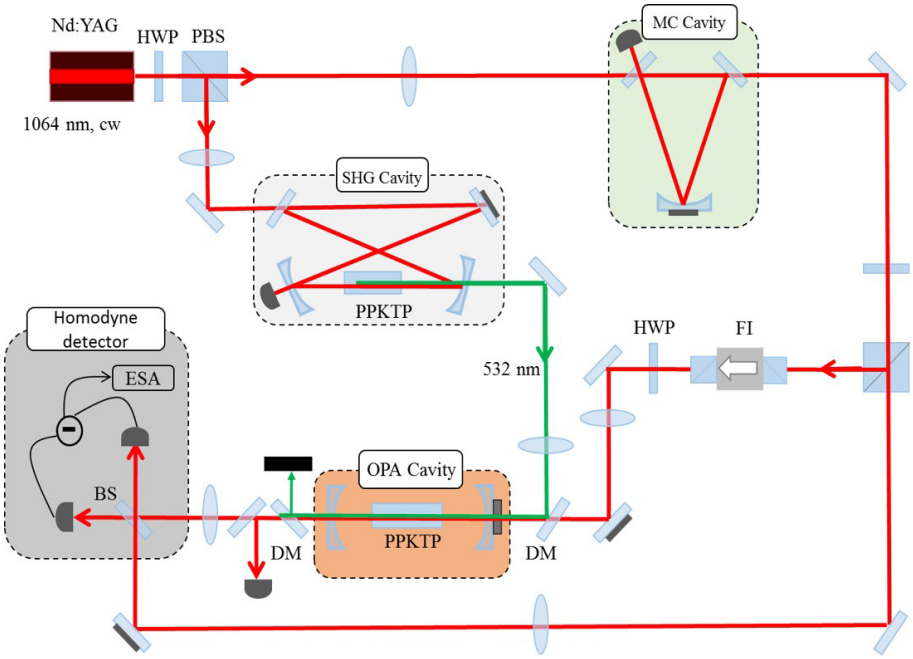

Fig. 3.3. Schematic of experimental setup.

light. The mirror M_2 is mounted on a piezo-electric transducer (PZT) which is used to control the length of the cavity and keep the cavity resonant with the input fundamental frequency. A type 0 periodically poled $KTiOPO_4$ (PPKTP) crystal, with both end facets anti-reflection coat for both 1064 nm and 532 nm, is used in the cavity. The PPKTP, with dimensions of $1mm \times 1mm \times 10mm$, is housed in a home-made oven and placed between the curved mirrors, where a smallest waist is 27 μm. The temperature of PPKTP was controlled to the optimal phase-matching temperature within an accuracy of 0.1 °C. In order to improve the stability of the cavity, we build SHG system in a single aluminum box where the PPKTP crystal, the oven, the thermal electric cooler and the four mirrors are fixed inside. The photograph of the SHG cavity is shown in Fig. 3.5.

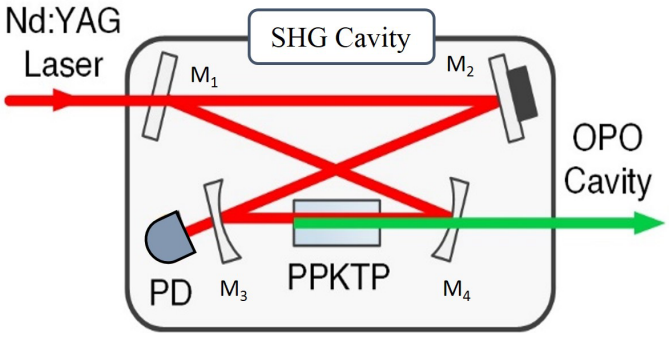

Fig. 3.4. experimental setup of SHG cavity.

The SHG cavity is locked using the dither-locking technique which has already been successfully used in lots of SHG and OPO experiments. In order to lock the cavity, the PZT of the cavity is dithered by a 30 kHz sinusoidal signal with a 500 mV amplitude and the light leaking from the cavity is monitored by a photodiode and then demodulated by a lock-in amplifier to provide an error signal for controlling the length of the cavity, then the error signal is fed back to PZT via a piezo driver.

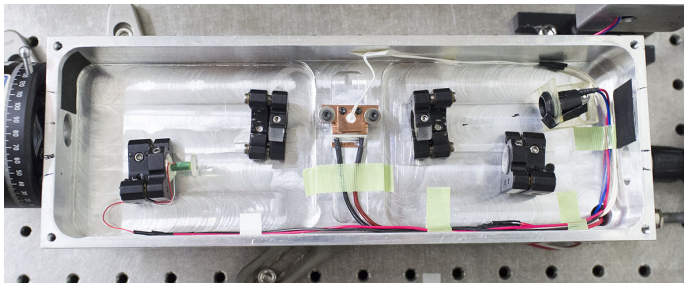

Fig. 3.5. The photograph of the SHG cavity.

To obtain the temperature characteristic of the PPKTP crystal, we measured the output power of the SHG as a function of temperature with a 1.7W input beam. The measured results is shown in Fig. 3.6. From the Fig. 3.6, we can find that the optimal phase matching temperature is about 32.5 °C and the full width at half maximum is about 5.5 °C. The measured results indicated that we can control the phase matching temperature near room temperature and stably operate the SHG.

We also measured the output power as a function of the input power for a single pass SHG configuration with the optimal phase matching temperature 32.5 °C. The measured results is shown in Fig.3.7. When the input power is 1.7W, a 29.8mW output power is obtained. The theoretical curve is given by

$$P_{SHG} = \gamma P_{in}^2. \tag{3.3.1}$$

where the γ is the single pass conversion coefficient. When $\gamma = 0.01W^{-1}$, the measured results are fitting with the theoretical values.

In order to obtain a high conversion efficiency for the SHG system, we locked the external cavity to an incidence fundamental resonance. Then, we measured the output power as the function of the input power with the optimal matching temperature and calculated the conversion efficiency respectively. The results is shown in Fig. 3.8. For 1.7W input power, we obtained a 1.23W of green light from the output of the SHG cavity and about 72% conversion efficiency. Further more, the maximum output power can be stably stayed for 4 hours with only 0.5% fluctuation. It indicates that we can obtain a sufficient stability and high power pump light to pump the OPA and generate squeezed vacuum state.

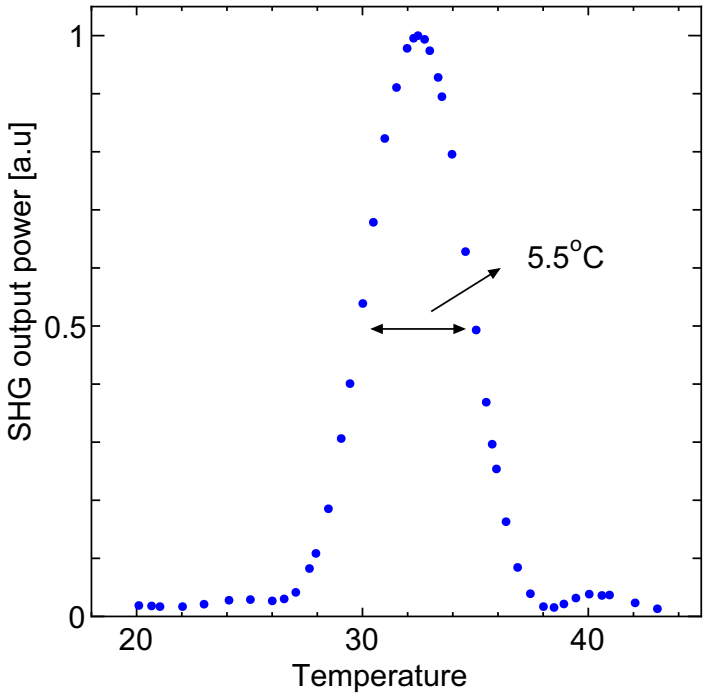

Fig. 3.6. Temperature characteristic for single-pass frequency doubling in PPKTP.

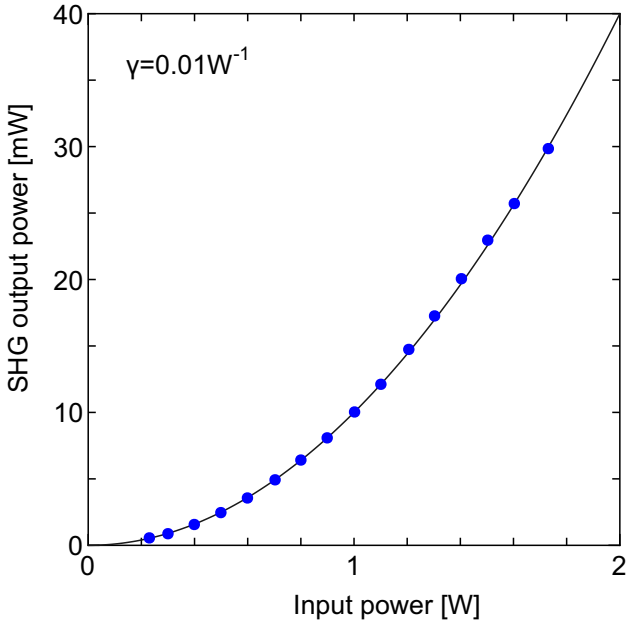

Fig. 3.7. SHG output power by a single-pass frequency doubling in PPKTP.

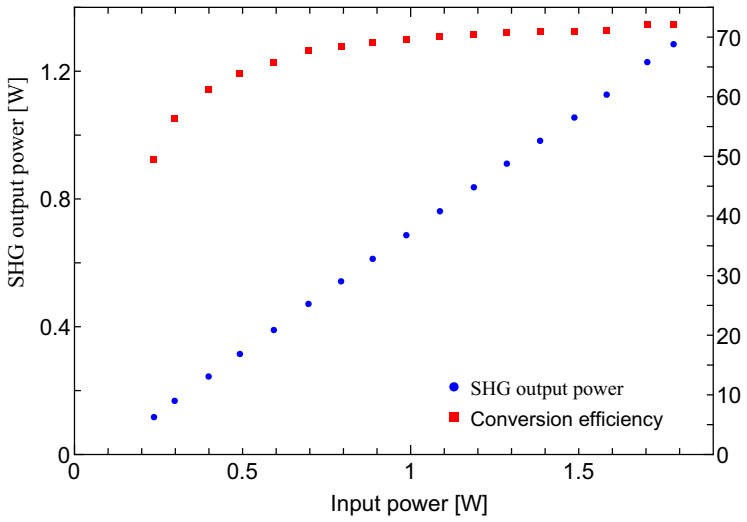

Fig. 3.8. SHG output power and the conversion efficiency as a function of the input power.

3.3.2 Mode cleaner cavity

A travelling-wave resonator is used in our experiment which serves as optical low-pass filter for high frequency phase noise on the laser beams as well as spatial mode cleaner cavity (MCC). Including the injection beam to OPA, the beam from the MCC was also used as coherent beam for two-photon interference and two local oscillators (LOs) for homodyne detectors.

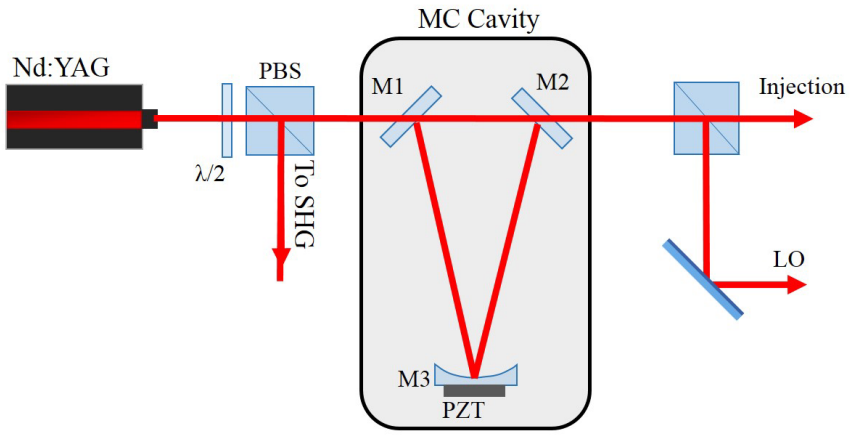

Fig. 3.9. The experimental setup of MCC.

As illustrated in Fig. 3.9, the resonator is set up as ring cavity with two flat mirrors and a curved mirror. The MCC consists of two identical at input-output mirrors with reflectivity of $R = 99\%$ and a curved mirror with a 1m radius of curvature and reflectivity of $R = 99.99\%$, and the total resonator length is 56cm. We observed a finesse of 160 and this provided a cavity linewidth of about 100 kHz. Since the light from the MCC is in TEM00 mode, it is very

convenient for mode matching with OPA and LO.

To characterize the MCC, we measured the intensity noise of the transmitted beam by a photodiode detection. The measured results is shown in Fig.3.10. In the figure, the measured data is normalized by quantum noise limit (QNL), the data which is closer to 0 indicates QNL. From Fig.3.10, we can find that the intensity noise of the input fundamental light closing QNL at 25 MHz, while the light transmitted through the MCC becomes at 11 MHz and the intensity noise decreased. This is because the light was filtered by the MC resonator. Since a higher squeezing level can be measured at lower frequency, we measured the squeezed state at 11 MHz in our experiment, and the measured results are in agreement with the theoretical value when the measured frequency is larger than 5MHz.

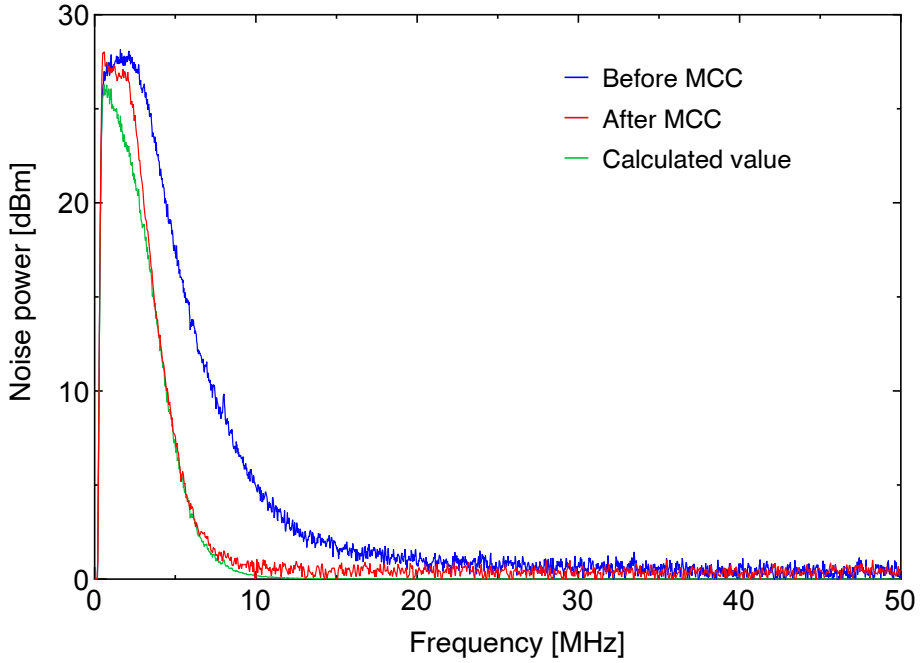

Fig. 3.10. The intensity noise reduction by MCC.

Since the output light from the MCC is used for injection light to OPA and LOs light for homodyne detectors, high stability without long term power fluctuation is required. So we locked the MCC using the dither-locking technique which was used in locking the SHG before. Fig. 3.11 shows a 135 mW transmitted light from the MCC stability stayed with 0.5% fluctuation for 3 hours, and input power is 180mW.

3.3.3 Optical parameter amplifier

The squeezed light source in our experiment is a linear Optical parameter amplifier (OPA) cavity. The layout of the OPA cavity is shown in Fig. 3.12. It consists of a $1mm \times 1mm \times 15mm$ type 0 PPKTP crystal and two concave mirrors. The input coupler is optically coated so that

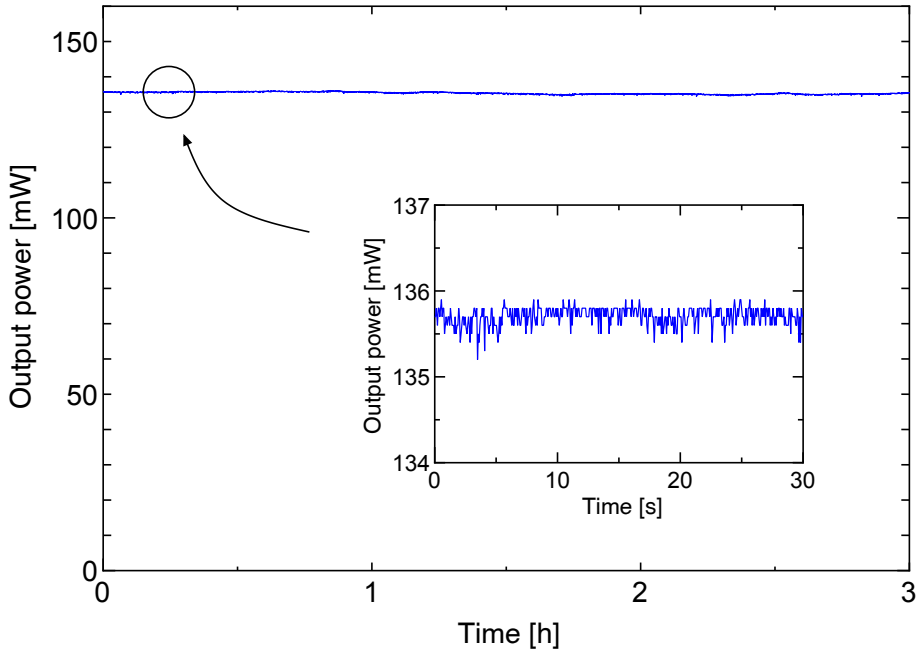

Fig. 3.11. Long-term stability of MCC.

it is highly reflective at 1064 nm. The output coupler has a measured transmission of 5% at 1064nm. One of the concave mirrors is mounted on a pizoelectric transducer (PZT) so that the OPA cavity length can be actively controlled for tuning onto the resonance with the laser frequency. Both the input coupler and output coupler are coated high transmission at 532nm so that the pump field interacts only once with the nonlinear medium. The length of the OPA cavity is about 54mm, the FSR and FWHM are 2775 MHz and 277.4MHz, respectively, thus the finesse can be calculated as 100. The OPA could be controlled so as to deamplify or amplify the injection beam by choosing the relative phase between pump and injection coherent beams. This ensures to produce the amplitude quadrature or phase quadrature squeezed state. The photograph of the OPA cavity in our experiment is shown in Fig. 3.13.

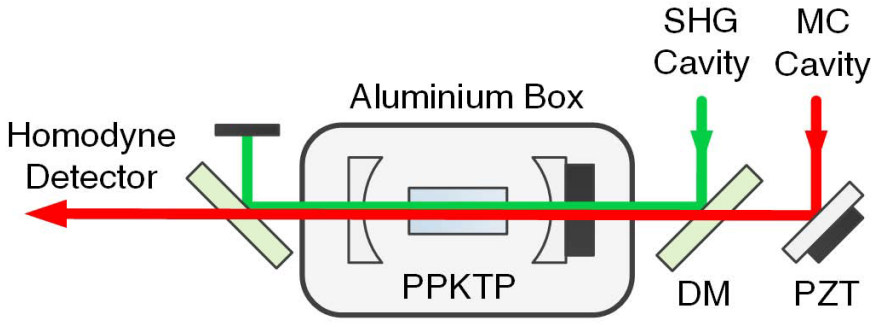

Fig. 3.12. The experimental setup of the OPA cavity.

The 1064nm light from MCC was used to inject the OPA cavity, and was mode matched into resonator by two lens with f=100mm and f=200mm. An isolator is used to prevent the reflectivity light from the OPA. The 532nm light from SHG was mode matched into resonator through another two lens with f=200mm and f=750mm. The two light were combined on a dichroic mirror. The relative phase between the pump beam and injection beam was controlled via an external PZT actuated mirror. Monitoring the injection beam that was transmitted through the OPA, showed alternating de-amplification and amplification when the phase of injection beam was scanned. The relative phase was locked using a dither lock from a phase modulation on the injection beam. The gain of the OPA was maximized by tuning the phase-matching condition of the nonlinear crystal which was adjusted by an servo-control of the temperature. The generated squeezed vacuum beam interfered with a LO beam on a 50:50 beam splitter and measured using homodyne detection.

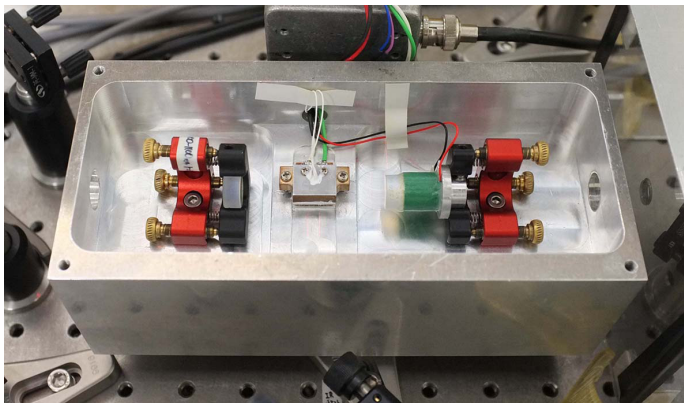

Fig. 3.13. The photograph of the OPA cavity.

1. The temperature characteristic of the PPKTP crystal in OPA cavity

Similar to SHG cavity, we also need to measure the single pass temperature characteristic of the PPKTP crystal in OPA cavity. To measure the temperature characteristic, we removed the M1 and M2 of the OPA, and only measured the power of the second harmonic light with a power meter. We chose the injection beam with 711mW and tuned the temperature by the temperature control, and the result is shown in Fig.3.14. From the figure, we can see that the optimal phase-matching temperature is 36°C and the FWHM is 2.9°C. The results also indicate that we can obtain the optimal phase-matching temperature near room temperature. Then we also measured the output power as a function of the input power for a single pass SHG configuration with the optimal phase matching temperature 36 °C. As shown in Fig. 3.15, the measured results are fitting with the theoretical values when $\gamma = 0.003W^{-1}$.

2. The amplification of injection beam in OPA cavity

In order to produce the squeezed vacuum beam from OPA, it is necessary to overlap the

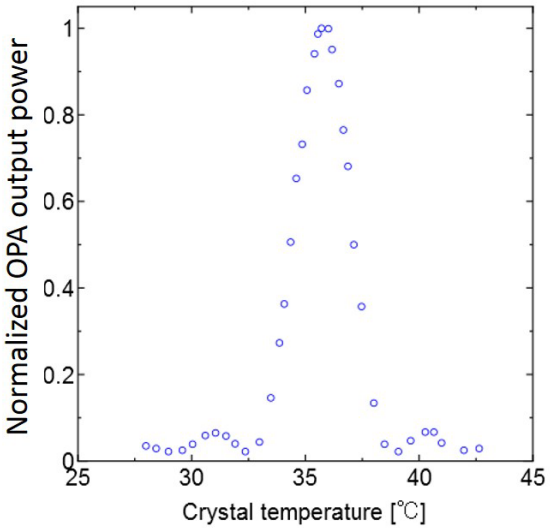

Fig. 3.14. Temperature characteristic of the PPKTP in OPA cavity.

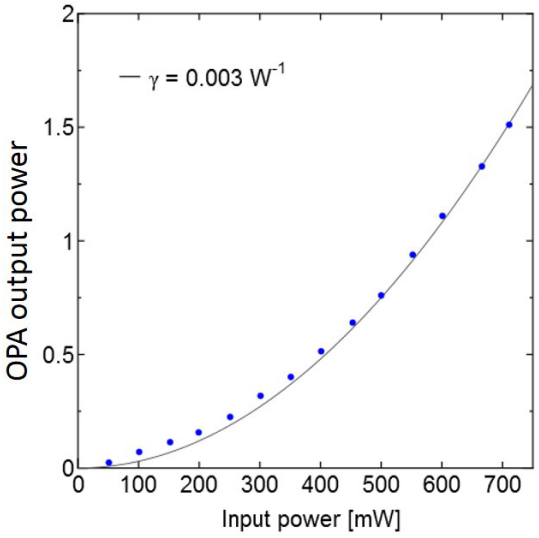

Fig. 3.15. OPA output power as a function of input power .

injection beam and the pump beam inside the OPA cavity and measure the classical gain which indicates the power of the injection beam increase or not. Since the classical gain varied depending on the relative phase between the injection beam and pump beam, a external PZT actuated mirror was inserted in the optical path of the injection beam. A triangle wave was sent to the PZT to control the relative phase.

For the injection beam, mode matching was performed to the mode of resonator. Thus we simulated and measured the waist of the injection beam, then inserted the crystal into the path of the injection beam, and overlapped the beam waist with the center of the crystal. At the center of the crystal, the beam waist is $91\mu m$ and $252\mu m$ at the end surfaces. After adjusting the mirrors in the OPA cavity, the injection beam was mode matched into the resonator where the resonance signal increased to the peak.

Similar to the injection beam, we simulated and measured the waist of the pump beam, and adjusted the two lens (f=200 and f=750) in the path of pump beam, and made the beam waist at the center of crystal where the beam waist is $65\mu m$ and $230\mu m$ at the end surfaces. Throughout the processes, the injection beam and pump beam keep parallel and the beams height were 75mm. A detector was placed after the OPA resonator and the classical gain was

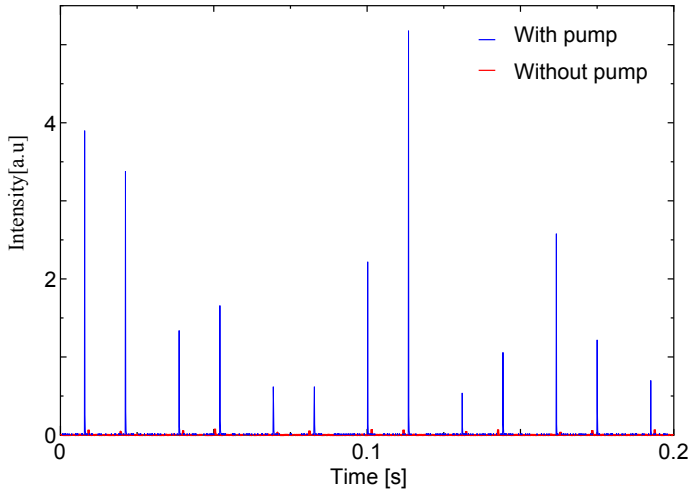

Fig. 3.16. The amplification of injection beam in OPA cavity

measured. In order to observe the amplification of the injection beam, we inserted a dichroic mirror between the OPA cavity and the detector. The dichroic mirror was used to cut the pump light of 532 nm. Fig. 3.16 showed the intensity of the injection beam was amplified when relative phase between the injection beam and the pump beam was scanned. From the figure, we can see that the injection beam is amplified for about 530 times. Since the peak of the classical gain changed, which indicated it is a phase sensitive amplification.

3. Locking the relative phase between the pump beam and injection beam

In order to produce different squeezed states, we should choose different relative phases be-

tween injection beam and pump beam. Thus we should lock the relative phase . A dichroic mirror was placed at the output of the OPA to remove the 532nm light from the OPA. The 1064nm light was transmitted to a 98% reflectivity mirror. the reflected light reached to homodyne detector, and the 2% transmitted light reached to a highly sensitive detector and used to lock the relative phase. The AC signal of the photodetector was divided into two parts by an RF splitter, one of the signal was used to lock the OPA cavity to control the length of the cavity, the other signal was used to lock the relative phase between the injection beam and pump beam. Fig. 3.17 shows the results of locking the classical gain which control the relative phase of injection beam and pump light.

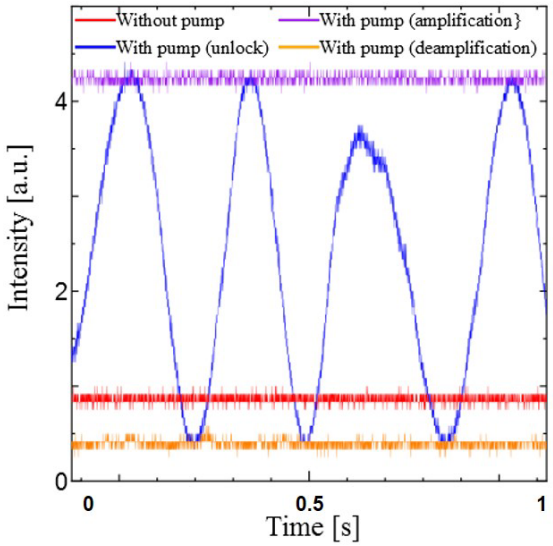

Fig. 3.17. Locking the relative phase between the pump beam and the injection beam.

When we locked the relative phase at de-amplification, we produced amplitude squeezed vacuum state, and the phase squeezed vacuum state was generated when the relative phase was locked at amplification.

3.3.4 Homodyne detector

To observe the quadrature squeezed state, a homodyne detector was used in our experiment. It is a most traditional detection scheme in continuous variable quantum optics region. Since both the amplitude and phase quadrature variances of the generated squeezed state should be measured. As shown in Fig.3.18, the homodyne detector consists of a 50:50 beam splitter, a pair of photodetectors and a subtractor. A signal light is mixed with a strong LO on the 50:50 beam splitter. Hence, only one mode, which is matched to the LO, is probed. Each beam splitter output light was focused on a photodiodes (ETX500). By choosing the relative phase between the measured signal and the LO light, the quadrature information of the measured signal can be recorded. Using a PZT mirror in the path of LO beam, the relative phase between the both

lights can be well controlled. The subtracted electronic signal of the homodyne detectors can be directly observed on a spectrum analyzer (SA) or an oscilloscope.

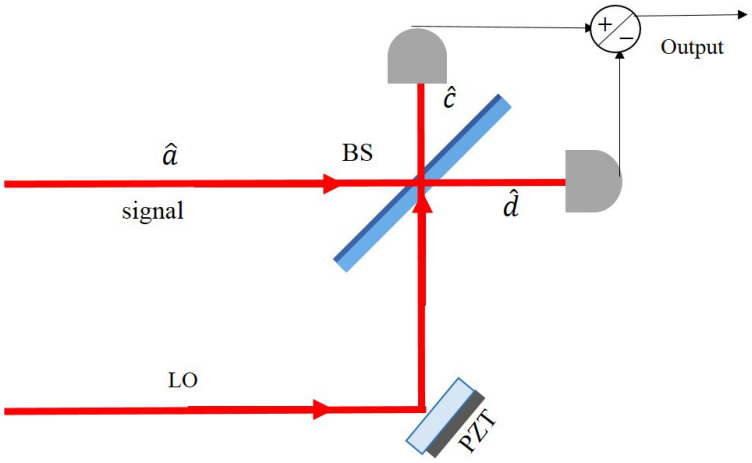

Fig. 3.18. Principle of homodyne detector.

We first checked the linearity of the homodyne detector by measuring shots noise levels as a function of LO powers by a oscilloscope (OSC). With the signal beam blocked, the shot noise of the homodyne detector can be recorded by sending only LO beam into the detector. Fig. 3.19 shows measured results which present eight measurement values with a LO power of 2mW, 4mW, 6mW, 8mW, 10mW, 12mW, 14mW and 16mW (measured the DC component of the electronic signal from the homodyne detector). Fig.3.19 shows the linear fit to eight measurement values and the detector can be used in our experiment.

In order to obtain a precise squeezed level of the squeezed state, the signal-to-noise ratio of the detector should be increased. We know that the dark noise of detector can not be ignored if it is larger than 10 dB below the shot noise. With both the signal beam and LO beam blocked, the dark noise of the homodyne detector can be recorded. And then we measured the shot noises by sending the LO light into the homodyne detector with different LO power of 2mW, 4mW, 8mW, 16mW and 32mW. Fig.3.20 shows the dark noise clearance with different LO beam power by measuring the AC component of the electronic signal from the homodyne detector on a spectrum analyzer. From Fig. 3.20, we can see that when the LO power is larger than 8 mW, the shot noise is larger than 10dB above the dark noise. In this experimnt, we used a 16mW local oscillator beam, and the dark noise clearance was approximately 13 dB at a measurement frequency of 11MHz. The spectrum analyzer was set with a resolution bandwidth (RBW) of 100 kHz and video bandwidth (VBW) of 100Hz.

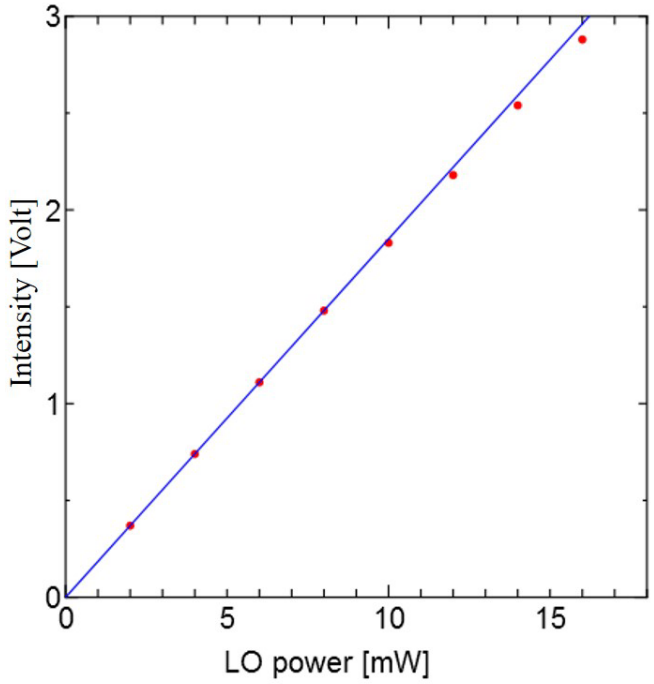

Fig. 3.19. The linearity of the homodyne detector.

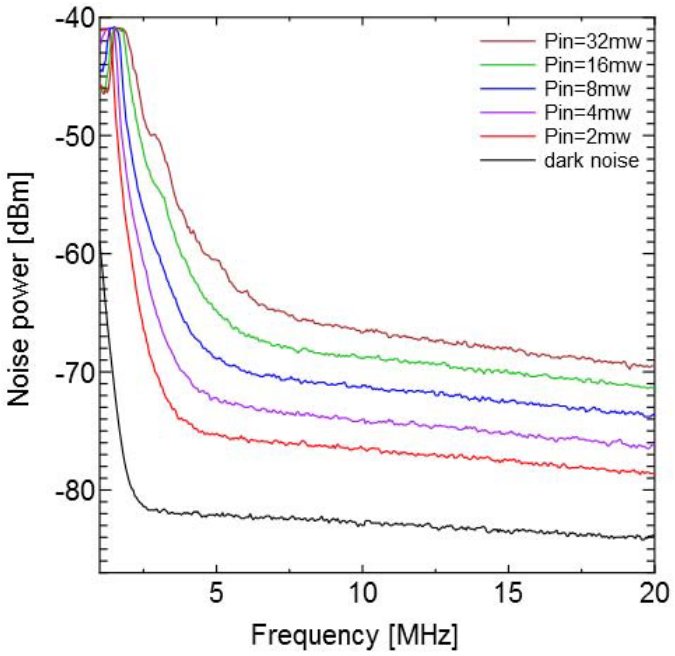

Fig. 3.20. The dark noise clearance with different LO beam powers.

3.4 Detection of squeezed vacuum state

3.4.1 Experimental procedure

The experiment was performed according to a strict produce of alignment and characterisation of mode matching or visibility of the optical paths, followed by the data acquisition. The steps of the experiment are given as,

1. Mode match the 1064nm laser coherent light into SHG resonator and MCC resonator. Lock the length of the SHG cavity and lock the laser frequency to MCC, respectively.
2. Adjust the injection light into OPA cavity for optimal mode matched into resonator. Then, incident the pump light into the OPA and adjusted the two mirrors in the path of the pump beam so as to obtain the maximum classical gain. Check that the lock is stable for de-amplification or amplification.
3. Adjust and measure the fringe visibility between LO beam and injection beam using a homodyne detector.
4. Confirm the power balance for all beams on a spectrum analyzer.
5. Set the power of the pump beam, injection beam and LO beam with ($P_p = 365mW$, $P_{in} = 1mW$ and $P_{LO} = 16mW$.
6. Re-lock the relative phase between pump beam and injection beam for de-amplification, re-lock the OPA cavity.
7. Observe the squeezing level on a spectrum analyzer.
8. Acquire the experimental data.
9. Re-lock the relative phase in step 6 for amplification and repeat the step 7 and step 8.
10. Choose another pump power and repeat the experimental procedure mentioned above.

3.4.2 Detection of squeezed vacuum state

In order to measure the squeezed vacuum state, we measured the generated state with a homodyne detector. The output of the homodyne detector was recorded with a spectrum analyzer. The experimental setup is shown in Fig. 3.21.

When we performed the measurement with homodyne detection, the most important step is to overlap the generated beam from the OPA and the LO beam. Hence, choosing an appropriate injection beam power which made the power of the generated beam from the OPA equal the power of LO beam , and interfered on the 50:50 beam splitter. A larger spatial overlapping between them, a higher fringe visibility can be observed, and a higher detection efficiency can

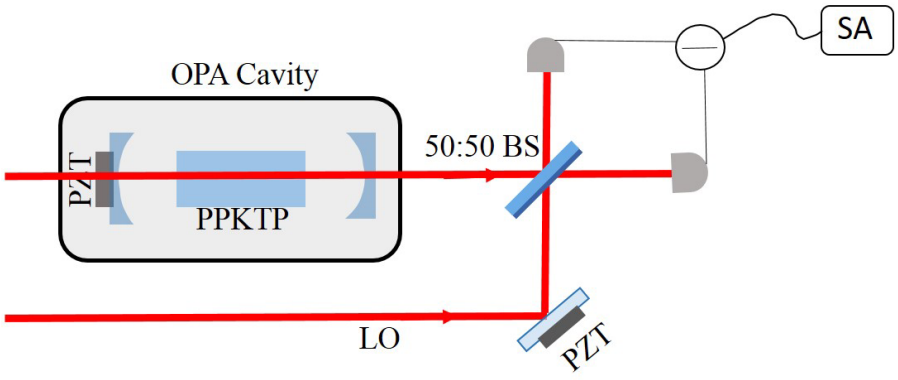

Fig. 3.21. The experimental setup of homodyne detection.

be obtained. As shown in Fig. 3.22, we obtained a visibility with 98%, which can be calculated as,

$$V = \frac{I_{max} - I_{min}}{I_{max} + I_{min}} \tag{3.4.1}$$

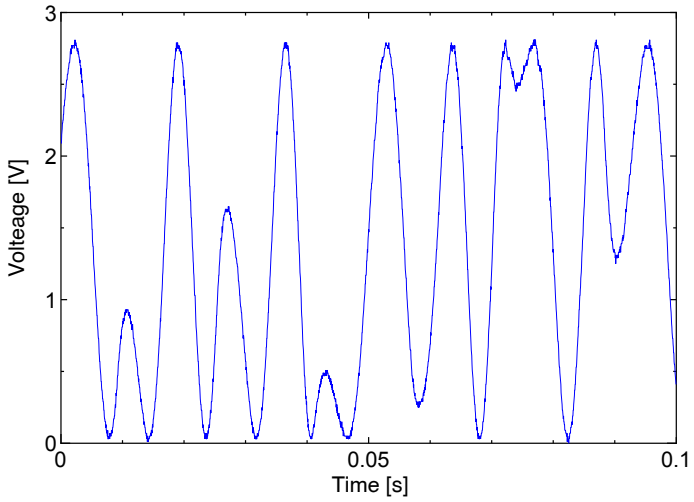

Fig. 3.22. The visibility between squeezed vacuum beam and LO beam.

Another important step is to align the balance between the two electronic signal from the two detectors. We can directly checked the balance with spectrum analyzer. In our experiment, the balance between the two electronic signal matched very well, as shown in Fig.3.23. It ensured the accuracy of our measurement results.

As shown in Fig.3.21, the homodyne detection was performed when the relative phase between the generated squeezed vacuum beam and LO beam was scanned by driving the PZT mirror, and the squeezing level was observed on a spectrum analyzer. We set the pump beam with$P_p = 540mW$, injection beam with $P_{in} = 1mW$ and LO beam with $P_{LO} = 16mW$, and set the

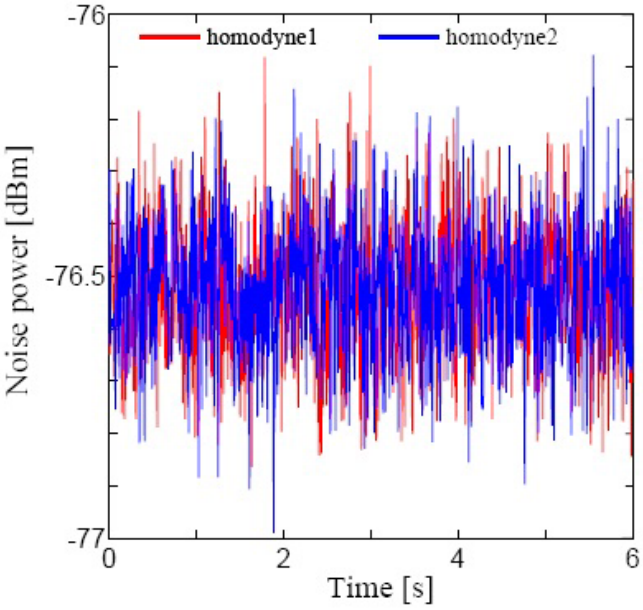

Fig. 3.23. The balance of homodyne detector.

spectrum analyzer with RBW =100kHz and VBW =100Hz. Fig.3.24 shows the measured noise power in frequency domain. From Fig.3.24, We can see that the squeezing can be observed from 5MHz to 35MHz. We can also find that as the analysis frequency increases, the generated squeezed state becomes purer. Since the purity of the squeezed state is very important for two-photon interference in next chapter, we choose an analysis frequency with 11MHz, and observed an amplitude or phase quadrature squeezed state with squeezing level of -1dB and anti-squeezing of 1.7dB which is shown in Fig. 3.25. The upper and under transverse line show the generated squeezed vacuum state is locked at squeezing and anti-squeezing, respectively. The principle of amplitude or phase locking technique will be discussed in next chapter.

3.5 Reconstruction of the Wigner function using the homodyne tomography

In classical physics, we can completely characterise an state by measuring the position and momentum of the state simultaneously. On the other hand, in quantum physics, it is impossible due to Heisenberg uncertainty principle. If we want to fully describe a quantum state, we have to know its wave function or some other equivalent information. However, the wave function is normally not measurable. In experiment, we usually reconstruct the Winger function and density matrix of a quantum state, which are the equivalent information to the quantum wave function.

In 1932, Wigner introduced a quasi-probability distribution into quantum mechanics [77] for the first time , which is known as Wigner function. Using the Wigner function, we can eas-

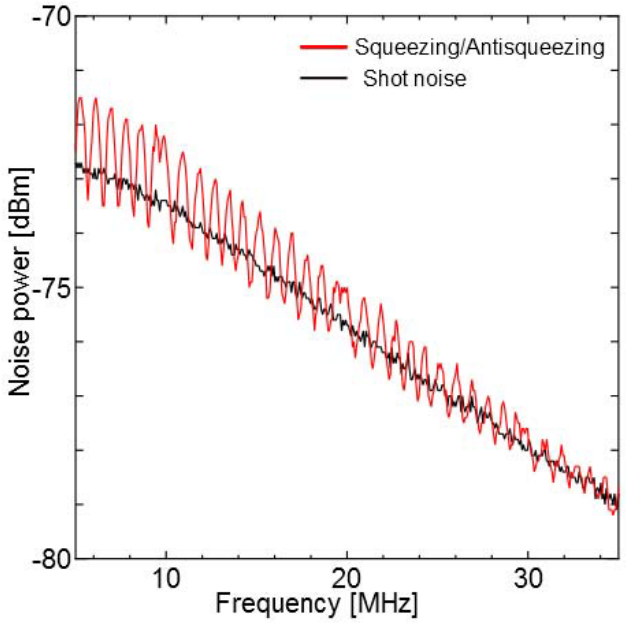

Fig. 3.24. Measurement of squeezed vacuum state with all frequencies.

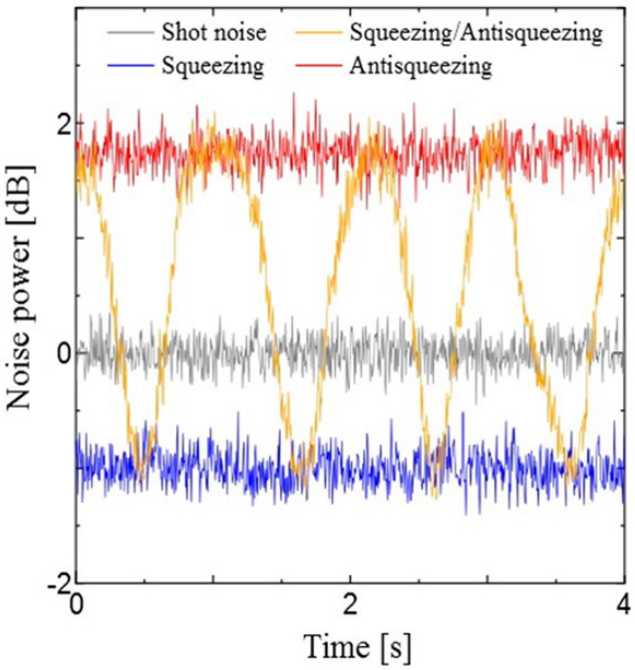

Fig. 3.25. Measurement of squeezed vacuum state at 11MHz.

ily obtain the probability distribution of a observable variable. Wigner function contains all information of a quantum state in phase space evolution. Unlike the classical probability distribution, the Wigner function can give a negative value with quantum state, and it is described as a quasi-probability distribution function.

The Wigner function was firstly reconstructed using a tomography technique by Bertrand in 1987 [78]. Soon after that, Vogel, et al described another way to reconstruct Wigner function from the measured quadrature amplitude distributions by optical homodyne measurement [79]. The first experiment of quantum state reconstruction was carried out by Smithey, et al [80]. The Wigner function of a vacuum and a quadrature squeezed state were reconstructed, in which the signal field was combined with a strong local oscillator field at a 50:50 beam splitter and measured by a balanced homodyne detection. We call this technique optical homodyne tomography. Using the Winger function, we can reconstruct the density matrix of a quantum state in Fock representation. It can directly provide the density matrix elements $\rho_{mn} = \langle m| \hat{\rho} |n\rangle$ of the state. In our work, we reconstructed the Wigner state to confirm the light fields which were generated in our experiment.

In this section, we will introduce the reconstruction of the Winger function by homodyne tomography [81–88] with inverse Radon transform and reconstruct the generated states in our experiment. We first discuss the principle of the homodyne tomography and explain the method of program, then introduce the experimental setup of homodyne tomography and give the experimental results.

3.5.1 The Wigner function

The Wigner function of quantum state is defined as a real function in phase space, which has the basic characteristics of quasi probability distribution. Considering a quantum state $|\varphi\rangle$ in two-dimensional space, the Wigner function can be defined as (For discussing convenience, we use x, p replace the $X^0, X^{\frac{\pi}{2}}$.)

$$W(x,p) = \frac{1}{2\pi\hbar}\int_{-\infty}^{\infty} \langle x + \frac{x'}{2}|\varphi\rangle \langle\varphi|x - \frac{x'}{2}\rangle \exp(-\frac{ipx'}{h})dx'. \tag{3.5.1}$$

The main properties of Wigner function are shown as

1. The Wigner function is a real function in phase space, namely,

$$W(x,p) = W^*(x,p). \tag{3.5.2}$$

2. The Wigner function is a quasi-probability distribution function which satisfies

$$\int W(x,p)dp = P_p(x), \int W(x,p)dx = P_x(p),. \tag{3.5.3}$$

where $P_p(x)$ and $P_x(p)$ are the probability distribution function of the particle in momentum and position space, respectively.

3. The Wigner is normalized in x,p space,

$$\int_{-\infty}^{\infty}\int_{-\infty}^{\infty} W(x,p)dxdp = Tr\hat{\rho} = 1. \tag{3.5.4}$$

4. The Wigner function can be either positive or negative, which is different from the classical probability distribution function. But for classical state, $W(x,p) \geq 0$.

The Wigner function can be used to uniquely defined a quantum state, and it is directly related to the quadrature probability distribution $pr(x_\theta, \theta)$ which can be experimentally measured with homodyne detection via

$$pr(x_\theta,\theta) = \int_{-\infty}^{\infty} W(x_\theta\cos\theta - p_\theta\sin\theta, x_\theta\sin\theta + p_\theta\cos\theta)dp_\theta. \tag{3.5.5}$$

That is to say, the quadrature probability distribution $pr(x_\theta, \theta)$ is a integral projection of the Winger function $W(x, y)$ onto a vertical plane defined by the phase of the local oscillator.

We consider the quadrature probability distribution $pr(x)$ and $pr(p)$ for $\theta = 0$ and $\theta = \frac{\pi}{2}$ as

$$pr(x) = \langle x|\hat{\rho}|x\rangle = \int_{-\infty}^{\infty} W(x,p)dp, \tag{3.5.6}$$

$$pr(p) = \langle p|\hat{\rho}|p\rangle = \int_{-\infty}^{\infty} W(x,p)dx. \tag{3.5.7}$$

Then we can calculate the Winger function for some quantum states. For a vacuum state, Using $\hat{a}\,|0\rangle = 0$ and $\hat{a} = \hat{x} + i\hat{p}$, we can obtain the wave function of a harmonic oscillator,

$$\phi_0(x) = (\frac{2}{\pi})^{\frac{1}{4}} e^{-x^2} \tag{3.5.8}$$

Using the density operator of vacuum state $\hat{\rho} = |0\rangle\langle 0|$, The Wigner function of vacuum state can be calculated as,

$$\begin{aligned} W_0(x,p) &= \frac{1}{\pi}\int_{-\infty}^{\infty} \langle x + \frac{x'}{2}\,|0\rangle\langle 0|\,x - \frac{x'}{2}\rangle \exp(-i2px')dx' \\ &= \frac{1}{\pi}\int_{-\infty}^{\infty} \phi_0(x+\frac{x'}{2})\phi_0(x-\frac{x'}{2})dx' \\ &= \frac{2}{\pi}\exp(-2x^2 - 2p^2). \end{aligned} \tag{3.5.9}$$

here $\hbar = 1/2$ is used.

Similarly, we can calculate the Wigner function of coherent state, squeezed vacuum state and displaced squeezed state.

$$W_\alpha(x,p) = \frac{2}{\pi}\exp[-2(x-x_0)^2 - 2(p-p_0)^2], \tag{3.5.10}$$

$$W_s(x,p) = \frac{2}{\pi}\exp(-2e^{2r}x^2 - 2e^{-2r}p^2), \tag{3.5.11}$$

$$W_d(x,p) = \frac{2}{\pi}\exp[-2e^{2r}(x-x_0)^2 - 2e^{-2r}(p-p_0)^2]. \tag{3.5.12}$$

3.5.2 Inverse Radon transform

As described in the previous section, in order to reconstruct the Wigner function using the data from the Homodyne detection, one of traditional methods is the inverse Radon transform. The probability distribution $pr(x_\theta, \theta)$ obtained from homodyne detection and the Wigner function have the relation as

$$pr(x_\theta, \theta) = \int_{-\infty}^{\infty} W(x_\theta \cos\theta - p_\theta \sin\theta, p_\theta \sin\theta + p_\theta \cos\theta) dp. \tag{3.5.13}$$

The relation is called Radon transform. In experiment, we usually use an reverse transform to reconstruct the Wigner function from the probability distribution $pr(x_\theta, \theta)$, this method is called inverse Radon transform. First, we perform a Fourier transform on Eq.(3.5.13) into

$$\begin{aligned} pr(\xi, \theta) &= \int_{-\infty}^{\infty} pr(x_\theta, \theta) \exp(-i\xi x_\theta) dx_\theta \\ &= \int_{-\infty}^{\infty}\int_{-\infty}^{\infty} W(x_\theta \cos\theta - p_\theta \sin\theta, p_\theta \sin\theta + p_\theta \cos\theta) \exp(-i\xi x_\theta) dx_\theta dp_\theta \\ &= \int_{-\infty}^{\infty}\int_{-\infty}^{\infty} W(x, p) \exp(-i\xi x \cos theta - i\xi p \sin\theta) dx dp, \end{aligned} \tag{3.5.14}$$

here we set $x = x_\theta \cos\theta - p_\theta \sin\theta$ and $p = p_\theta \sin\theta + p_\theta \cos\theta$.

Then we perform a Fourier transform on Wigner function,

$$\tilde{W}(\upsilon, \nu) = \int_{-\infty}^{\infty}\int_{-\infty}^{\infty} W(x, p) \exp(-i\upsilon x - i\nu p) dx dp, \tag{3.5.15}$$

which has the same form with Eq.(3.5.14), thus we can obtain

$$pr(\xi, \theta) == \int_{-\infty}^{\infty} pr(x_\theta, \theta) \exp(-i\xi x_\theta) dx_\theta = \tilde{W}((\xi \cos\theta, \xi \sin\theta). \tag{3.5.16}$$

Then we perform a inverse Fourier transform on Eq. (3.5.15),

$$\begin{aligned} W(x, p) &= \frac{1}{(2\pi)^2} \int_{-\infty}^{\infty}\int_{-\infty}^{\infty} \tilde{W}(\upsilon, \nu) \exp(-i\upsilon x - i\nu p) d\upsilon d\nu \\ &= \frac{1}{(2\pi)^2} \int_{-\infty}^{\infty}\int_{0}^{\pi} \tilde{W}((\xi \cos\theta, \xi \sin\theta)|\xi| \exp(ix\xi \cos\theta + ip\xi \sin\theta) d\theta d\xi \\ &= \frac{1}{(2\pi)^2} \int_{-\infty}^{\infty}\int_{0}^{\pi}\int_{-\infty}^{\infty} pr(x_\theta, \theta)|\xi| \exp[i\xi(x \cos\theta + p \sin\theta - x_\theta)] dx_\theta d\theta d\xi. \end{aligned} \tag{3.5.17}$$

This equation is known as inverse Radon transform. In Eq.(3.5.17), the ξ integration term is independence with the probability distribution $pr(x_\theta, \theta)$, and we can write it as

$$K(\alpha) = \frac{1}{2} \int_{-\infty}^{\infty} |\xi| \exp(i\xi\alpha) d\xi \tag{3.5.18}$$

Thus we can obtain the Wigner function by inverse Radon transform as

$$W(x, p) = \frac{1}{2\pi^2} \int_{0}^{\pi}\int_{-\infty}^{\infty} pr(x_\theta, \theta) K(x \cos\theta + p \sin\theta - x_\theta) dx_\theta d\theta. \tag{3.5.19}$$

3.5.3 Data processing of inverse Radon transform

In experiments, the probability distribution $pr(x_\theta, \theta)$ can be obtained from homodyne detection. Actually, the Eq.(3.5.19) and $pr(x_\theta, \theta)$ are function with continuous value with $-\infty \leq x \leq \infty$ and $0 \leq \theta \leq \pi$, but the data from the experiment is discrete value, hence, the Eq.(3.5.19) should be calculated not as integral but as a sum of discrete value. First, to calculate the $pr(x_\theta, \theta)$, we divided the x_θ and θ into N equal parts and every part is δx and $\delta\theta$, thus the Eq.(3.5.19) is re-written as

$$W(x,p) = \frac{1}{2\pi^2} \sum_{i=1}^{N_x} \sum_{j=1}^{N_\theta} pr(x_i, \theta_j) K(x\cos\theta_j + p\sin\theta_j - x_i)\delta x \delta\theta. \tag{3.5.20}$$

and the Eq. (3.5.18) is approximated as,

$$\begin{aligned} K(\alpha) &\cong \frac{1}{2}\int_{-k_c}^{k_c} |\xi| \exp(i\xi\alpha) d\xi \\ &= \frac{1}{\alpha^2}[\cos(k_c\alpha) + k_c\alpha \sin(k_c\alpha) - 1]. \end{aligned} \tag{3.5.21}$$

where k_c is cut off parameter. In experiment, $K(\alpha)$ acts as a low pass filter. With this filter function, we can reproduce the continuous Wigner function by using discrete data which measured from homodyne detection. We should choose an appropriate $K(\alpha)$ to reconstruct the Wigner function in our experiment. The Fig.3.26 shows $K(\alpha)$ as a function of α when $k_c = 5$.

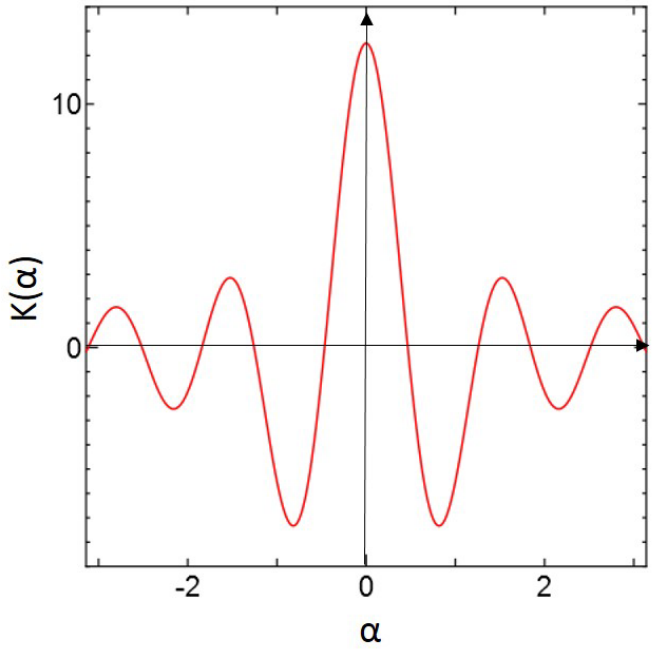

Fig. 3.26. $K(\alpha)$ as a function of α when $k_c = 5$.

3.5.4 Experimental setup and results of homodyne tomography

The experimental setup is shown in Fig. 3.27. The electronic signal of the homodyne detector was amplified, band-pass filtered, mixed-down at 11 MHz, and low-pass filtered. Then they were sampled by a 12-bit digital-analog-convertor (DAC) at the rate of 240 kS/s. And the relative phase of the squeezed beam and the LO beam is driven by a PZT with amplitude 12 V_{p-p} and frequency with 0.05 Hz.

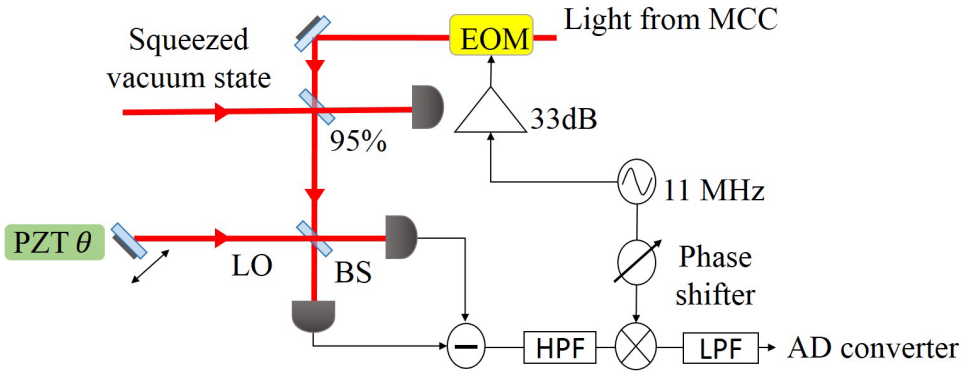

Fig. 3.27. Experimental set up of homodyne tomography.

In our experiment, we reconstruct the Wigner function of vacuum state, coherent state, amplitude quadrature squeezed state and phase quadrature squeezed state. The measurement results are shown in Fig.3.28 and Fig.3.29, respectively.

3.6 Summary

In this chapter, we experimentally produced squeezed vacuum state from a DOPA. By choosing appropriate relative phase between the pump beam and injection beam, the OPA can be controlled to deamplify or amplify the injection beam, the amplitude quadrature and phase quadrature squeezed state with the squeezing -1dB and anti-squeezing of 1.7 dB in the range of 5MHz to 35MHz were generated. To obtain a purer squeezed state which is very important in two-photon interference, we detected the squeezed state at the 11MHz, and obtained the amplitude quadrature squeezed state with purity of $V^0 * V^{\frac{\pi}{2}} = 1.13$ and the phase quadrature squeezed state with purity of $V^0 * V^{\frac{\pi}{2}} = 1.04$.

We also introduced the Wigner function and the principle of reconstruction of Wigner function by inverse Radon transform. Using the data from homodyne tomography, we reconstructed the Winger function of different states which were generated in our experiment. The reconstructed states are consistent with the results which were observed on the spectrum analyzer (SA).

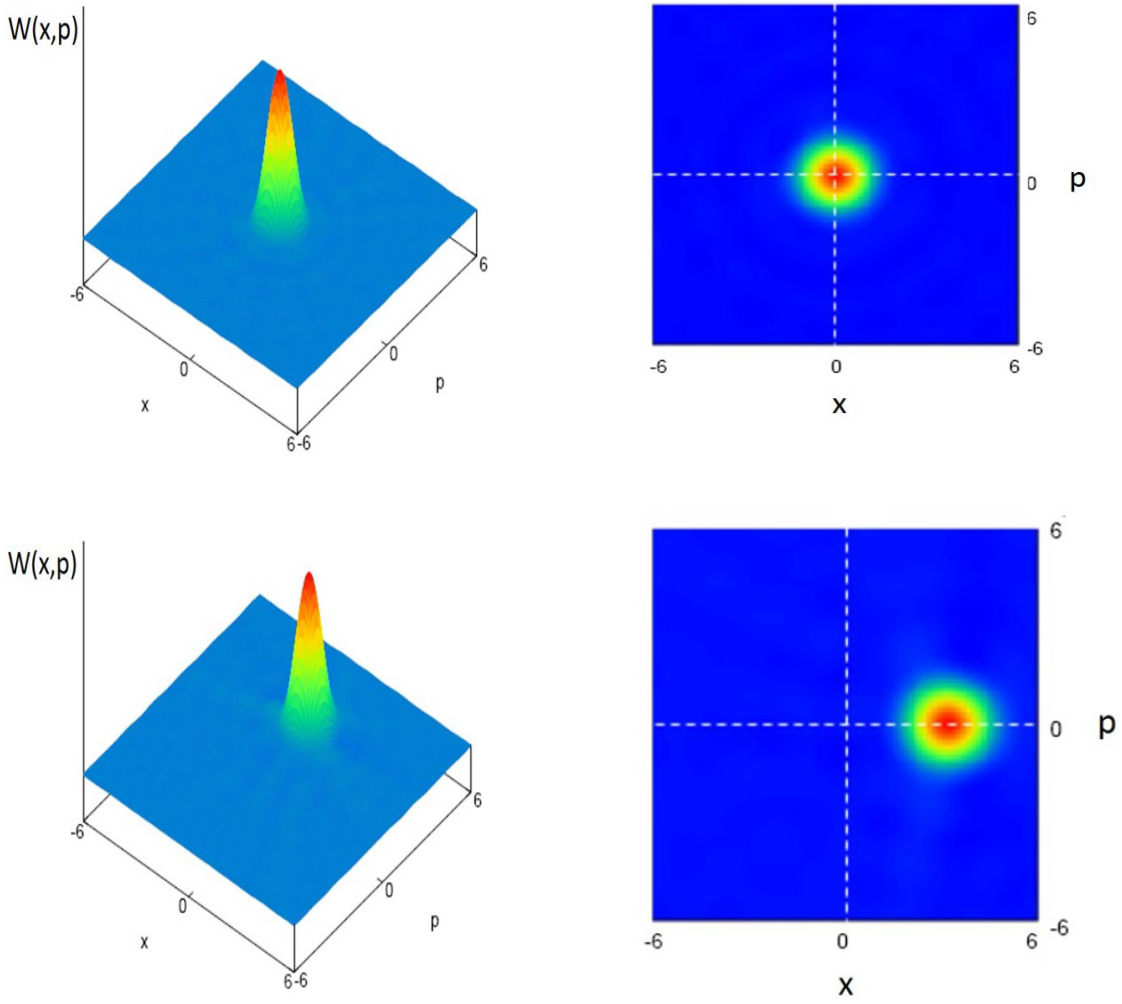

Fig. 3.28. Wigner function of light states. above: vacuum state, below: coherent state. left: Wigner function, right: Wigner function observing from the top

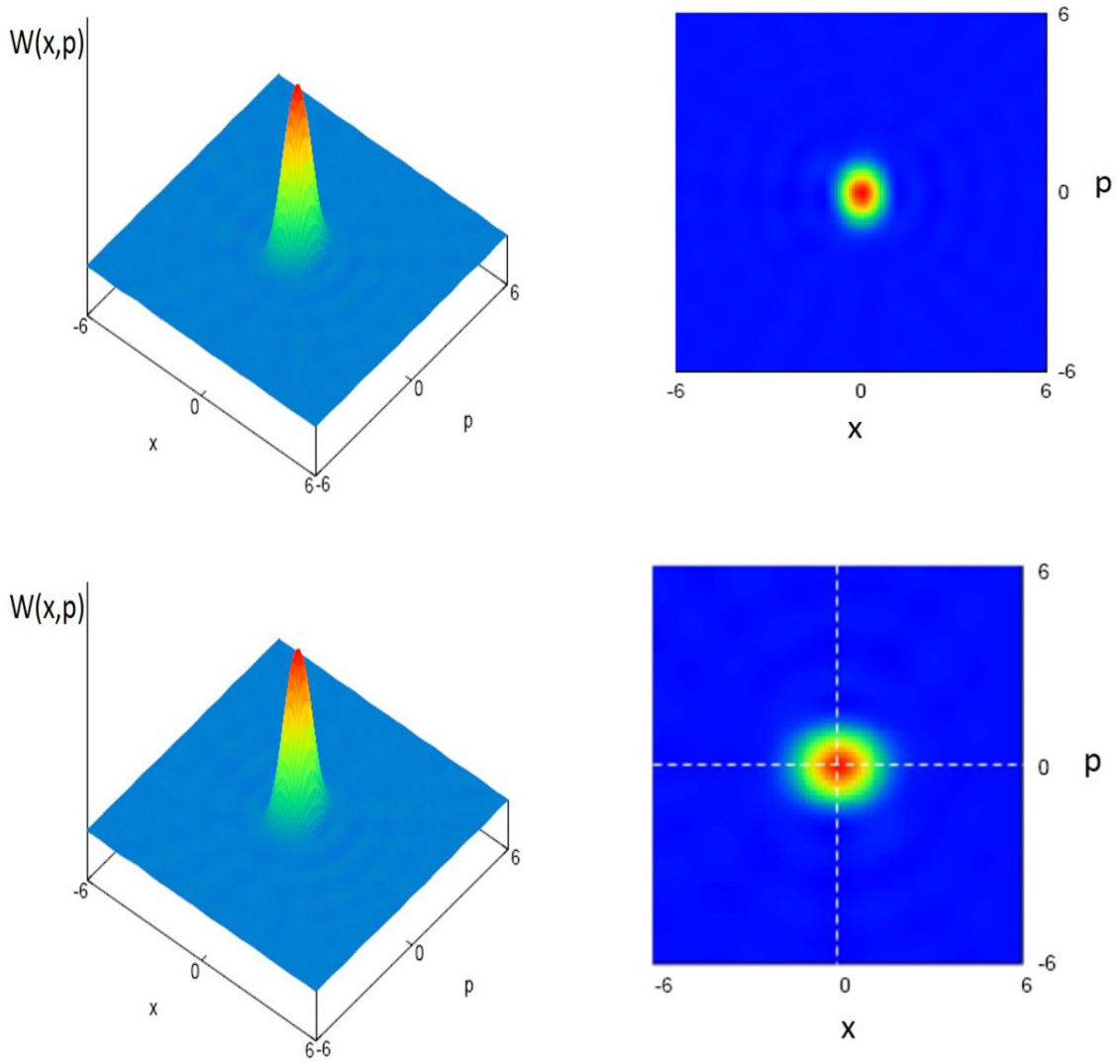

Fig. 3.29. Wigner function of a squeezed vacuum state. above: amplitude quadrature state, below: phase quadrature state. left: Wigner function, right: Wigner function observing from the top.

Chapter4 Two-photon interference with continuous variables

In this chapter, we will report an experimental observation of a two-photon interference between a squeezed vacuum state from an optical parametric amplifier and a weak coherent state on a beam splitter with continuous variables. In the first section, we will briefly introduce the two-photon interference between a squeezed vacuum state and a weak coherent state. secondly, we will introduce the principle of the two-photon interference with continuous wave light. Thirdly, we will introduce the generation of displaced squeezed state. The measurement system will be introduced in the fourth section. At last, the experimental results and discussion will be introduced.

4.1 Introduction

In 1974, Stoler [89] proposed a theoretical scheme to observe anti-bunching effect, where a squeezed vacuum state from parametric down-conversion and a coherent state were used. This phenomenon was first demonstrated experimentally by Koashi [10] with two-photon interference between a squeezed vacuum state and a weak coherent state using a pico-second pulse laser in 1993. Later, such a two-photon interference was also observed by interfering the squeezed vacuum state with a coherent state on a beam splitter [11]. Since then, both the two-photon interference and its applications with pulsed laser source have been extensively studied in experiment [90–95]. Recently, , the complex wave functions, which provides complete information of a quantum state, for biphoton state have also been measured by two-photon interference [72, 73]. In most of these experiments, the coherence length and time delay between two photons were measured when interference occurred. Thus, a technique of single photon counting and modules (SPCM) was usually employed to interrogate the strong correlation between photons, and pulsed lasers were the most suitable light sources. For a continuous wave light source, it was also suggested that an anti-bunched field can be produced by homodyning of an output from an OPO with a strong coherent local oscillator. It is also turned out that the underlying principle is two-photon interference [96, 97]. However, it is not easy to observe continuous wave two-photon interference because it is difficult to separate correlated photon pairs from the broadband emission of a sub-threshold OPO. Recently, this shortcoming was overcome by an optical filter cavity [98] or an atomic filter [72], and two-photon interference with continuous wave field was observed by employing an OPA with the technique of SPCM. Yet, the observation of two-photon interference on a beam splitter still remains a technical challenge.

Different from previous experiments, we used homodyne detection technique in our experiment. Hence, the output beam from the OPA is mixed with a strong LO beam on a beam splitter, and only one mode, which is completely matched to the LO, is probed. By choosing the phase of the LO, two orthogonal amplitude quadratures of a signal are recorded. To investigate photon statistics, one of important approaches is reconstruct the photon number probability distributions using homodyne tomography technique. This technique has been widely used to characterize aggregate measures of a quantum state in the past decade [99]. On the other hand, using the measured amplitude quadratures, we can also obtain the second-order correlation function of measured field [71]. Up to now, the correlation measurement technique gives another important approach to investigate nonclassical properties of light fields in quantum optics [71]. This approach is first used to measure the entanglement between two light fields [100]. Recently, it was also employed to characterize squeezed state by analyzing the correlation between two output photocurrents of two balanced homodyne detectors [101]. It was found that the estimation of squeezing degree is independent of the amount of electronic noise, which is a crucial issue in homodyne detection system. In this thesis, we will give the correlation between two amplitude quadratures which can estimate the photon statistics and demonstrate two-photon interference.

In this chapter, we will experimentally observe a two-photon interference between a squeezed vacuum state and a coherent state with continuous variables for the first time. The homodyne detection technique will be used to select two-photon state for interference from the broadband emission of the OPA. The photon anti-bunching or bunching , which is corresponding to destructive or constructive two-photon interference, will be observed when amplitude squeezed vacuum state or phase squeezed vacuum state interfere with a coherent field, respectively.

4.2 Continuous wave two-photon interference

4.2.1 Principle of continuous wave two-photon interference

To understand how two-photon interference occurs, let us consider a principle scheme shown in Fig. 4.1. A continuous wave coherent state and a squeezed vacuum state from OPA are interfered on an arbitrary beam splitter. We consider one of the output states which is split by a 50:50 beam splitter and measured by two set of homodyne detectors. For simplicity, we only treat it with a simple single mode model and both parametric gain of the OPO and the amplitude of coherent state are not significant. It means that the average photon number of both squeezed vacuum state and coherent sate are far less than one. Thus, we can write the input states as below,

$$|\Psi_{in}\rangle \approx |0,0\rangle + \alpha|0,1\rangle + \frac{\alpha^2}{\sqrt{2}}|0,2\rangle - \frac{\zeta}{\sqrt{2}}|2,0\rangle, \tag{4.2.1}$$

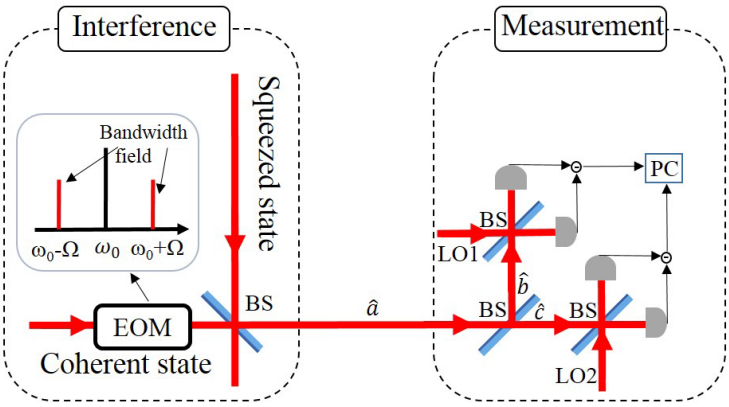

Fig. 4.1. Principle scheme of cw two-photon interference.

in which the squeezed vacuum state is generated from an OPA,

$$|\Psi_{\text{OPO}}\rangle \approx |0\rangle - \frac{\zeta}{\sqrt{2}}|2\rangle, \tag{4.2.2}$$

where ζ is proportional to the level of squeezing and $|\zeta| \ll 1$ (it is a weak squeezed vacuum state) and the coherent state is

$$|\alpha\rangle \approx |0\rangle + \alpha|1\rangle + \frac{\alpha^2}{\sqrt{2}}|2\rangle, \tag{4.2.3}$$

where α is complex amplitude of the coherent state with $|\alpha| \ll 1$. In chapter 2, a beam splitter of 50:50 was given to demonstrate the two-photon interference between a squeezed vacuum state and a coherent state. Here, without loss of generality, an arbitrary beam splitter with transmissivity (t) and reflectivity (r) [44] is used, and the output states can be listed as:

$$|0,0\rangle_{out} = |0,0\rangle \tag{4.2.4}$$
$$|0,1\rangle_{out} = r\,|0,1\rangle + t\,|1,0\rangle \tag{4.2.5}$$
$$|0,2\rangle_{out} = r^2\,|2,0\rangle + t^2\,|0,2\rangle + \sqrt{2}tr\,|1,1\rangle \tag{4.2.6}$$
$$|2,0\rangle_{out} = t^2\,|2,0\rangle + r^2\,|0,2\rangle - \sqrt{2}tr\,|1,1\rangle\,. \tag{4.2.7}$$

Up to two-photon term, we then have the output state as

$$\begin{aligned}|\Psi_{out}\rangle = |0,0\rangle + r\alpha|1,0\rangle + t\alpha|0,1\rangle + (\alpha^2+\zeta)tr|1,1\rangle \\ + \frac{1}{\sqrt{2}}[(r^2\alpha^2 - t^2\zeta)|2,0\rangle + (t^2\alpha^2 - r^2\zeta)|0,2\rangle].\end{aligned} \tag{4.2.8}$$

We are only interested in the state from one output of the beam splitter, it can be writen as

$$\begin{aligned}|\Psi_{out1}\rangle &= |0\rangle + [r\alpha + (\alpha^2+\zeta)tr]|1\rangle + \frac{1}{\sqrt{2}}(r^2\alpha^2 - t^2\zeta)|2\rangle \\ &\approx |0\rangle + r\alpha|1\rangle + \frac{1}{\sqrt{2}}(r^2\alpha^2 - t^2\zeta)|2\rangle.\end{aligned} \tag{4.2.9}$$

where $|r^2\alpha^2| \sim |t^2\zeta| << |r\alpha|$ is used since $|\alpha| << 1$, and $|r|^2, |t|^2 < 1$. The two-photon rate is given by

$$R_2 = |\frac{1}{\sqrt{2}}(r^2\alpha^2 - t^2\zeta)|^2. \tag{4.2.10}$$

When $r^2\alpha^2 = t^2\zeta$, the two-photon rate can be completely cancelled and destructive two-photon interference occurs by interfering an amplitude squeezed state with a coherent state. On the other hand, the two-photon rate can be larger than that of the coherent sate by employing phase squeezed state and constructive two-photon interference occurs. To suppress the optics loss and maximally utilize the squeezed vacuum state, we may choose a beam splitter with $|r|^2 \approx 1$. In our experiment, we choose a beam splitter with reflectivity of 95%.

Up to now, most of experiments on two-photon interference were extensively demonstrated by directly measuring the two-photon rate with two single photon counting modules (SPCMs). One click of SPCM mean that an individual photon was detected on the central frequency of the measured field with a bandwidth of from several MHz to THz. The two-fold coincidence only measured two-photon rate of the output state in Eq. (4.2.9). For continuous wave field, homodyne detection is a traditional detection technique. In a homodyne detection system, a measured field is mixed with a LO on a symmetric beam splitter. This means that the output of the homodyne detection gives the information of the complex amplitudes of whole wave light field but not only the two-photon rate. Unlike SPCM system, the homodyne detection technique gives the quadrature amplitude of the measured field on a given sideband frequency. Fortunately, it is possible to calculate the photon statistics of the field with the measured quadrature amplitudes. One of well-known techniques is quantum tomography. Another method is to calculate the second-order correlation function from the measured quadrature amplitudes [71].

The second-order correlation function of the output state in Eq. (4.2.9) can be given as

$$\begin{aligned} g^{(2)}(0) &= \frac{\langle a^\dagger a^\dagger a a\rangle}{\langle a^\dagger a\rangle^2} \\ &= \frac{(\alpha^2 r^2 - \eta t^2)^2}{(\alpha^2 r^2 - \eta t^2)^4 + \alpha^4 r^4 + 2\alpha^2 r^2(\alpha^2 r^2 - \eta t^2)^2} \\ &= \begin{cases} 0 & \alpha^2 r^2 = \eta t^2, \\ \frac{4}{1+8\alpha^2 r^2 + 16\alpha^4 r^4} \approx 4, & \alpha^2 r^2 = -\eta t^2, \end{cases} \end{aligned} \tag{4.2.11}$$

where $|\alpha r| << 1$ is considered. Obviously, $g^{(2)}(0) = 0$ indicates photon anti-bunching effect for completely destructive two-photon interference and $g^{(2)}(0) \approx 4$ displays photon bunching effect for constructive two-photon interference. In a practical experiment, it is difficult to observe $g^{(2)}(0) = 0$ due to the purity of the squeezed state and un-unity detection efficiency. Hence, $g^{(2)}(0) < 1$ indicates the two-photon destructive interference and $g^{(2)}(0) > 1$ gives the two-photon constructive interference. Thus the second-order correlation function can be used to interrogate two-photon interference.

Since using homodyne detection which is sensitive to the quadrature amplitudes of the measured state, we should re-write the Eq. (4.2.11) in term of two quadrature amplitudes. Using

$\hat{a} = \frac{1}{2}(\hat{X}_{\hat{a}}^{0} + i\hat{X}_{\hat{a}}^{\frac{\pi}{2}})$ and $\hat{a^{\dagger}} = \frac{1}{2}(\hat{X}_{\hat{a}}^{0} - i\hat{X}_{\hat{a}}^{\frac{\pi}{2}})$, Eq. (4.2.11) can be re-written as

$$g^{(2)}(0) = \frac{\sum_{\varphi}[\left\langle (\hat{X}_a^{\varphi})^4 \right\rangle + \left\langle (\hat{X}_a^{\varphi})^2 (\hat{X}_a^{\frac{\pi}{2}-\varphi})^2 \right\rangle - 8\left\langle (\hat{X}_a^{\varphi})^2 \right\rangle] + 12}{(\sum_{\varphi}\left\langle (\hat{X}_a^{\varphi})^2 \right\rangle - 2)^2}, \tag{4.2.12}$$

where $\varphi = 0, \frac{\pi}{2}$. The Eq. (4.2.11) gives a another method to measure the second-order correlation function and provides a connection between discrete variables and continuous variables in quantum optics regime. Unfortunately, what makes this measurement impossible is that there are cross-quadrature terms for a single mode. However, in practice experiment, we can realize the measurement by separating the beam into two parts and detecting their correlation with a modified Hanbury-Brown and Twiss (HBT) interferometer. Since the second-order correlation function charactizes photon statistics while quadrature amplitudes come from complex amplitude of wave light field, Eq. (4.2.12) gives a direct evidence of wave-particle duality of light.

4.2.2 Second-order correlation function from a modified HBT interferometer

As mentioned in previous section, the second-order correlation function $g^{(2)}(0)$ is impossible to be measured in the form of Eq. (4.2.12) because there are cross-quadrature terms for a single mode, which can not be measured simultaneously. In experiment, we can separate the generated signal mode $\hat{a}$ into mode $\hat{b}$ and mode $\hat{c}$ with a 50:50 beam splitter, and measure the intensity correlation between them by a modified HBT interferometer, as shown in Fig. 4.2.

$$g_{b,c}^{(2)}(0) = \frac{\langle b^{\dagger}bc^{\dagger}c\rangle}{\langle b^{\dagger}b\rangle\langle c^{\dagger}c\rangle}. \tag{4.2.13}$$

If $\hat{b} = (\hat{a} + \hat{\nu})/\sqrt{2}$ and $\hat{c} = (\hat{a} - \hat{\nu})/\sqrt{2}$ with $\hat{\nu}$ is a vacuum mode, the Eq. (4.2.11) and Eq. (4.2.13) become equivalent, namely, $g_a^{(2)}(0) = g_{b,c}^{(2)}(0)$. Thus we can use this method to measure the $g_a^{(2)}(0)$.

As shown in Fig. 4.2, two homodyne detection systems are employed to record their quadrature amplitudes,

$$\hat{X}_{\hat{b}}^{\theta} = e^{i\theta}\hat{b}^{\dagger} + e^{-i\theta}\hat{b}, \tag{4.2.14}$$

$$\hat{X}_{\hat{c}}^{\phi} = e^{i\phi}\hat{c}^{\dagger} + e^{-i\phi}\hat{c} \tag{4.2.15}$$

where $\hat{b}^{\dagger}(\hat{c}^{\dagger})$ and $\hat{b}(\hat{c})$ are creation and annihilation operators for mode b and mode c. θ and ϕ are relative phase between beam $b(c)$ and LO and can be actively controlled to choose an appropriate value. $\theta(\phi) = 0$ and $\theta(\phi) = \frac{\pi}{2}$ indicate quadrature amplitude and quadrature phase of mode b and mode c, respectively. Thus we can obtain

$$\hat{b} = \frac{1}{2}(\hat{X}_b^{0} + i\hat{X}_b^{\frac{\pi}{2}}) \tag{4.2.16}$$

$$\hat{b}^{\dagger} = \frac{1}{2}(\hat{X}_b^{0} - i\hat{X}_b^{\frac{\pi}{2}}). \tag{4.2.17}$$

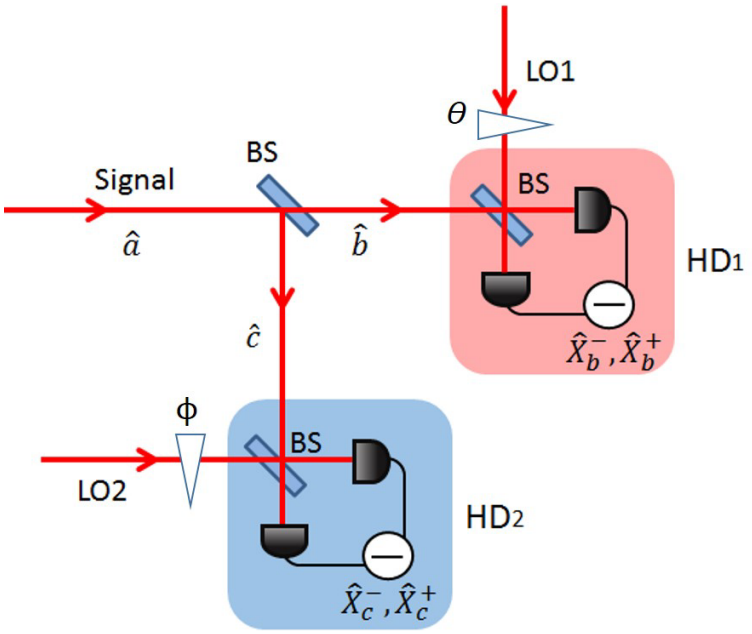

Fig. 4.2. Principle setup of measuring $g^{(2)}(0)$ with two HD systems.

Then we can calculate $\hat{b}^\dagger\hat{b}$ as,

$$\begin{aligned}\hat{b}^\dagger\hat{b} &= \frac{1}{4}[(\hat{X}_b^0)^2 + (\hat{X}_b^{\frac{\pi}{2}})^2 + i(\hat{X}_b^0\hat{X}_b^{\frac{\pi}{2}} - \hat{X}_b^{\frac{\pi}{2}}\hat{X}_b^0)] \\ &= \frac{1}{4}[(\hat{X}_b^0)^2 + (\hat{X}_b^{\frac{\pi}{2}})^2 - 2], \end{aligned} \tag{4.2.18}$$

here we used commutation relation

$$[\hat{X}_k^0, \hat{X}_l^{\frac{\pi}{2}}] = 2i\delta_{kl} = \begin{cases} 2i & k = l, \\ 0, & k \neq l. \end{cases} \tag{4.2.19}$$

Similarly, $\hat{c}^\dagger\hat{c}$ is obtained as

$$\hat{c}^\dagger\hat{c} = \frac{1}{4}[(\hat{X}_c^0)^2 + (\hat{X}_c^{\frac{\pi}{2}})^2 - 2], \tag{4.2.20}$$

Inserting Eq (4.2.18) and Eq (4.2.20) into Eq (4.2.13), and it can be re-expressed as

$$g^{(2)}(0) = g_{b,c}^{(2)}(0) = \frac{\sum_{\theta,\phi}\langle(\hat{X}_b^\theta)^2(\hat{X}_c^\phi)^2\rangle - 2[\sum_\theta\langle(\hat{X}_b^\theta)^2\rangle + \sum_\phi\langle(\hat{X}_c^\phi)^2\rangle] + 4}{(\sum_\theta\langle(\hat{X}_b^\theta)^2\rangle - 2)(\sum_\phi\langle(\hat{X}_c^\phi)^2\rangle - 2)}. \tag{4.2.21}$$

In this equation, summations are made over the quadrature indices, $\theta(\phi) = 0, \frac{\pi}{2}$. Obviously, the cross-quadrature terms for a single mode disappear and this technique can be used to measure photon statistics. The absence of cross-quadrature terms mean that each correlation term can be independently measured by recording the information from the outputs of homodyne detectors, and then the $g^{(2)}(0)$ can be reconstructed.

To understand Eq. (4.2.21) easily, we transform the equation into a correlation measurement form. Using

$$\langle AB\rangle = \langle A\rangle + \langle B\rangle + \mathrm{cov}(A,B). \tag{4.2.22}$$

We re-express the intensity correlation between mode b and mode c using quadrature amplitudes as

$$\begin{aligned} g^{(2)}_{b,c}(0) &= \frac{\sum_{\theta,\phi}[\langle(\hat{X}_b^\theta)^2\rangle\langle(\hat{X}_c^\phi)^2\rangle] + \sum_{\theta,\phi}[cov((\hat{X}_b^\theta)^2,(\hat{X}_c^\phi)^2)] - 2[\sum_\theta\langle(\hat{X}_b^\theta)^2\rangle + \sum_\phi\langle(\hat{X}_c^\phi)^2\rangle] + 4}{\sum_{\theta,\phi}[\langle(\hat{X}_b^\theta)^2\rangle\langle(\hat{X}_c^\phi)^2\rangle] - 2[\sum_\theta\langle(\hat{X}_b^\theta)^2\rangle + \sum_\phi\langle(\hat{X}_c^\phi)^2\rangle] + 4} \\ &= \frac{\sum_{\theta,\phi} cov((\hat{X}_b^\theta)^2,(\hat{X}_c^\phi)^2)}{(\sum_\theta\left\langle(\hat{X}_b^\theta)^2\right\rangle - 2)(\sum_\phi\left\langle(\hat{X}_c^\phi)^2\right\rangle - 2)} + 1, \end{aligned} \tag{4.2.23}$$

where $cov((\hat{X}_b^\theta)^2,(\hat{X}_c^\phi)^2)$, $\left\langle(\hat{X}_b^\theta)^2\right\rangle$ and $\left\langle(\hat{X}_c^\phi)^2\right\rangle$ are the covariance and means of squared quadratures of the measured states. In experiment, we measure four permutations of quadratures independently, then calculate the covariance and means of squared quadratures, and finally reconstruct $g^{(2)}(0)$ according to Eq. (4.2.23).

Actually, the two-photon interference between a squeezed state and a coherent state on a beam splitter can also be considered as displacing a squeezed vacuum state. The displaced result can be expressed as

$$|\Psi_{out1}\rangle = \hat{D}(\alpha)\hat{S}(r)|0\rangle, \tag{4.2.24}$$

where $\hat{D}(\alpha)$ and $\hat{S}(r)$ are displacement and squeezing operators, respectively. To calculate the $g^{(2)}(0)$ simply, we perform the calculation in Heisenberg picture, which means that we start with a mode from the vacuum state, and transform the creation operator and annihilation operator with

$$\hat{D}^\dagger(\alpha)\hat{S}^\dagger(r)\hat{a}\hat{D}(\alpha)\hat{S}(r) = \alpha + \hat{a}\cosh(r) - \hat{a}^\dagger\sinh(r) \tag{4.2.25}$$

$$\hat{D}^\dagger(\alpha)\hat{S}^\dagger(r)\hat{a}^\dagger\hat{D}(\alpha)\hat{S}(r) = \alpha + \hat{a}^\dagger\cosh(r) - \hat{a}\sinh(r) \tag{4.2.26}$$

For make the derivation simple, we restrict α and r to be real quantities, and calculate the second-order correlation function $g^{(2)}(0)$ as [71]

$$\begin{aligned} g^{(2)}(0) &= \frac{\langle a^\dagger a^\dagger a a\rangle}{\langle a^\dagger a\rangle^2} \\ &= 1 + \frac{\sinh^2(r)[2\alpha^2 + \cosh(2r) - 2\alpha^2\coth(r)]}{[\alpha^2 + \sinh^2(r)]^2}. \end{aligned} \tag{4.2.27}$$

This expression is specific to pure state. To make our analysis more applicable to experiments, we can generalize Eq.(4.2.27) for any state which has the quadrature variance $V_a^0, V_a^{\frac{\pi}{2}}$ and displacement value α as,

$$g^{(2)}(0) = 1 + \frac{16\alpha^2(e^{-2r} - e^{-r}e^r) + 2(e^{2r} + e^{-2r} - 2e^{-r}e^r)(e^{-2r} + e^{2r})}{(e^{-2r} + e^{2r} - 2e^{-r}e^r + 4\alpha^2)^2}, \tag{4.2.28}$$

where $\sinh r = \frac{e^r - e^{-r}}{2}$ and $\cosh r = \frac{e^r + e^{-r}}{2}$ are used and the displacement α is also restricted to be real. We use the measured quadrature variance V_a^0 and $V_a^{\frac{\pi}{2}}$ to replace the squeezing (e^{-2r}) and anti-squeezing (e^{2r}) and re-express the Eq. (4.2.28) as:

$$g^{(2)}(0) = 1 + \frac{16\alpha^2\left(V_a^0 - \sqrt{V_a^0 V_a^{\frac{\pi}{2}}}\right) + 2\left(V_a^{\frac{\pi}{2}} + V_a^0 - 2\sqrt{V_a^0 V_a^{\frac{\pi}{2}}}\right)\left(V_a^0 + V^{\frac{\pi}{2}}\right)}{\left(V_a^0 + V_a^{\frac{\pi}{2}} - 2\sqrt{V_a^0 V_a^{\frac{\pi}{2}}} + 4\alpha^2\right)^2}, \tag{4.2.29}$$

Here we use $V_a^0 * V_a^{\frac{\pi}{2}}$ represents the purity of the measured state and $V_a^0 * V_a^{\frac{\pi}{2}} = 1$ indicates a pure squeezed state. This equation is also used to curve theoretical predictions of $g^{(2)}(0)$ for two measured quadrature variances V_a^0 and $V_a^{\frac{\pi}{2}}$ with various displacement of coherent state α for a mode a.

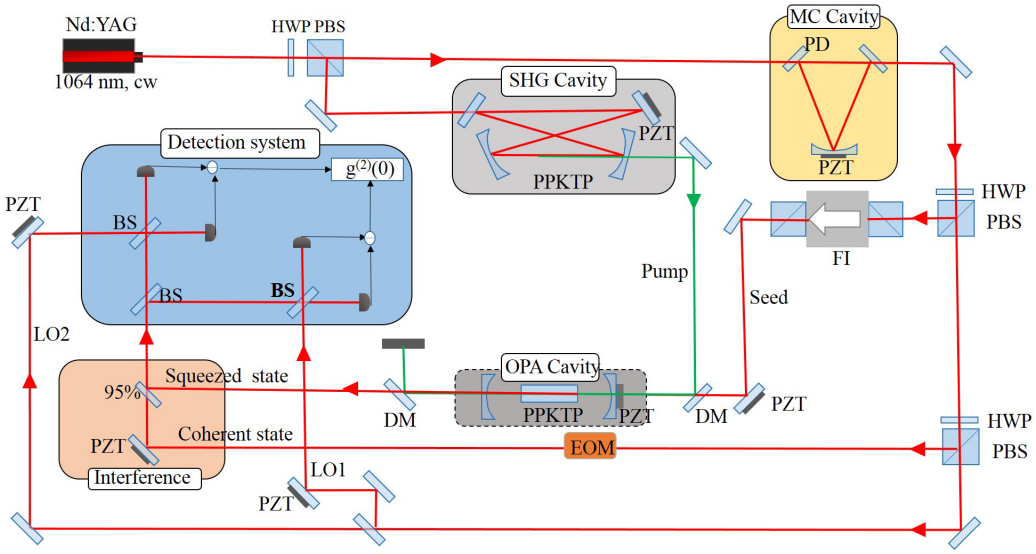

Fig. 4.3. Principle scheme of cw two-photon interference.

4.3 Two-photon interference between squeezed vacuum state and coherent state

The experimental setup is shown in Fig. 4.3. The experiment can be divided into three parts: preparation of coherent state, generation of displaced squeezed state and measurement of the second-order correlation function with homodyne detection. The coherent state is prepared by modulating the light from the MCC with a electro-optical modulator (EOM) on a sideband frequency 11MHZ, and then interfere with a squeezed vacuum state from the OPA, which is generate in the chapter 3, on a 95% beam splitter to generate a displaced squeezed state. The generated displaced squeezed state is split into two beams with a 50:50 beam splitter. Each of

the two output beam is measured a homodyne detector. After obtain the measured quadrature amplitude, we can calculate the correlation between the two mode b and c, and observe the photon anti-bunching and bunching effect of the measured state a.

4.3.1 Preparation of coherent state using a electro-optics modulator

Since the squeezed vacuum state was observed over a range of measurement frequencies, the interfered coherent state should be prepared on one of measurement frequencies by modulating the laser light with an electro-optical modulator (EOM). The principle of modulation has been discussed in chapter 2. Here we will discuss how to realize it in experiment, and we choose the modulation frequency at $\Omega = 11$MHz.

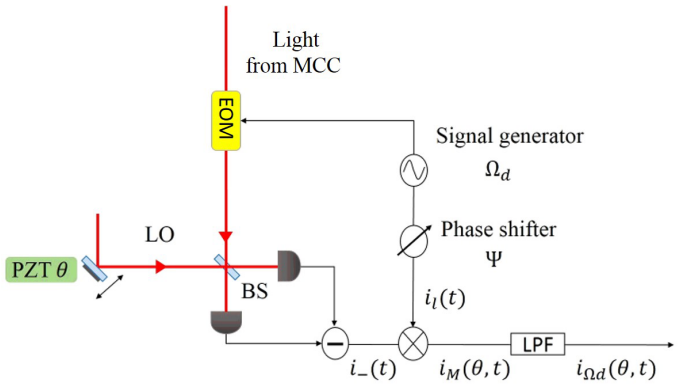

Fig. 4.4. Experimental setup of producing coherent state.

To realize a displacement of coherent state at the measurement frequency Ω, a part of power is transferred to the sidebands at Ω with a EOM driven by an wave function which provided an radio freqency (RF) signal at $\Omega = 11MHz$ with a modulation depth $M \ll 1$. The displacement depends on the modulation depth M, which can be actively controlled by varying amplitude of the modulation signal. As shown in Fig.4.4.

The modulated beam is measured by a homodyne detector, at whose a pair of matched photo-diodes (ETX500) with the quantum efficiency of 90% is employed. The output of the homodyne detector are amplified, band-pass filtered, mixed down at 11MHz, and low-pass filtered. Then they are sampled by a 12-bit DAC. To verify the system, we chose three different amplitudes of the signals from the wave function with $V_{p-p} = 0.5mV$, $0.8mV$ and $1.5mV$, and obtained coherent state with three different displacements with $\alpha = 0.2$, 0.6 and 1.2, as shown in Fig.4.5. This method obviously enables us to obtain an arbitrary displacement of coherent state as long as the power of the modulated sidebands is much smaller than that of the LO.

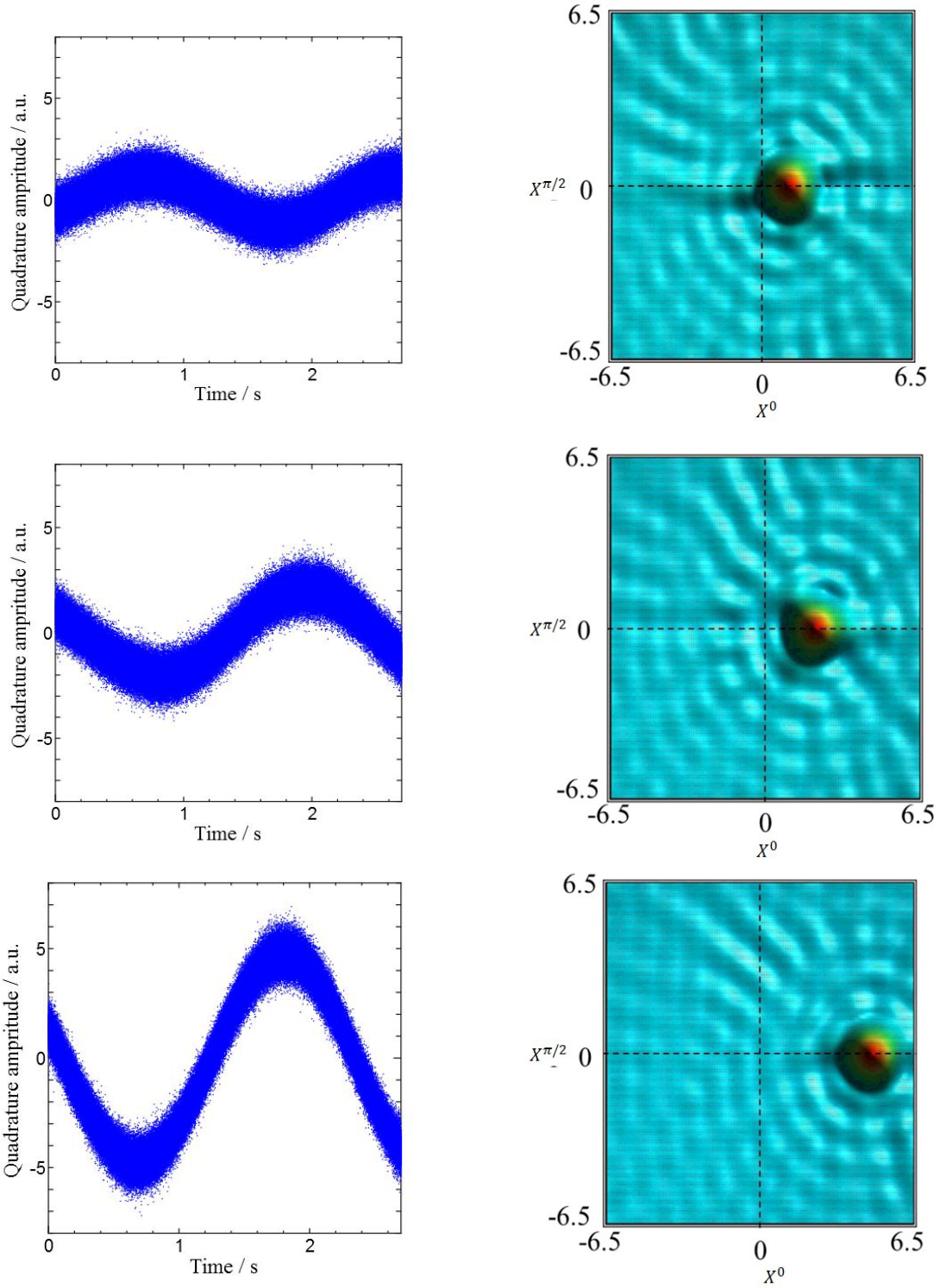

Fig. 4.5. Measured results of coherent state with different modulation depths

4.3.2 Interference between squeezed vacuum state and coherent state

As mentioned in previous section, the two-photon interference of a squeezed vacuum state and coherent state can be considered as displacing a squeezed vacuum state. Hence we will discuss the principle of generation displaced squeezed state in this section. We assume the modes of squeezed vacuum state and coherent state as $\hat{a}_{sq}$ and $\hat{a}_{coh}$, respectively. After combined on a high reflectivity beam splitter, the output state can be described as

$$\hat{a}_{out} = \sqrt{R}\hat{a}_{sq} + \sqrt{T}\hat{a}_{coh}, \tag{4.3.1}$$

where $R + T = 1$. We define the coherent state $\hat{a}_{coh} = \frac{\alpha}{\sqrt{T}} + \delta\hat{a}_{coh}$ with amplitude α,

$$\hat{a}_{out} = \sqrt{R}\hat{a}_{sq} + \alpha + \sqrt{T}\delta\hat{a}_{coh}, \tag{4.3.2}$$

For a high reflectivity beam splitter($R \to 1$), the output is re-expressed as

$$\hat{a}_{out} = \sqrt{R}\hat{a}_{sq} + \alpha. \tag{4.3.3}$$

In practice experiment, the transmissivity T can not be neglected, and this influence is treated as contamination of the vacuum field. In our experiment, we chose a beam splitter with reflectivity of 95%. The results can be further improved using a beam splitter with reflectivity of 98% or 99%.

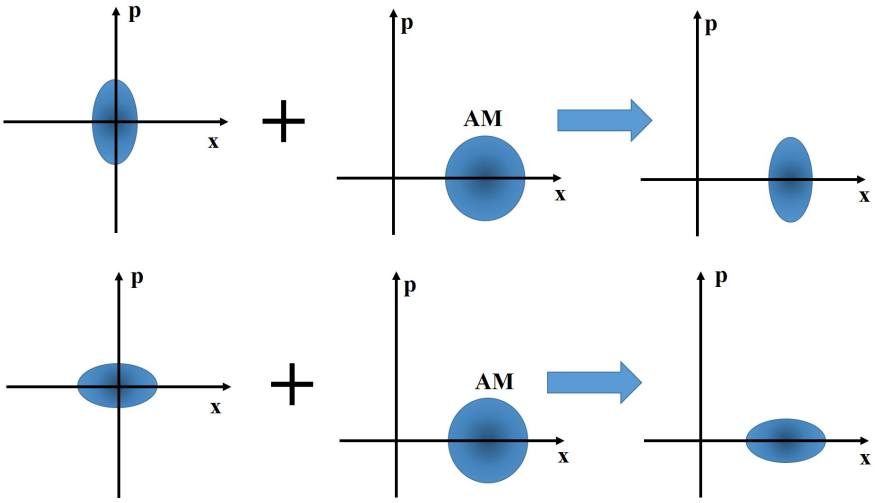

Fig. 4.6. Generation of displaced squeezed state.
above: displaced amplitude squeezed state, below: displaced phase squeezed state.

Then we introduce the effect of the displaced squeezed state. As discussed above, we can generate displaced squeezed state by interfering a squeezed vacuum state with a coherent state on a beam splitter. Actually, a displaced squeezed state also can be regarded as displacing a

squeezed vacuum state on a specific direction which was controlled by the phase of the coherent state. If the phase of the coherent state is 0, the generated displaced squeezed state can be regarded as displacing a squeezed vacuum state at amplitude direction or x direction. If the phase of the coherent state is $\frac{\pi}{2}$, the generated displaced squeezed state can be regarded as displacing a squeezed vacuum state at phase direction or p direction. In practice experiment, we can realize it by choosing different modulations (amplitude modulation and phase modulation). In our experiment, we generated two kinds of displaced squeezed states by displacing two kinds of squeezed vacuum state at x direction, as shown in Fig. 4.6.

We have produced two kinds of squeezed vacuum state (amplitude squeezed vacuum state and phase squeezed vacuum state) in chapter 3. Using these two kinds of squeezed vacuum states, we generated two kinds of displaced squeezed state by combining them with a coherent state produced by amplitude modulating the beam from the MCC on a 95:5 beam splitter. The principle setup is shown in Fig. 4.7.

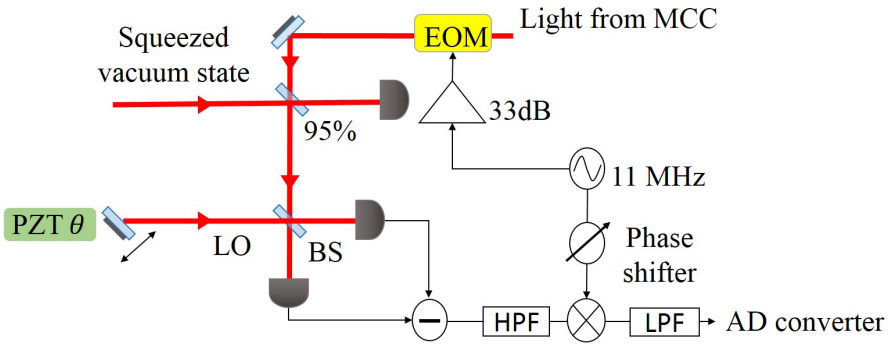

Fig. 4.7. The principle setup of two-photon interference.

The generated displaced squeezed beam combined with a LO beam on a 50:50 beam splitter and measured by a homodyne detector. The measurement and data acquisition systems (DAS) are as same as that in measurement of coherent state. To confirm the generated displaced squeezed states, we can reconstruct the Wigner function using the data from the homodyne tomography. As an example, we generated an amplitude squeezed state with $\{V^0 = 0.87, V^{\frac{\pi}{2}} = 1.27, \alpha = 0.39\}$ and a phase squeezed state with $\{V^0 = 0.88, V^{\frac{\pi}{2}} = 1.18, \alpha = 0.6\}$. The Winger function of the two displaced squeezed state were shown in Fig. 4.8. The obtained variance of quadrature amplitudes and the displacement will be inserted into Eq.(4.2.29) and used to plot the theoretical predictions of $g^{(2)}(0)$ for the two kinds of displaced squeezed states.

4.4 Measurement of second-order correlation function $g^{(2)}(0)$

4.4.1 Experimental setup of measurement system

In order to measure the second-order correlation function $g^{(2)}(0)$, we separated the generated displaced squeezed state into two beams with a 50:50 beam splitter, as shown in Fig. 4.10. The

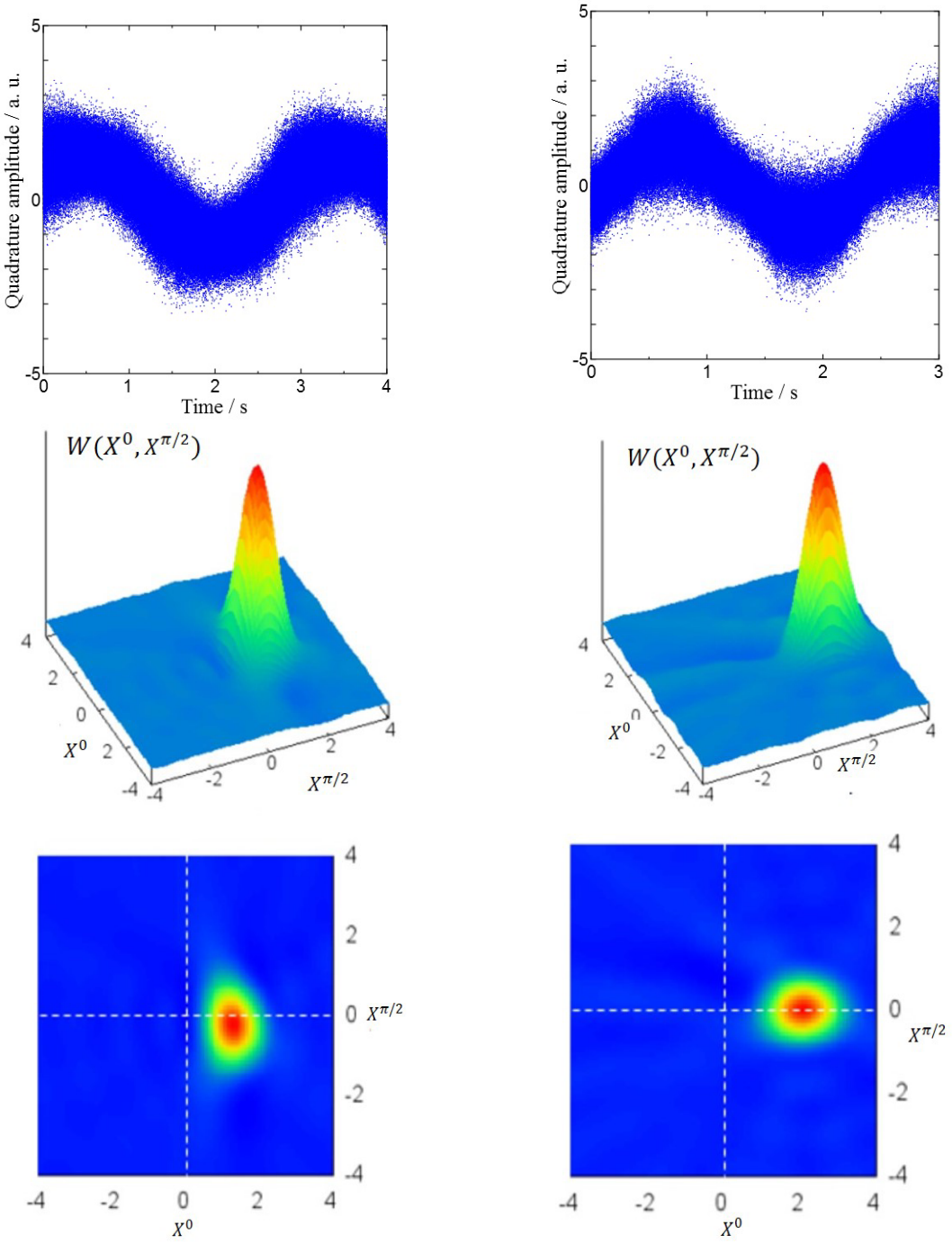

Fig. 4.8. Measurement results of displaced squeezed state.
left: displaced amplitude squeezed state, right: displaced phase squeezed state.

light from each output port of the beam splitter was received by two independent homodyne detector. The homodyne condition fulfilled by a signal/LO power ratio of 1:1000. The relative phase was actively controlled so as to measure the required either amplitude quadrature or phase

quadrature . We estimate the total detection efficiency of 83%. The fringe visibility among the LO beam, displaced beam and injection beam was shown in Table 4.1.

Table 4.1. Visibility among all beams.

	Visibility
LO1 and In1	98.%
LO2 and In2	98.%
LO1 and Dis1	92%
LO2 and Dis2	96%

LO:local oscillator beam, In: injection beam, Dis: displaced beam.

The photocurrents from the two photodiodes were subtracted from one another to give a signal that was proportional to the quadrature amplitudes of signal beam. The relative phase between the LO beam and displaced squeezed beam was controlled by a PZT mirror on the path of LO beam. It was used to adjust the optical path length of the LO beam. An error signal to lock the amplitude quadrature was accomplished by demodulating the amplitude modulation that was left over from the Pound-Drever-Hall (PDH) locking of the OPA cavity length (AC lock). The lock to the phase quadrature was obtained nulling the difference of the low-pass filtered photocurrents (DC lock).

After locking quadrature amplitudes stably, we can acquire the data from the homodyne detectors. The data acquired system is as same as that in homodyne tomography. Using the data from the homodyne tomography, we can calculate the covariance and means of squared quadratures, and finally reconstruct the $g^{(2)}(0)$ according to Eq.(4.2.23).

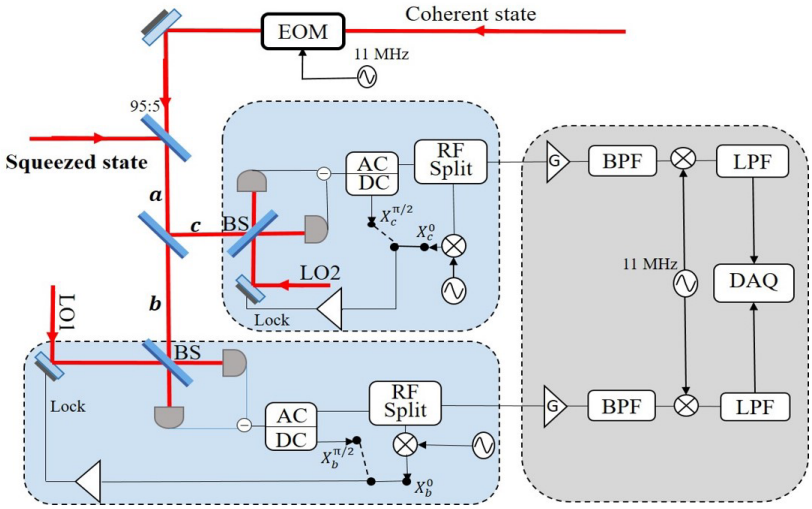

Fig. 4.9. Setup for measuring of $g^{(2)}(0)$.

4.4.2 Quadrature locking

To reconstruct the $g^{(2)}(0)$, we should first measure the amplitude quadrature and phase quadrature for the four permutations with $(X_b^0,\ X_c^0)$, $(X_b^0,\ X_c^{\frac{\pi}{2}})$, $(X_b^{\frac{\pi}{2}},\ X_c^0)$ and $(X_b^{\frac{\pi}{2}},\ X_c^{\frac{\pi}{2}})$. Hence, locking quadrature amplitudes stably is one of the most important and difficult work in our homodyne detection measurement. We locked the anti-squeezing phase with direct current (DC) lock and locked the squeezing phase with alternative current (AC) lock, respectively.

1. Locking quadrature phase using DC signal of the homodyne detector

To measure the phase quadrature of the electromagnetic field using homodyne detection signals, we locked the relative phase between the signal beam and LO beam on 0 or π. When the relative phase between signal beam and LO beam is 0 or π, after mixing the two beams on a 50:50 beam splitter, the two output intensities from the beam splitter are equal. The principle setup is shown in Fig. 4.11.

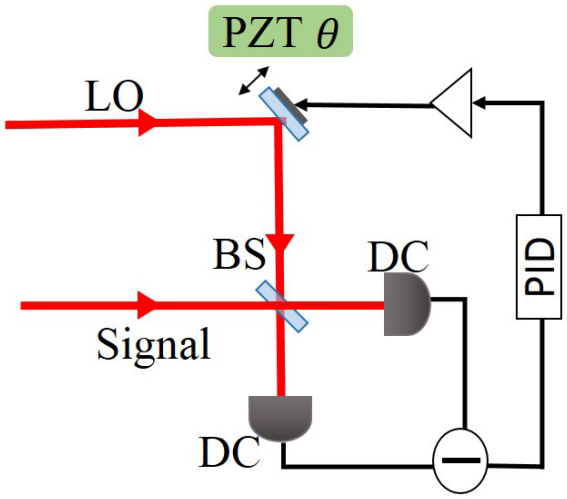

Fig. 4.10. The principle setup of locking quadrature phase.

As shown in Fig.4.11, the DC components from the two detectors are subtracted from one another and sent to proportional integral derivative controller (PID). By adjusting the PID, The feedback signal from PID is sent to a high-voltage amplifier and send to the PZT mirror on the LO beam. The optical path of the LO beam is controlled by scanning the PZT mirror which is driven by the amplified feedback signal. Thus the relative phase between the signal beam and LO beam can be controlled. The locking system locks the relative phase of the two beams to the position where the output from the subtractor is zero.

2. Locking quadrature amplitude using AC signal of the homodyne detector

Similarly, to measure the amplitude quadrature of the electromagnetic field with homodyne detector, we should lock the relative phase between the signal beam and LO beam on 0 or π.

When the relative phase between signal beam and LO beam is $\frac{\pi}{2}$ or $-\frac{\pi}{2}$, after interfering the two beams on a 50:50 beam splitter, one of the output intensity is maximum, while another is minimum. Hence we can lock one of the output beams at the maximum or minimum to make the relative phase between the signal beam and LO beam is $\frac{\pi}{2}$ or $-\frac{\pi}{2}$. The principle setup is shown in Fig. 4.12.

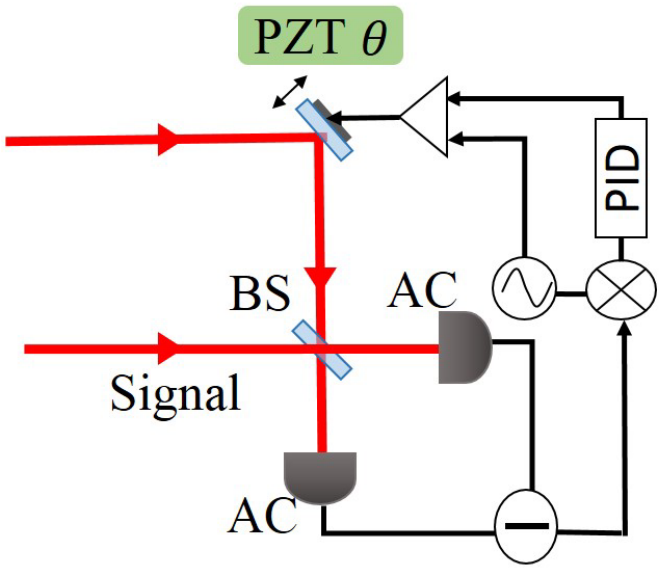

Fig. 4.11. The principle setup of locking quadrature amplitude.

As shown in Fig. 4.12, a 13 kHz sinusoidal modulation signal is generated from wave-function and sent to a high-voltage amplifier. Then the amplified modulation signal is sent to PZT mirror on the LO beam, and modulate the relative phase between the signal beam and LO beam. The AC components from the beam splitter are subtracted from one another and mix with a sinusoidal signal. Then the mixed signal is sent to PID and produce a error signal. The error signal is also sent to high-voltage amplifier and PZT mirror on the LO beam.

4.4.3 Experimental procedure for whole experiment

Then we will introduce the whole experimental procedure for measuring the $g^{(2)}(0)$, including producing the squeezed vacuum state, preparing the coherent state and acquiring the data. The main steps of the experiment are given as,

1. Mode match the 1064nm laser coherent light into SHG resonator and MCC resonator. Lock the length of the SHG cavity and lock the laser frequency to MCC, respectively.

2. Adjust the injection light into OPA cavity for optimal mode matched into resonator. Then, incident the pump light into the OPA and adjusted the two mirrors in the path of

the pump beam so as to obtain the maximum classical gain. Check that the lock is stable for de-amplification or amplification.

3. Adjust and measure the fringe visibility between LO beam1 & injection beam1, LO beam2 & injection beam2, LO beam1 & coherent beam1 and LO beam2 & injection beam2 by using two set of homodyne detectors.

4. Confirm the power balance for all beams on a spectrum analyzer.

5. Set the power of the pump beam, injection beam, coherent beam and LO beam with $P_p = 365mW$, $P_{in} = 1mW$, $P_{co} = 1.3mW$ and $P_{LO} = 32mW$

6. Re-lock the relative phase between pump beam and injection beam for de-amplification, re-lock the OPA cavity.

7. Check the squeezing level on a spectrum analyzer.

8. Adjust a modulation depth for EOM.

9. Lock the relative phase between the generated squeezed vacuum state and coherent state to produce a displaced squeezed beam.

10. Lock relative phase between LO beam and generated displaced squeezed state on two homodyne detectors and acquire the data. First lock to (X_b^0, X_c^0) and record data; then lock to (X_b^0, $X_c^{\frac{\pi}{2}}$) and record data; then lock to ($X_b^{\frac{\pi}{2}}$, X_c^0) and record data, then lock to ($X_b^{\frac{\pi}{2}}$, $X_c^{\frac{\pi}{2}}$) and record data. Block the squeezed vacuum beam and coherent beam, and detect the shot noise. Block all beam and detect the dark noise.

11. Change the modulation depth for EOM, and repeat the step 10.

12. Re-lock the relative phase in step 3 to amplification, and repeat the experiments for the same modulation depth.

13. Choose another squeezing level by adjusting the pump power and repeat the experimental procedure mention above.

4.5 Experimental results

The first step of our measurement is to measure the shot noise for the vacuum state, which is used to calibrate the displacement (α) of coherent state and the noise of all states generated in our experiment. The shot noise is obtained by measuring the noise current from one of homodyne detectors by blocking the signal beam, and this value serves as the unit of measurement for all the measured states.

4.5.1 The variance and the mean of the quadrature amplitudes

To investigate the two-photon interference, we should construct the second-order correlation function with Eq. (4.2.23) which can be calculated with covariances and means of squared quadrature of the mode b and c. Hence, we should first calculate the variances and means of the quadrature amplitudes of the mode b and c, respectively.

After the phase of the LO beams are actively locked, The amplitude quadrature and phase quadrature for beams b and c are recorded. After the data are stored, the variance, the mean, and covariance between beams b and c can be calculated. Here, we give two measured results for amplitude squeezed state with $\{V^0 = 0.87, V^{\frac{\pi}{2}} = 1.27, \alpha = 0.39\}$ and phase squeezed state with $\{V^0 = 0.88, V^{\frac{\pi}{2}} = 1.18, \alpha = 0.39\}$ from our series of measured data as example. Table 4.2 shows the means and the variances of four permutations of the quadrature measurements for amplitude squeezed state (ASS) and phase squeezed state (PSS).

Table 4.2. Variances and means of generated states.

	Quadrature	$\hat{X}_b^{\pi/2}$	$\hat{X}_b^0$	$\hat{X}_c^{\pi/2}$	$\hat{X}_c^0$
ASS	Variance	1.30	0.95	1.22	0.93
	Mean	0	0.82	0	0.75
PSS	Variance	0.99	1.06	0.97	1.06
	Mean	0	0.80	0	0.75

ASS: amplitude squeezed state, PSS: phase squeezed state.

Obviously, for the amplitude squeezed state, the variance of amplitude quadrature is below the shot noise limit, while the phase quadrature is above the shot noise limit. One the other hand, the variance of phase quadrature is below the shot noise limit and the variance of amplitude quadrature is above the shot noise limit for the phase squeezed state. The means of the quadrature amplitudes are used to determine the displacement (α) of the coherent state which can be controlled by amplitude modulating the laser light with an EOM.

4.5.2 Calculation of $g^{(2)}(0)$ with correlation measurement

To calculate $g^{(2)}(0)$, a convenient approach is to construct its covariance matrix for the squared quadratures of the four permutations. The covariance matrix is described as

$$\sigma_{b,c} = \begin{pmatrix} \langle((\hat{X}_b^{\frac{\pi}{2}})^2)^2\rangle & \langle(\hat{X}_b^{\frac{\pi}{2}})^2(\hat{X}_b^0)^2\rangle & \langle(\hat{X}_b^{\frac{\pi}{2}})^2(\hat{X}_c^{\frac{\pi}{2}})^2\rangle & \langle(\hat{X}_b^{\frac{\pi}{2}})^2(\hat{X}_c^0)^2\rangle \\ \langle(\hat{X}_b^0)^2(\hat{X}_b^{\frac{\pi}{2}})^2\rangle & \langle((\hat{X}_b^0)^2)^2\rangle & \langle(\hat{X}_b^0)^2(\hat{X}_c^{\frac{\pi}{2}})^2\rangle & \langle(\hat{X}_b^0)^2(\hat{X}_c^0)^2\rangle \\ \langle(\hat{X}_c^{\frac{\pi}{2}})^2(\hat{X}_b^{\frac{\pi}{2}})^2\rangle & \langle(\hat{X}_c^{\frac{\pi}{2}})^2(\hat{X}_b^0)^2\rangle & \langle((\hat{X}_c^{\frac{\pi}{2}})^2)^2\rangle & \langle(\hat{X}_c^{\frac{\pi}{2}})^2(\hat{X}_c^0)^2\rangle \\ \langle(\hat{X}_c^0)^2(\hat{X}_b^{\frac{\pi}{2}})^2\rangle & \langle(\hat{X}_c^0)^2(\hat{X}_b^0)^2\rangle & \langle(\hat{X}_c^0)^2(\hat{X}_c^{\frac{\pi}{2}})^2\rangle & \langle((\hat{X}_c^0)^2)^2\rangle \end{pmatrix} \tag{4.5.1}$$

We use the same data which was obtained above as example. For the amplitude squeezed state with $\{V^0 = 0.87, V^{\frac{\pi}{2}} = 1.27, \alpha = 0.39\}$, the covariance matrix is given by

$$\sigma_{b,c} = \begin{pmatrix} 3.32 & 0 & 0.10 & 0 \\ 0 & 4.78 & 0 & -0.19 \\ 0.10 & 0 & 2.98 & 0 \\ 0 & -0.19 & 0 & 3.78 \end{pmatrix}. \tag{4.5.2}$$

It clearly shows that the squared quadrature amplitude between mode b and c displays anti-correlation ($\langle(\hat{X}_b^0)^2(\hat{X}_c^0)^2\rangle = \langle(\hat{X}_c^0)^2(\hat{X}_b^0)^2\rangle = -0.19$) and the squared quadrature phase between mode b and c exhibits correlation ($\langle(\hat{X}_b^{\frac{\pi}{2}})^2(\hat{X}_c^{\frac{\pi}{2}})^2\rangle = \langle(\hat{X}_c^{\frac{\pi}{2}})^2(\hat{X}_b^{\frac{\pi}{2}})^2\rangle = 0.10$), respectively. Actually, these measured correlations come from the entanglement correlation which were produced by combining a squeezed vacuum state and a coherent state on a beam splitter. Inserting the covariances and means of squared quadratures into Eq.(4.2.23), a second-order correlation function of $g^{(2)}(0) = 0.81 < 1$ is obtained. It clearly shows that photon anti-bunching effect is observed and two-photon destructive interference occurs.

On the other hand, for the phase squeezed state with $\{V^0 = 0.88, V^{\frac{\pi}{2}} = 1.18, \alpha = 0.39\}$, the covariance matrix of squared quadratures from four permutations can be calculated as

$$\sigma_{b,c} = \begin{pmatrix} 1.97 & 0 & 0.04 & 0 \\ 0 & 8.42 & 0 & 0.32 \\ 0.04 & 0 & 1.90 & 0 \\ 0 & 0.32 & 0 & 6.33 \end{pmatrix}. \tag{4.5.3}$$

Different from the previous case, there are only positive covariances or correlations of the squared quadratures between the two modes b and c. In original entanglement correlation, there are both correlations and anti-correlations between the two modes. Again inserting the values of covariances and means into the Eq. (4.2.23), we can calculate a $g^{(2)}(0) = 1.37 > 1$ which indicates photon bunching effect due to two-photon constructive interference.

4.5.3 Second-order correlation function as a function of displacement

To find the effect of two-photon interference, we measured the second-order correlation function $g^{(2)}(0)$ for a small range of displacements α for the amplitude squeezed state with $\{V^0 = 0.87, V^{\frac{\pi}{2}} = 1.27\}$ and the phase squeezed state with $\{V^0 = 0.88, V^{\frac{\pi}{2}} = 1.18\}$, respectively. Fig. 4.13 shows the experimental results of $g^{(2)}(0)$ for the two different squeezed states with various displacements of coherent state α.The displacement of coherent state can be controlled by the amplitude of the modulation signal which is driven on the EOM for the coherent beam. From Fig. 4.13, we can find that the plotted $g^{(2)}(0)$ shows appreciable deviation from one when the displacement of the coherent state is less than a specific value, while approaching one when the displacement is lager than this value. The measurement of $g^{(2)}(0)$ for the amplitude squeezed state first decreases and finds a minimum value $g^{(2)}(0) = 0.81 < 1$ at $\alpha = 0.39$ on increasing the

displacement of the coherent state. As the displacement increases further, $g^{(2)}(0)$ monotonically approached one. While $g^{(2)}(0)$ for the phase squeezed state decreases monotonously to one as the displacement of the coherent state increases.

The behavior of $g^{(2)}(0)$ indicates the photon statistics of generated field, photon anti-bunching effect and photon bunching effect, which corresponded to destructive and constructive two-photon interference between the squeezed vacuum state and the coherent state, respectively.

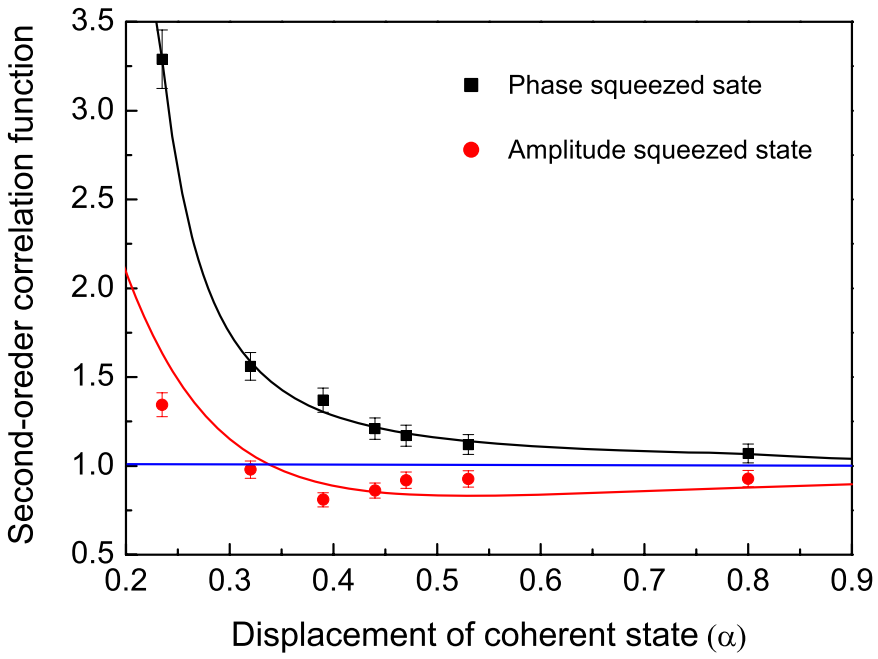

Fig. 4.12. Experimental measurement of $g^{(2)}(0)$ as a function of displacement α

4.6 Discussion of the results

It should be borne in mind that the second-order correlation function in Eq. (4.2.12) is extremely sensitive to the purity of the squeezed vacuum state and the coherent state. The best results will be obtained only when both the squeezed state and coherent state are the minimum uncertainty states ($V^0 * V^{\frac{\pi}{2}} = 1$). For the coherent state, it was produced by transferring a part of the optical power to the sidebands which makes it is almost a pure state. Hence, in order to obtain a better $g^{(2)}(0)$, we should generate a higher purity squeezed vacuum state. In the present experiment, we prepared the amplitude squeezed vacuum state with a purity of $V^0 * V^{\frac{\pi}{2}} = 0.87 * 1.27 = 1.13$ and the phase squeezed vacuum state with a purity of $V^0 * V^{\frac{\pi}{2}} = 0.88 * 1.18 = 1.04$, respectively. Recently, lots of techniques have been demonstrated to purify

a squeezed state [**?**, 102, 103]. In our experiment, it can be realized by reducing the injection beam power to decouple the extraneous noise and operate the OPA at far below threshold. We can also obtain a higher purity squeezed vacuum state by choosing a larger analysis frequency. We believe that the results can be significantly improved when a higher purity squeezed vacuum state is used.

Another limitation of the experiment is the efficiency of the homodyne detector. The efficiency of the homodyne detector can be written as $\eta_{det} = \eta_q V^2$ (η_q is the quantum efficiency of the detector and V^2 is the visibility of the signal beam and LO beam). Since the weak squeezed vacuum state was used in our experiment in our experiment, the limitation of the quantum efficiency is small and can be ignored. Thus the largest limitation of the detector is the visibility of the signal beams and LO beam. We measured the visibility between the squeezed vacuum state and the LO beam with 98% and visibility between the coherent state and the LO beam with 92%. Obviously the visibility between the coherent state and LO beam can be improved and a better results can be obtained.

4.7 Summary

We experimentally observed a continuous wave two-photon interference between a squeezed vacuum state from an optical parametric amplifier and a weak coherent state on a beam splitter by measuring the second correlation function with the homodyne detection system. A second-order correlation function of $g^{(2)}(0) = 0.81 < 1$, indicating the two-photon destructive interference, was observed when an amplitude squeezed vacuum state acts as one of interference sources. On the other hand, the two-photon constructive interference of $g^{(2)}(0) = 1.37 > 1$ was also obtained when the phase squeezed vacuum state is employed as one of interference sources.

Chapter5 Summary and outlook

In this chapter, brief summary of the key results of this thesis are provided. From these results, a number of future goals and investigations are identified.

5.1 Summary

Two-photon interference between a squeezed vacuum state from OPA and a weak coherent state is of fundamental interest in quantum optics and widely used in in quantum information, such as quantum communications generation of quantum state and quantum metrology. In this thesis, we experimentally observed a two-photon interference between a squeezed vacuum state and a coherent state on beam splitter with continuous variables by homodyne detection for the first time. Two different photon statistics (photon bunching and photon anti-bunching) were investigated by calculating the second-order correlation function from the measured quadrature amplitudes, which are corresponding to constructive interference and destructive interference, respectively. This provides another method to observe two-photon interference, and the main work of this thesis are followed as:

A squeezed state with best squeezing of -1dB and anti-squeezing of 1.7dB at a wavelength of 1064nm was produced from a below threshold optical parametric amplifier (OPA) with periodically poled $KTiOPO_4$ (PPKTP) crystal. The squeezing levels was controlled by the pump power, thus we can obtain an appreciate squeezing level, such as 0.3dB in our experiment, to realize the two-photon interference which was the core work of this thesis. By choosing an appropriate relative phase between the pump beam and injection beam, the OPA could be controlled so as to de-amplify or amplify the injection beam. This ensures to produce the amplitude quadrature and phase quadrature squeezed state which were used as one of interference source to realize the destructive interference and constructive interference, respectively.

With inverse Radon transform, we also reconstructed the Wigner function of different states with by homodyne tomography. The reconstructed states intuitively characterizes the generated vacuum states, coherent states, squeezed vacuum states and displaced squeezed states generated in our experiment. They are consistent with the results which were observed on the spectrum analyzer.

In this research, two-photon interference between a squeezed vacuum state and a weak coherent state with continuous wave laser source by homodyne detection system for the first time. Photon anti-bunching and bunching of the mixed field were investigated by calculating the correlations among four permutations of measured quadratures components, which were obtained by two

homodyne detection systems. The nonclassical effect of photon anti-bunching of $g^{(2)}(0) = 0.81 < 1$, indicating the two-photon destructive interference, was observed when an amplitude squeezed vacuum state was used as one of interference sources. On the other hand, the two-photon constructive interference of $g^{(2)}(0) = 1.37 > 1$ was also observed when the phase squeezed vacuum state was used.

5.2 Outlook

What follows are some ideas that can build on the work that we have done so far.

Firstly, observation of the two-photon interference at multi-analysis frequencies. Two-photon interference was widely used for generation of a single-photon state and entangled photon states for quantum information technology [105, 106]. In our experiment, the two-photon interference occurs at sidebands of the laser frequency. Hence, this makes it possible to produce quantum states at the sidebands of the laser frequency. It is easy to further extend sideband components using optical frequency comb technique [107]. Adding the generation of the wideband squeezed state [108], this opens an approach to produce a single-photon frequency comb. We believe it leads to potential applications for future multi-channel quantum communications technology [109–111].

Secondly, extending the two-photon interference to multi-photon interference. In our present experiment, we observed the two-photon interference by measuring the second-order correlation function of mixed states with a modified HBT interferometer, and it was mainly composed of two homodyne detections. According to our theoretical prediction, the value of the third-order [112] and four-order correlation function is oscillating by the change of displacement of the coherent state. There must be more information contained in third-order or four-order correlation functions, which will exist some interesting ptoperties of light. We can develop our experimental setup to divide our mixed state into three or four equal intensity beams, and each of them is combined with a strong local oscillator and measure the two quadrature components. Using this equipment and signal algorithm, we could measure the third-order and four-order correlation function which clearly demonstrate the quantum mechanical nature of light. Actually, the physical principle behind the measuring process is three-photon and four-photon interference [113].

Acknowledgements

The last four years of my life have been amazing and I would like to thank everyone who has contributed and supported me over this time.

First of all I gratefully acknowledge the help of my supervisor, associate professor Yun Zhang and professor Masayoshi Watanabe, who have offered me valuable suggestions in the academic studies. Associate professor Zhang has offered constant assistance and insight and understanding into many areas of quantum optics pursued in this thesis and also in my prior research. Professor Watanabe's outstanding abilities as a group leader have been made apparent to me many times and his enthusiasm for his work is very addictive.

I sincerely thank professor Kenichi Nakagawa, professor Yasuo Tomita, and associate professor Ryosuke Shimizu, who read my thesis and gave me some constructive suggestions on my thesis.

I also deeply indebted to the same group's Kota Kawamoto, Masato Wakuda, Yuki Fujita, Naoki Ishino. Almost none of my research was accomplished by me alone. From the beginning of my studies until now I worked together with them. I hope they had as much fun working with me as I had working with them.

Thanks to all of the other folks: Saburo Sakurai, Motoki Kaneyasu, Yuya Shimo, Syoma Hattori, Fumino Yamada, Syun Takeuchi, Horofumi Fujii, Syouta Nakagawa, Takahiro Izumi, Syouta Akazawa, Syouta Sugimoto, Daiki Nagao , and all the other students in Watanabe-zhang lab for their kindness。

Finally I send my deepest appreciations to my parents, my wife and my lovely son for supporting and encouraging me all the years. I am proud to share this thesis with you.

Reference

[1] M. Koashi, K. Kono, M. Matsuoka, and T. Hirano, Probing the two-photon phase coherence of parametrically down-converted photons by a local oscillator, Phys. Rev. A **50**, R3605 (1994).

[2] M. Matsuoka and T. Hirano, Quantum key distribution with a single photon from a squeezed coherent state, Phys. Rev. A **67**, 042307 (2003).

[3] Y. J. Lu, L. B. Zhu, and Z. Y. Ou, Security improvement by using a modified coherent state for quantum cryptography, Phys. Rev. A **71**, 032315 (2005).

[4] H. Wang and T. Kobayashi, Phase measurement at the Heisenberg limit with three photons, Phys. Rev. A **71**, 021802 (2005).

[5] R. Schnabel, N. Mavalvala, D. E. McClelland, and P. K. Lam, Quantum metrology for gravitational wave astronomy, Nat. Commun. **1**, 121 (2010).

[6] J. W. Pan, Z. B. Chen, C. Y. Lu, H. Weinfurter, A. Zeilinger, and M. Zukowski, Multiphoton entanglement and interferometry, Rev. Mod. Phys. **84**, 777 (2012)

[7] L. Mandel, Quantum effects in one-photon and two-photon interference, Rev. Mod. Phys. **71**, S274 (1999).

[8] G. Jaeger and A. V. Sergienko, Multi-photon quantum interferometry, Progress in Optics **42**, 277 (2001).

[9] R. Ikuta, T. Kobayashi, H. Kato, S. Miki, T. Yamashita, H. Terai, M. Fujiwara, T. Yamamoto, M. Koashi, M. Sasaki, Z. Wang, and N. Imoto, Nonclassical two-photon interference between independent telecommunication light pulses converted by difference-frequency generation, Phys. Rev. A. **88**, 042317 (2013).

[10] M. Koashi, K. Kono, T. Hirano, and M. Matsuoka, Photon antibunching in pulsed squeezed light generated via parametric amplification, Phys. Rev. Lett. **71**, 1164 (1993).

[11] M. Koashi, M. Matsuoka, and T. Hiraro, Photon antibunching by destructive two-photon interference, Phys. Rev. A. **53**, 3621 (1996).

[12] T. Legero, T. Wilk, M. Hennrich, G. Rempe, and A. Kuhn, Quantum beat of two single photons, Phys. Rev. Lett. **93**, 070503 (2004).

[13] M. G. Raymer, S. J. van Enk, C. J. McKinstrie, and H. J. McGuinness, Interference of two photons of different color, Opt. Commun. **283**, 747 (2010).

[14] R. B. Patel, A. J. Bennett, I. Farrer, C. A. Nicoll, D. A. Ritchie, and A. J. Shields, Two-photon interference of the emission from electrically tunable remote quantum dots, Nature Photon. **4**, 632 (2010).

[15] S. L. Braunstein and P. V. Loock, Quantum information with continuous variables, Rev. Mod. Phys. 77, 513 (2005)

[16] J. Etesse, M. Bouillard, B. Kanseri, and R. Tualle-Brouri, Experimental generation of squeezed cat states with an operation allowing iterative growth, Phys. Rev. Lett. **114**, 193602 (2015).

[17] K. Makino, Y. Hashimoto, J. Yoshikawa, H. Ohdan, T. Toyama, P. van Loock, and A. Furusawa, Synchronization of optical photons for quantum information processing, Sci. Adv. **2**, e1501772 (2016).

[18] T. F. Silva, G. C. Amaral, D. Vitoreti, G. P. Temporao, and J. P. Weid, Spectral characterization of weak coherent state sources based on two-photon interference, J. Opt. Soc. Am. B. **32**, 545 (2015).

[19] D. Bouwmeester, Jian-Wei Pan, K Mattle, M. Eibl, and H. Weinfurter, Experimental quantum teleportation, Nature **390**, 575 (1997)

[20] A. Furusawa, J. L. Srensen, S. L. Braunstein, C. A. Fuchs, H. J. Kimble, and E. S. Polzik, Unconditional quantum teleportation, Science **282**, 706 (1998)

[21] A. Ourjoumtsev, R. Tualle-Brouri, J. Laurat, and P. Grangier, Generating optical schrodinger kittens for quantum information processing, Science **312**, 83 (2006)

[22] A Ourjoumtsev, H Jeong, R Tualle-Brouri, and P Grangier, Generation of optical Schrodinger cats' from photon number states, Nature 448, 784 (2007)

[23] A. I. Lvovsky, H. Hansen, T. Aichele, O. Benson, J. Mlynek, and S. Schiller, Quantum state reconstruction of the single-photon fock state, Phys. Rev. Lett. **87**, 050402 (2001)

[24] A. Zavatta, S. Viciani, and M Bellini, Tomographic reconstruction of the single-photon Fock state by high-frequency homodyne detection, Phys. Rev. A **70**, 053821 (2004)

[25] U. L. Andersen, J. S. Neergaard-Nielsen, P. van Loock, and A. Furusawa, Hybrid discrete- and continuous-variable quantum information. Nature Physics 11, 713 (2015)

[26] W. K. Wootters and W. H. Zurek, Complementarity in the double-slit experiment: Quantum nonseparability and a quantitative statement of Bohr's principle, Phys. Rev. D **19**, 473 (1973)

[27] P. Mittelstaedt, A. Prieur, and R. Schieder, Unsharp particle-wave duality in a photon split-beam experiment, Foundations of Physics **9**, 891 (1987)

[28] V. Jacques, E. Wu, F. Grosshans, F. Treussart, P. Grangier, A. Aspect, and J. Roch, Experimental realization of wheeler's delayed-choice gedanken experiment, Science **315**, 966 (2007)

[29] R. Ionicioiu and D. R. Terno, Proposal for a quantum delayed-choice experiment, Phys. Rev. lett. **107**, 230406 (2011)

[30] J. S. Tang, Y. L. Li, X. Y. Xu, G. Y. Xiang, C. F. Li, and G. C. Guo, Realization of quantum Wheeler's delayed-choice experiment, Nature Photonics **6**, 600 (2012)

[31] L. Piazza, T. T. A. Lummen, E. Quionez, Y. Murooka, B. W. Reed, B. Barwick, and F Carbone, Simultaneous observation of the quantization and the interference pattern of a plasmonic near-field, . Nature Communications **6**, 6407 (2015)

[32] R. Hanbury-Brown and R. Q. Twiss, Correlation between photons in two coherent beams of light, Nature. **177**, 27 (1956).

[33] R. J. Glauber, The quantum theory of optical coherence, Phys. Rev. **130**, 2529 (1963).

[34] J. A. Zielinska, F. A. Beduini, V. G. Lucivero, and M. W. Mitchell, Atomic filtering for hybrid continuous-variable/discrete-variable quantum optics, Opt. Express **22**, 25307 (2014).

[35] H. Vahlbruch, Squeezed light for gravitational wave astronomy, Ph.D. thesis (The University of Hannover , 2008).

[36] N. B. Grosse, Harmonic entanglement & Photon anti-bunching, Ph.D. thesis (The Australian National University, 2009).

[37] D. F. Walls and G. J. Milburn, Quantum optics, (Springer US, 1994).

[38] C. C. Gerry and P. L. Knight, Introductory quantum optics (Cambridge University Press, Cambridge, UK, 2004).

[39] M. S. Stefszky, Generation and detection of low-frequency squeezing for gravitational-wave detection, Ph.D. thesis (The Australian National University 2012).

[40] H. P. Yuen and V. W. S. Chan, Noise in homodyne and heterodyne detection, Opt. Lett. **8**, 177 (1983).

[41] G. L. Abbas, V. W. S. Chan, and T. K. Yee, Local-oscillator excess-noise suppression for homodyne and heterodyne detection, Opt. Lett. **8**, 419 (1983).

[42] B. L. Schumaker, Noise in homodyne detection, Opt. Lett. **9**, 189 (1984).

[43] H. A. Bachor and T. C. Ralph, Guide to Experiments in Quantum Optics, Wiley-VCH (2004).

[44] Z. Y. Ou, Multi-photon quantum interference, (Springer US, 2007)

[45] Z. Y. Ou, S. F. Pereira, H. J. Kimble, and K. C. Peng, Realization of the einstein-podolsky-rosen Paradox for continuous variables, Phys. Rev. Lett. **68**, 3663 (1992).

[46] K. Wakui, H. Takahashi, A. Furusawa, and M. Sasaki, Photon subtracted squeezed states generated with periodically poled $KTiOPO_4$, Opt. Express **15**, 3568 (2007).

[47] N. B. Grosse, W. P. Bowen, K. McKenzie, and P. K. Lam, Harmonic entanglement with second-order nonlinearity , Phys. Rev. Lett. **96**, 063601 (2006).

[48] P. van Loock and S. L. Braunstein, Multipartite entanglement for continuous variables: a quantum teleportation network, Phys. Rev. Lett. **84**, 3482 (2000).

[49] J. S. Neergaard-Nielsen, B. M. Nielsen, C Hettich, K. Molmer and E. S. Polzik, Generation of a superposition of odd photon number states for quantum information networks, Phys.Rev. Lett. 97, 083604 (2006).

[50] K. Jung and J. Kim, Characterization of timing jitter spectra in free-running mode-locked lasers with 340 dB dynamic range over 10 decades of fourier frequency, Opt. Lett. **40**, 316 (2015).

[51] M. M. Nieto, The discovery of squeezed states in 1927, The 5th Int. Conference on Squeezed States and Uncertainty Relations (Balatonfured, 1997)

[52] V. V. Dodonov, "Nonclassical" states in quantum optics: a "squeezed" review of the first 75 years, J. Opt. B: Quantum Semiclass. Opt. **4**, R1 (2002)

[53] E. H. Kennard, Quantum mechanics of simple motion types, Z. Phys. **44**, 326 (1927) (German)

[54] R. E. Slusher, L. W. Hollberg, B. Yurke, J. C. Mertz, and J. F. Valley, Observation of squeezed states generated by four-wave mixing in an optical cavity, Phys. Rev. Lett. **56**, 788 (1986)

[55] L. A. Wu, H. J. Kimble, J. L. Hall, and H. Wu, Generation of squeezed states by parametric down conversion, Phys. Rev. Lett. **57**, 2520 (1986).

[56] R. E. Slusher, P. Grangier, A. LaPorta, B. Yurke, and M. J. Potasek, Pulsed squeezed light, Phys. Rev. Lett. **59**, 2566 (1987)

[57] E. S. Polzik, J. Carri, and H. J. Kimble, Atomic spectroscopy with squeezed light for sensitivity beyond the vacuum state limit, Appl. Phys. B. **55**, 279, (1992).

[58] K. Schneider, M. Lang, J. Mlynek, and S. Schiller. Generation of strongly squeezed continuous-wave light at 1064 nm, Opt. Express. **2**, 59 (1998).

[59] H. Vahlbruch, S. Chelkowski, M. Mehmet, B. Hage, A. Franzn, N. Lastzka, S. Goler, K. Danzmann, and R. Schnabel, Observation of squeezed light with 10-dB quantum noise reduction, Phsy. Rev. Lett. **100**, 033602 (2008).

[60] M. Mehmet, S. Ast, T. Eberle, S. Steinlechner, H. Vahlbruch, and R. Schnabel, Squeezed light at 1550nm with a quantum noise reduction of 12.3 dB, Opt. Express. **19**, 25763 (2011).

[61] T. Eberle, S. Steinlechner, J. Bauchrowitz, V. Handchen, H. Vahlbruch, M. Mehmet, H. Muller-Ebhardt, and R. Schnabel, Quantum enhancement of the zero-areasagnac interferometer topology for gravitational wave detection, Phys. Rev. Lett. **104**, 251102 (2010).

[62] H. Vahlbruch, M. Mehmet, K. Danzmann, and R. Schnabel, Detection of 15 dB squeezed states of light and their application for the absolute calibration of photoelectric quantum efficiency, Phys. Rev. Lett. 117 110801 (2016).

[63] P. K. Lam, T. C. Ralph, B. C. Buchler, D. E. McClelland, H. A. Bachor, and J. Gao, Optimization and transfer of vacuum squeezing from an optical parametric oscillator, J. Opt. B. **1**, 469 (1999).

[64] W. P. Bowen, R. Schnabel, N. Treps, H-A. Bachor, and P. K. Lam, Recovery of continuous wave squeezing at low frequencie, J. Opt. B: Quantum Semiclass. Opt. **4**, 421(1992).

[65] S. Suzuki, H. Yonezawa, F. Kannari, M. Sasaki, and A. Furusawa, 7dB quadrature squeezing at 860 nm with periodically poled KTiOPO4, Appl. Phys. Lett. **89**, 061116 (2006).

[66] Y. Takeno, M. Yukawa, H. Yonezawa, and A. Furusawa, Observation of -9 dB quadrature squeezing with improvement of phase stability in homodyne measurement, Opt. Express. **15**, 4321 (2007).

[67] M. Mehmet, H. Vahlbruch, N. Lastzka, K. Danzmann, and R. Schnabel, Observation of squeezed states with strong photon-number oscillations. Phys. Rev. A. **81**, 013814 (2010).

[68] M. S. Stefszky, C. M. Mow-Lowry, S. S. Y. Chua, D. A. Shaddock, B. C. Buchler, H. Vahlbruch, A. Khalaidovski, R. Schnabel, P. K. Lam, and D. E. McClelland, Balanced homodyne detection of optical quantum states at audio-band frequenices and below, Class. Quantum Grav. **29**, 14 (2012).

[69] C.M. Caves, Quantum-mechanical noise in an interferometer, Phys. Rev. D, **23**, 1693 (1981).

[70] M. Xiao, L.-A. Wu, and H. J. Kimble, Precision measurement beyond the shot-noise limit, Phys. Rev. Lett. **59**, 278 (1987).

[71] N. B. Grosse, T. Symul, M. Stobiska, T. C. Ralph, and P. K. Lam, Measuring photon antibuching from continuous variables sideband squeezing, Phys. Rev. Lett. **98**, 153603 (2007).

[72] F. A. Beduini, J. A. Zieliska, V. G. Lucivero, Y. A. Astiz, and M. W. Mitchell, Interferometric measurement of the biphoton wave function, Phys. Rev. Lett. **113**, 183602 (2014)

[73] P. Chen, C. Shu, X. Guo, M. M. T. Loy, and S. Du, Measuring the biphoton temporal wave function with polarization-dependent and time-resolved two-photon interference, Phys. Rev. Lett. **114**, 010401 (2015)

[74] P. A. Franken, A. E. Hill, C. W. Peters, and G. Weinreich, Generation of optical harmonics. Phys. Rev. Lett. **7**, 118 (1961).

[75] Y. Zhang, N. Hayashi, H. Matsumori, R. Mitazaki, Y. H. Xue, Y. Okada-Shudo, M. Watanabe, and K. Kasai, Generation of1.2W green light using a resonant cavity-enhanced second-harmonic process with a periodically poled $KTiOPO_4$, Opt. Commun. **294**, 271 (2013).

[76] H. Matsumori, Generation of squeezed vacuum state and measurement of photon anti-bunching effect, Master thesis (The University of Electro-Communications, 2013).

[77] E. Winger, On the quantum correction for thermodynamic equilibrium, Phys. Rev. **40**, 749 (1932).

[78] J. Bertrand and P. Bertrand, A tomographic approach to Wigner's function, Foundations of Physics 17, 397 (1987).

[79] K. Vogel and H. Risken, Determination of quasiprobability distributions in terms of probability distributions for the rotated quadrature phase, Phys. Rev. A 40, 2847 (1989).

[80] D. T. Smithy, M. Beck, and M. G. Raymer, Measurement of the Wigner distribution and the Density matrix of a light mode using optical homodyne tomography: application to squeezed states and vacuum, Phys. Rev. Lett. 70, 1244 (1993).

[81] U. Leonhardt, Measuring the quantum state of light, Cambridge University Press (1997).

[82] A. I. Lvovsky, Continuous-variable optical quantum state tomography, Rev. Mod. Phys. **81**, 299 (2009).

[83] J. W. Wu, P. K. Lam, M. B. Gray, and H. A. Bachor, Optical homodyne tomography of information carrying laser beams, Opt. Express. **4**, 154 (1998).

[84] J. W. Wu, Applications of Optical Homodyne Tomography, Ph.D. thesis (The Australian National University, 2000).

[85] G. Breitenbach and S. Schiller, Homodyne tomography of classical and non-classical light, J. Mod. Opt. **44**, 2207 (1997).

[86] G. Breitenbach, S. Schiller, and J. Mlynek, Measurement of the quantum states of squeezed light, Nature **387**, 471 (1997).

[87] C. G. Ye, Investigation on squeezing light and observation of electromagnetically induced transparency-like effect in phase-sensitive optical prametric amplifier, Ph.D.thesis (The Shanxi University, 2009).

[88] K. Kawamoto, Measurement of photon anti-bunching with homodyne detection, Master thesis (The University of Electro-Communications, 2015)

[89] D. Stoler, Photon antibunching and possible ways to observe it, Phys. Rev. Lett. **33**, 1397 (1974).

[90] H. J. Kimble, M. Dagenais, and L. Mandel, Photon Antibunching in Resonance Fluorescence, Phys. Rev. Lett. **39**, 691 (1977).

[91] M. S. Zubairy and J. J. Yeh, Photon statistics in multiphoton absorption and emission processes, Phys. Rev. A **21**, 1624 (1980).

[92] J. Mostowski and K. Rzazewski, Photon bunching and antibunching in second harmonics generation, Phys. Lett. A **66**, 275 (1978).

[93] H. P. Yuen, Two-photon coherent states of the radiation field, Phys. Rev. A **13**, 2226 (1976).

[94] K. J. Resch, J. S. Lundeen, and A. M. Steinberg, Nonlinear optics with less than one photon, Phys. Rev. Lett. **87**, 123603 (2001).

[95] J. H. Kim, T. Cai, C. J. K. Richardson, R. P. Leavitt, and E. Waks, Two-photon interference from a bright single-photon source at telecom wavelengths, Optica **3**, 577 (2016).

[96] A. B. Dodson and R. Vyas, Homodyne photon statistics of the subthreshold degenerate parametric oscillator, Phys. Rev. A **47**, 3396 (1993).

[97] H. Deng, D. Erenso, R. Vyas, and S. Singh, Entanglement, interference, and measurement in a degenerate parametric oscillator, Phys. Rev. Lett. **86**, 2770 (2001).

[98] Y. J. Lu and Z. Y. Ou, Observation of nonclassical photon statistics due to quantum interference, Phys. Rev. Lett. **88**, 023601 (2002).

[99] D. T. Smithey, M. Beck, J. Cooper, and M. G. Raymer, Measurement of number-phase uncertainty relations of optical fields, Phys. Rev. A **48**, 3159 (1993).

[100] Y. Zhang, R. Okubo, M. Hirano, Y. Eto, and T. Hirano, Experimental realization of spatially separated entanglement with continuous variables using laser pulse trains, Sci. Rep. 5, 13029 (2015).

[101] L. A. Krivitsky, U. L. Andersen, R. Dong, A. Huck, C. Wittmann, and G. Leuchs, Correlation measurement of squeezed light, Phys. Rev. A 79, 033828 (2009).

[102] Y. Kurochkin, A. S. Prasad, and A. I. Lvovsky, Distillation of the two-mode squeezed state, Phys. Rev. Lett. **112**, 070402 (2014).

[103] J. Yoshikawa, T. Hayashi, T. Akiyama, N. Takei, A. Huck, U. L. Andersen, and A. Furusawa, Demonstration of deterministic and high fidelity squeezing of quantum information, Phys. Rev. A **76**, 060301 (2007).

[104] J. Heersink, Ch. Marquardt, R. Dong, R. Filip, S. Lorenz, G. Leuchs, and U. L. Andersen, Distillation of squeezing from non-Gaussian quantum states, Phys. Rev. Lett. **96**, 253601 (2006).

[105] A. Beveratos, R. Brouri, T. Gacoin, A. Villing, J. Poizat, and P. Grangier, Single photon quantum cryptography, Phys. Rev. Lett. **89**, 187901 (2002).

[106] J. P. Olson, K. R. Motes, P. M. Birchall, N. M. Studer, M. LaBorde, T. Moulder, P. P. Rohde, and J. P. Dowling, Linear optical quantum metrology with single photons: Experimental errors, resource counting, and quantum Cramr-Rao bounds, Phys. Rev. A **96**, 013810 (2017).

[107] Y. Zhang, J. Ishikawa, and F. L. Hong, Accurate frequency atlas of molecular iodine near 532nm measured by an Optical Frequency comb generator, Opt. Commun. **200** 209-215 (2001).

[108] M. Kobayashi, Y. Kadoya, H. Yuji, R. Masuyama, and M. Yamanishi, Squeezing of photon-number fluctuations in the frequency range wider than 300 MHz in light-emitting diodes at room temperature, J. Opt. Soc. Am. B **17**, 1257 (2000).

[109] M. Pysher, Y. Miwa, R. Shahrokhshahi, R. Bloomer, and O. Pfister, Parallel generation of quadripartite cluster entanglement in the optical frequency comb, Phys. Rev. Lett. **107**, 030505 (2011).

[110] B. Hage, A. Samblowski, and R. Schnabel, Towards einstein-podolsky-rosen quantum channel multiplexing, Phys. Rev. A. **81**, 062301 (2010)

[111] J. Lu, L. Zhou, L. M. Kuang, and F. Nori, Single-photon router: Coherent control of multichannel scattering for single photons with quantum interferences, Phys. Rev. A **89**, 013805 (2014)

[112] M. J. Stevens, S. Glancy, S. W. Nam, and R. P. Mirin, Third-order antibunching from an imperfect single-photon source, Opt. Express. **22**, 3244 (2014) .

[113] Y. H. Xue, T. Y. Li, K. Kasai, Y. Okada-Shudo, M. Watanabe, Y. Zhang, Controlling quantum interference in phase space with amplitude, Sci. Rep. **7**, 2291(2017).

Publications

Paper

1. Daohua Wu, Kota Kawamoto, Xiaomin Guo, Katsuyuki Kasai, Masayoshi Watanabe, and Yun Zhang,

   Observation of two-photon interference with continuous variables by homodyne detection,

   The European Physical Journal D **71**, 260 (2017) Corresponding chapter 4

International Conference

1. Daohua Wu, Kota Kawamoto, Masato Wakuda Masayoshi Watanabe and Yun Zhang

   Measuring photon anti-bunching and photon statistics of continuous-wave light by homodyne detection,

   The 22nd International Conference on Laser Spectroscopy. Mon-56

   Singapore, June 28〜July 3, 2015.

2. Daohua Wu, Kota Kawamoto, Katsuyuki Kasai, Masayoshi Watanabe and Yun Zhang

   Observation of two-photon interference for continuous-wave light with homodyne detection,

   The 24th Congress of the International Commission for Optics. Th3H-05

   Tokyo, Japan, Aug.21〜 Aug.25, 2017.

Domestic Conference

1. Daohua Wu, Kota Kawamoto, Masato Wakuda Masayoshi Watanabe and Yun Zhang

   Observation of photon statistics in two-photon interference for continuous variables,

   The 64th JSAP Spring Meeting, 17p-414-12

   Yokohama, Mar.14〜Mar.17, 2017.

Resume

呉　道華　(Daohua Wu) 昭和 54 年 01 月 14 日　中国で生まれる

学　　歴

平成 09 年 09 月 01 日	安徽師範大学物理子信息工程学部	入学
平成 13 年 06 月 30 日	同上	卒業
平成 18 年 09 月 01 日	安徽大学大学院物理と材料科学研究科光学専攻修士課程	入学
平成 21 年 06 月 30 日	同上	修了
平成 26 年 03 月 28 日	電気通信大学大学院　情報理工研究科　先進理工学専攻	入学

職　　歴

平成 13 年 07 月 01 日	安徽中医薬高等専門学校	教員
平成 26 年 02 月 28 日	同学	退職